Sensitivity of Precipitation to Land-use Changes in a Regional Climate Model of West Africa

By

Patric Ryser

M.A., Climate and Society
Columbia University, 2021

Submitted to the MIT Civil and Environmental Engineering Department
in partial fulfillment of the requirements for the degree of

Master of Science in Civil and Environmental Engineering
at the

MASSACHUSETTS INSTITUTE OF TECHNOLOGY

February 2024

Authored by: Patric Ryser
MIT Civil and Environmental Engineering
August 31st, 2023

Certified by: Elfatih A.B. Eltahir
Professor of Civil and Environmental Engineering
MIT Civil and Environmental Engineering
Thesis Supervisor

Accepted by: Heidi Nepf
Professor of Civil and Environmental Engineering
Chair, Graduate Program Committee

Sensitivity of Precipitation to Land-use Changes in a Regional Climate Model of West Africa

By
Patric Ryser

Submitted to the MIT Civil and Environmental Engineering Department on August 31st, 2023 in partial fulfillment of the requirements for the degree of
Master of Science in Civil and Environmental Engineering

Abstract

Limited water resources, climate change and food security needs in West Africa present a special set of challenges in the years to come as the population grows. An optimized irrigation scheme for agriculture can change regional climate by increasing rainfall in specific areas, possibly increasing the water availability for agricultural activities by causing changes in the background large-scale climate circulations which could lead to more precipitation overall in areas with water scarcity.

Both observational and model studies have looked at irrigation impacts around the world, including West Africa. However, the intermediate mechanisms, such as specific roles of the atmospheric structures of the Planetary Boundary Layer (PBL) and Lifting Condensation Level (LCL), or how background wind patterns are affected under certain land-use changes have not been thoroughly explored.

This thesis analyzes the atmospheric changes due to land-use and land-cover changes (LULCC) by analyzing the PBL, the LCL, surface wind, surface pressure and other atmospheric variables to quantify the underlying physical mechanisms which shape rainfall. We analyze this by using the MIT Regional Climate Model (MRCM) to test different LULCC scenarios. For the irrigation experiment, LCL is more sensitive and drops more than does PBL especially in the north, yet rainfall only increases south of the irrigation area. There also exists a transitional zone, north of which there is less rainfall. Desertification increases both the PBL and LCL heights, but the increase in LCL is greater. This pushes the cloud base higher than the PBL, preventing cloud formation and rainfall. However, the simulated rainfall changes do not mirror this development. At a certain latitude, there is again a transitional zone, north of which the rainfall decreases and south of which the rainfall increases intermittently. Given the patterns of the precipitation changes, we believe that different mechanisms are at work for both the desertification and irrigation experiments. This study hypothesizes a blocking mechanism that prevents the monsoon from travelling northward due to the presence of a high surface pressure anomaly being observed in the north of the irrigated zone under the irrigation scenario.

The changes of the atmospheric structure, specifically the PBL and LCL, surface pressure, and wind patterns, as analyzed in this thesis, provide us with another dimension to understand the effects of irrigation and desertification on rainfall, enabling more optimal irrigation strategies. It also provides insights on the locations where natural vegetation or croplands may benefit from the additional rainfall, which could facilitate soil carbon sequestration, a nature-based solution for combatting climate change.

Thesis Supervisor: Elfatih A.B. Eltahir
Title: H.M. King Bhumibol Professor, Professor of Civil and Environmental Engineering

Contents

Acknowledgements

I would like to thank most dearly Professor Elfatih A.B. Eltahir for having gone through this academic journey with me which culminated in this thesis after 2 years together. I have learned many valuable things and Prof. Eltahir was always an inspirational and supportive advisor to me even in the toughest of times. I will always be grateful for the great opportunity that I got to spend time here in this wonderful lab at MIT. I would also like to thank the other faculty members at Parsons who took the time to teach me certain topics to broaden my horizons and show me why they enjoyed the things they were researching. I would also like to thank my lab mates Yeonwoo, Muhammad and Kasia for always having been supportive and for helping me out with the day-to-day operations in the lab. I have learned many tips and tricks for programming on the Linux server, using ArcGIS and opening NetCDF files that would have otherwise cost me many extra hours. I believe that we will stay friends forever. Then I would also like to thank the wider Parson community, thank Sarah Smith for having patiently explained me things again and again and other colleagues and staff who always helped me out and were kind to me to make life just that little more enjoyable at times when life seemed frustrating. I will always remember and cherish the times I spent here.

1. Introduction

1.1 Large Scale Agricultural Trends in West Africa

Agricultural expansion has been rapid in the 20th century, with around 40% of the earth's ice-free surface being transformed into agricultural land (Turner et al., 2007). Agricultural activity accounts for roughly 85% of all water withdrawals in the world, which fundamentally alters the water and energy balances between the surface and the atmosphere. These big scales of water-use, often associated with irrigated agriculture and associated land-use land-cover changes, have strong impacts on regional climate and more specifically on rainfall. More recently, land-use changes continue to happen at a fast pace in the 21st century, with cropland area increasing globally by 9% and notably in Africa by more than 30% from 2003 to 2019 alone. In the same time frame, the global per capita agricultural land-use has decreased by roughly 10%. This is due to an all-round increase in productivity in agriculture, including the expansion of irrigated croplands, more efficient farming techniques such as the adequate use of fertilizers in conjunction with the growing global population (Potapov et al., 2022).

Agricultural activities are a key component not only for meeting the ever-larger demands for food with a growing global population, but are also an indispensable part of contributing to the African economic growth in conjunction with the foreign aid flowing into certain countries (McArthur & Sachs, 2019). The correct strategic development of resources, including agricultural planning in African countries, can result in synergies that increase food production and contribute to economic growth. However, agricultural expansion also has many detrimental side effects such as causing a rapid loss of biodiversity (Tripathi et al., 2021) and changing the regional climate patterns, including temperature and rainfall, in sometimes unforeseen ways (Alter et al., 2015, 2015; Berg et al., 2014; Betts et al., 1996; Findell & Eltahir, 1997; Kang & Eltahir, 2018; Lobell et al., 2009; Santanello et al., 2018; Zhou et al., 2019, 2021). Furthermore, it is assumed that the implementation of irrigated agriculture will continue to expand in West Africa to meet the growing population. Therefore, understanding the consequences of increasing irrigated agriculture at specific times and locations is important to avoid some of the unwanted climate conditions associated with specific implementations of agricultural expansion. In the following, this introduction will first present background about West African agricultural challenges and opportunities, then provide a summary of the West African climate, and finally touch on the variables that affect rainfall in West Africa.

1.2 Challenges and Opportunities for West African Agriculture

Challenges and opportunities for agriculture in West Africa are due to several trends and drivers of change. These trends include demographic trends and socio-economic trends. For demographics, there is a strong growth rate, specifically for poorer countries, with an average growth rate of about 2.7% and is projected to reach 490 million by 2050. There are also strong migration trends, specifically migration from rural areas into cities and geographically from Sahelian to Sudano-Guinean zones. However, despite urbanization, the rural populations continue to grow in absolute terms. Socio-economically, the middle-classes, defined as people who are above the poverty line, earning more than 2 dollars per day, are growing, despite still not constituting most of the population (Hollinger & Staatz, 2015). The socio-economic and demographic trends cause an increase in the total demand for food as well as an increase in the diversity for different kinds of food due to urbanization and globalization. However, there are also downsides to globalization, such as being part of an increased volatile international market environment for agricultural products, driven by climate change, climate variability and increased links between financial, energy and agricultural markets. Climate variability which is likely to increase in the future (Teye & Nikoi, 2022), causes yields each year to be more unpredictable, due to events such as droughts and floods. Financial pressure comes from fast growing agriculture producers such as Brazil that are leveraging advanced technologies to increase their agricultural productivity as well as from other socio-economic trends, such as urbanization. There are also many deficiencies when it comes to risk management for farmers, such as a lack of agricultural insurance and other financial instruments as well as more basic technological solutions, such as improved soil and water management as irrigation (Hollinger & Staatz, 2015).

Market risks combined with the lack of risk management techniques combines to make agricultural activities to be a risky endeavor. However, some of these challenges can be overcome through technical solutions, such as the expansion of irrigation infrastructure and understanding on how regional climate change due to land-use changes can be quantified to improve water resources management. This specifically will be the challenge this study aims to better overcome.

1.3 West African Climate

West Africa is the study area of this research. West Africa can be subdivided into 3 different regions: the Sahara (north of 20N), the Sahel (roughly between 10N and 20N) and the Tropics (below 10N). It is a semiarid region where climate variability, climate change and topography all play an important role on rainfall patterns (Figure 1.1). Climate variability is driven primarily by the West African Monsoon (WAM), which has strong seasonal characteristics, bringing the Inter-Tropical Convergence Zone (ITCZ) from the tropics around the equator up north in the rainy season between June and August/September and then back south again. Due to this latitudinal shift in rain, West African climate is characterized by a strong north-south gradient (Figure 1.2). WAM itself is influenced by both natural variability, such as the El Niño/Southern Oscillation (ENSO) associated with abnormal sea surface temperatures, and anthropogenic forcings such as greenhouse gas emissions. The rainfall pattern of the WAM is characterized mainly by two rainfall events that are spread over two time periods in two different locations: (1) intense rains near the Gulf of Guinea (around 5N) between June and July which roughly follows the seasonality of the Atlantic Sea Surface Temperature (SST),

and (2) strong rainfall bands along the interior of the West African continent at about 10N starting in July and continuing until about late August/early September. During July to September, westward propagating wave signals [African easterly waves (AEWs)] dominate the synoptic-scale variability (Gu & Adler, 2004). In addition, human-induced land-use change is a key element in conjunction with natural variability that controls and influences the WAM system. (Biasutti, 2019; Im, Marcella, et al., 2014a; Zheng & Eltahir, 1998).

Historically, land use has changed dramatically in this area, with cultivated land expanding 5-fold in the Sahel when comparing the 1950s to the 2000s. This area, however, does not have good water resources for agriculture and the amount of irrigated area is estimated to be a very small percentage of the total cultivated area (CGIAR, 2015; Hollinger & Staatz, 2015; Tripathi et al., 2021). Furthermore, West Africa is considered a "hot spot" for soil moisture-rainfall feedbacks (Koster et al., 2004; Wang & Eltahir, 2007), which means that if land-use and land cover changes (LULCC) occur there, such as an expansion of irrigated agriculture, it might have a disproportionately large impact on atmospheric conditions and subsequently rainfall patterns. This thesis will discuss the possible effects of irrigation and desertification on the alteration of regional climate in West Africa, such as affecting the wind patterns, PBL, LCL, and precipitation amounts associated with the WAM.

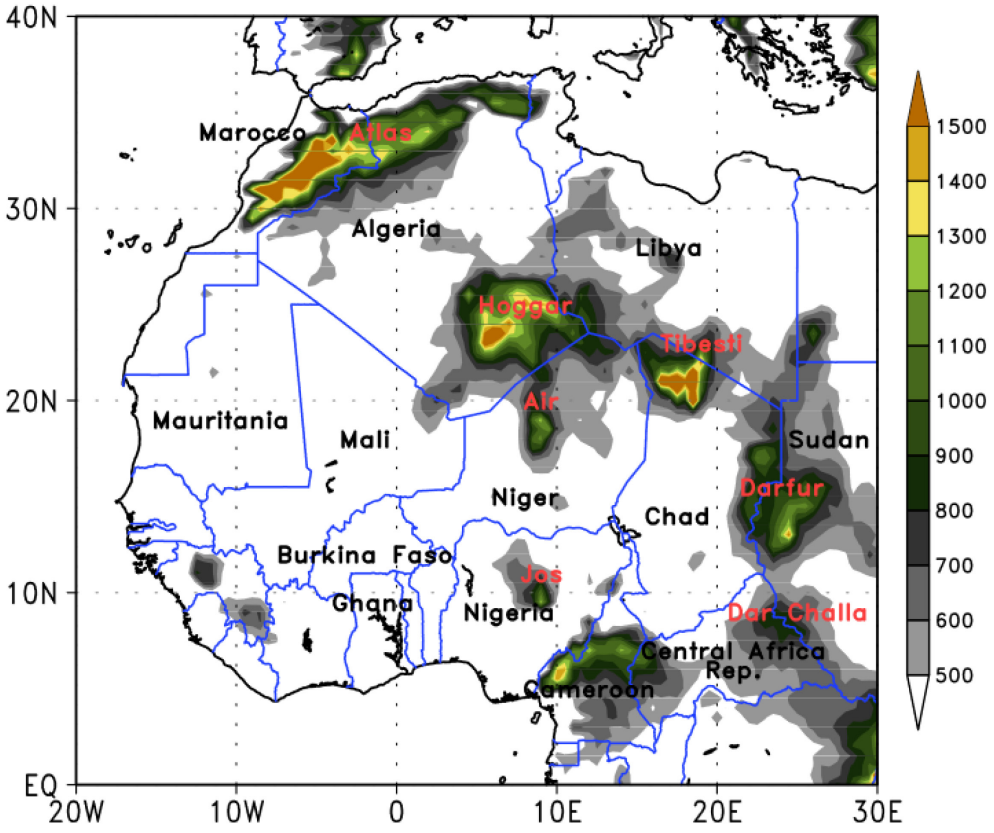

Figure 1.1 Elevation Map showing different mountain ranges in Africa. Graph extracted from (Lavaysse et al., 2009).

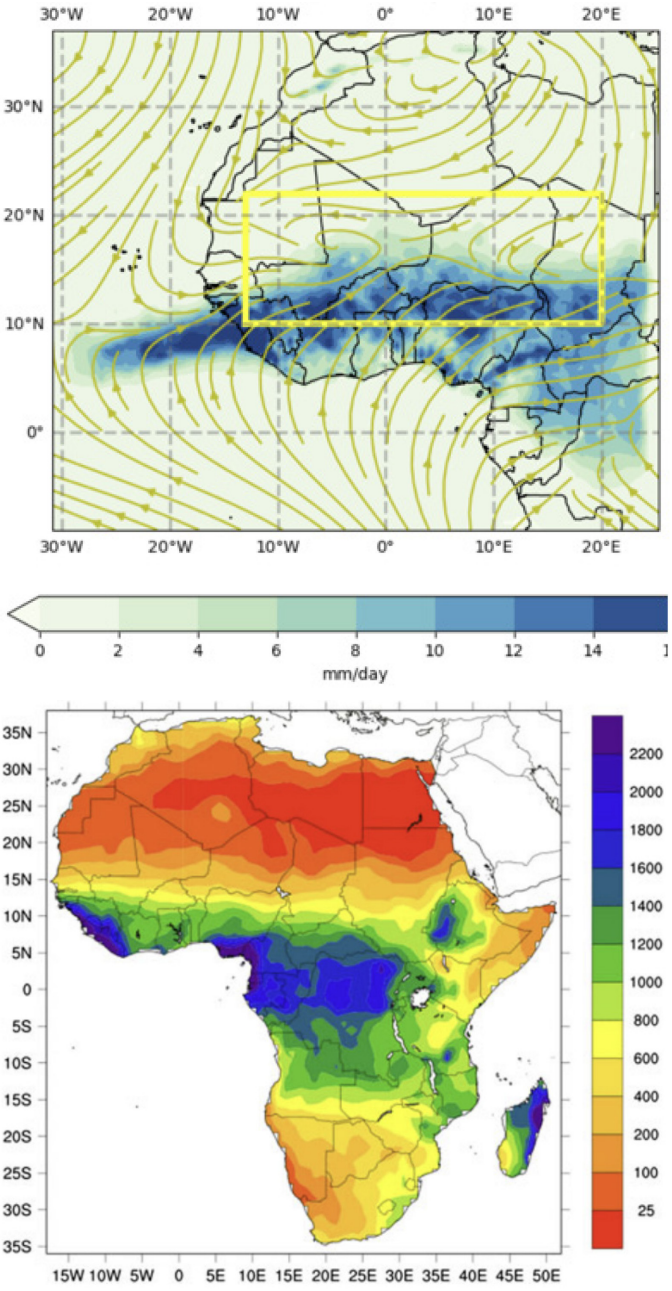

Figure 1.2 Top: July precipitation amounts (mm/day) from MRCM control (CONT) simulation. Bottom: Annual average precipitation (mm) in Africa from the Global Precipitation Climatology Center (GPCC) 1979-2010 rainfall data (graph extracted from (A. Siebert, 2014)).

1.4 Variables Affecting West African Rainfall

West African rainfall is heavily influenced by different climate phenomena. Studies in the past on West African rainfall can generally be categorized into 3 categories: There are those that investigate the teleconnections of remote oceanic forcings such as from Atlantic ocean SST (Rodríguez-Fonseca et al., 2011; Thorncroft et al., 2011; Zheng et al., 1999), or effects from the El Nino Southern Oscillation (ENSO) from the Pacific ocean on larger scales (Atiah et al., 2020; Camberlin et al., 2001; Dai & Wigley, 2000); those that focus on local atmospheric to land-surface level perturbations (Kang & Eltahir, 2019; Qian et al., 2013) such as due to irrigated agricultural activities; and more recently, studies that look at the effects of aerosols both remotely through ocean-mediated processes and locally through direct-atmospheric processes on rainfall (Deser et al., 2020; Hirasawa et al., 2022). Studies in this third category see the effects on rainfall in this region as being linked to the Hadley cells as well as the regional monsoonal circulations, which causes it to be susceptible to influences from both remote oceans and local land surfaces (Biasutti, 2019).

West African summer rainfall variability is strongly influenced by SST in the Atlantic ocean and has strong interannual variability (Thorncroft et al., 2011; Worou et al., 2021; Zheng et al., 1999). Despite some recent studies that have suggested a weakening role of Atlantic SSTs on West African rainfall (Worou et al., 2021), there have been many studies on WAM which have shown a strong correlation between interannual WAM variability in rainfall to other ocean characteristics such as the South Atlantic Ocean Dipole (Nnamchi & Li, 2011). Some also actively use this relationship to predict seasonal rainfall in the future (A. Siebert et al., 2021). Physical mechanisms associated with SST effects on rainfall are related to the temperature differences between the equatorial Atlantic and the Sahara, which drives the timing and intensity of coastal rainfall and the moisture flux convergence north of the main rainfall band (Thorncroft et al., 2011). It can

therefore be concluded from previous studies that one of the main drivers of interannual rainfall variability are the conditions of ocean temperatures in the Atlantic and in other oceans.

At the same time, another driver of rainfall anomalies in West Africa are local perturbations in moisture and temperature which can lead to changes in the fluxes of energy and matter. These changes in surface conditions, such as a change in land-use type, can alter the large-scale circulations and change rainfall patterns in the region. Some of the theories involving land-atmosphere interactions have been well-studied and there are many different feedback loops proposed on how surface conditions affect circulations and ultimately rainfall (Liu et al., 2022; Seneviratne et al., 2010). Specifically for rainfall, there are generally different ways to look at it, either through the lens of water recycling or through the lens of convective activity, which are both valid. However, these feedback loops are usually best understood at different spatial scales. If one looks at smaller spatial scales, theories proposed in past studies indicate a negative feedback loop between wet patches and local convective initiation, as wet patches decrease the surface temperature, which causes the planetary boundary layer to lower, which in turn decreases convective activity (Im & Eltahir, 2014; Klein & Taylor, 2020; Taylor et al., 2012). At larger spatial scales however, water recycling is generally still considered one potential factor and leads to a feedback mechanism in which wet soils tend to increase regional rainfall as the extra moisture is evaporated and then falls back to earth as rain at a later time in the same mesoscale region (Brubaker et al., 1993; Gong & Eltahir, 1996). No matter the mechanisms involved, there is no denying the direct effects of local land surface effects on rainfall variability in West Africa, and the region of West Africa is considered to be a hotspot when it comes to land-atmosphere feedbacks (Koster et al., 2004).

More recently, newer studies have pointed to the fact that aerosols can also have a strong impact on rainfall (Camberlin et al., 2001; Deser et al., 2020; Monerie et al., 2023). Anthropogenic aerosols are dominated by sulfate emissions, but effects have also been documented for black carbon (Huang et al., 2009). Aersol emissions can both have local

and remote impacts on rainfall in West Africa through both local, i.e. West African aerosol emissions and remote, i.e. emissions from the US and Europe. This is due to the aerosol properties such as altering the shortwave radiation, and the changing of cloud albedo and lifetime (Collins et al., 2017). These effects explain the West African droughts in the past, as the emissions of European and North American aerosols caused a decrease in surface air temperature in those areas, weakening the interhemispheric temperature gradient and causing the WAM to move southward. This in turn caused droughts in West Africa as WAM did not transport as much water northward. Since the 1980s, emissions of aerosols in Europe and North America have decreased, causing the WAM to move northward and contribute to more rainfall. However, the local effect of aerosol emissions in West Africa itself have become more dominant as aerosol emissions increased for both sulfates and black carbon. This in turn is responsible for drying in recent years and will likely be the dominant pathway to drying in the years to come as these aerosols scatter shortwave radiation over Africa, enhance cloud cover, which cools the surface and decreases the amount of local rainfall (Hirasawa et al., 2022; Shindell et al., 2023).

2. Literature Review

In the Introduction section, we have introduced the notion that West African rainfall is mainly affected by three aspects, local land and atmospheric feedbacks, remote ocean drivers, and aerosols, which themselves have both a remote and a local effect on rainfall. The experiments that we conducted are focused on understanding the effects on rainfall due to land-use and land-cover changes. For this reason, we will dive deeper into the first driver of change from previous studies.

The current state of the land-use types in Africa are mostly comprised of grasslands, savannas, and croplands (Figure 2.1), of which most of the existing croplands are rainfed due to a lack of irrigation infrastructure. This causes agriculture to be less productive as it suffers more from negative impacts caused by climate variability, which will likely increase in the future (Teye & Nikoi, 2022). One of the possible solutions would be to implement more irrigation infrastructure to minimize unwanted climate risks (Hollinger & Staatz, 2015) for the future. One of the consequences of increasing irrigation, is the wetting of the soils and the increase of evapotranspiration of the crops. It is therefore important to better understand the consequences of wet soils and LULCC more broadly on climate as well as precipitation. In the following, we will review different studies in the past that have already looked at the topic of LULCC as well as irrigation on precipitation and other intermediate mechanisms that lead to a change in rainfall as well as other water resources.

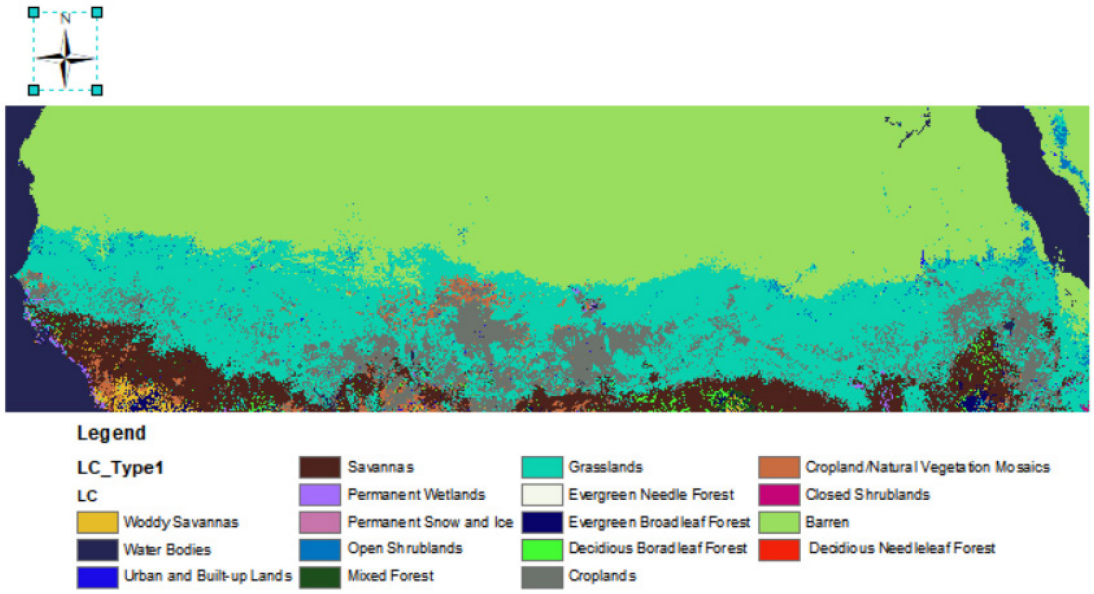

Figure 2.1: MODIS data showing the current land-cover types of the Sahelian region.

Studies proposing that land-use change in the Sahel cause a change in rainfall have dated back to the 1970s, where Charney et al. (1975) proposed that a decrease in plant-cover would lead to a decrease in rainfall based on changing the albedo of the surface inside a simulation study. Comprehensive theoretical frameworks of land-atmosphere interactions that included vegetation feedbacks on the atmosphere and many different processes were presented in the 1990s. Some of these studies focused more on water recycling (Savenije, 1995) and suggested that decreased vegetation would increase the runoff and thus decrease the amount of water that is being recycled and subsequently decrease precipitation. Other studies focused more on the energy balance, planetary boundary layer (PBL) stability, effects on rainfall (te Wierik et al., 2021), and how these effects feed back to the surface water and energy balances which also includes effects on vegetation (Betts et al., 1996; Eltahir, 1998; Pal & Eltahir, 2001). These studies benefitted from the availability of observations, such as the First International Satellite Land Surface Climatology Project (ISLSCP) Field Experiment (FIFE) (P. J. Sellers et al., 1992) and the Boreal Ecosystem Atmosphere Study (BOREAS) (P. Sellers et al., 1995). These studies have shown many important relationships (Figure 2.2), for example on the

radiative feedback loops, which means that wet soils tend to lower the surface albedo, increasing the amount of radiation absorbed by the surface, thus increasing the net radiation at the surface. At the same time, it would lower the Bowen ratio (sensible to latent heat flux), moistening the lower atmosphere. This is however counter-acted by the cloud effects, which then reduce the incoming radiation. Feedback regarding the boundary layer height (PBL height) and moist static energy (MSE) would result in a lower PBL height and an overall increased amount of MSE per unit mass of air within the PBL. It also suggests a theory that wet soils tend to decrease the cloud base height, which should increase the magnitude of convective rainfall. For the above explained mechanisms, we see that there is both a positive feedback loop with the increase in the unit MSE within the PBL, which causes increased rainfall, as well as a potential negative feedback loop, caused by the build-up of clouds, which might decrease the amount of radiation reaching the Earth's surface, thus decreasing the amount of potential energy available for convective activities. With this in mind, we can assume that there may be different locations on Earth under different climate conditions, which may exhibit positive or negative feedback loops on rainfall caused by the same wet soil conditions.

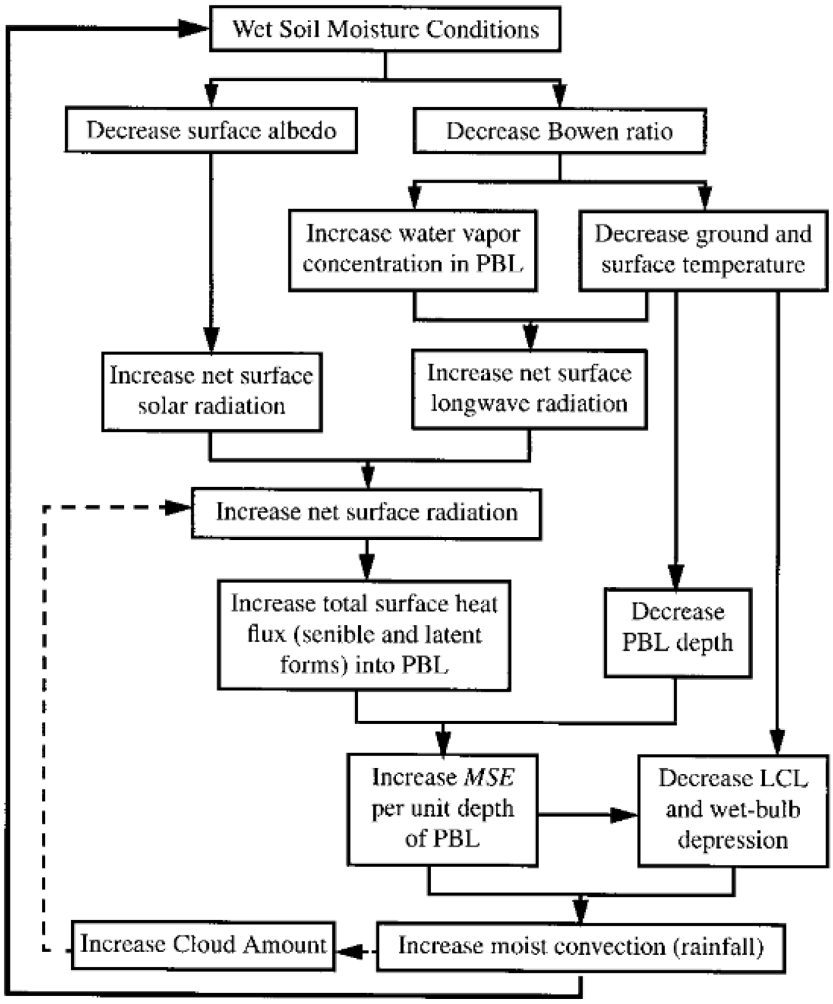

Fig. 2.2: This figure is extracted from Pal & Eltahir (2001) , highlighting the different pathways on how wet soil conditions lead to increased rainfall (positive feedback loops) as well as negative feedback loops.

Findell & Eltahir (2003a) developed a framework with a one-dimensional boundary layer model and using two thermodynamic features of the atmosphere to analyze the soil-moisture – atmospheric boundary layer interactions under different early morning atmospheric conditions. The 2 thermodynamic features observed are the Convective Triggering Potential (CTP) and the Humidity Index (HI_{low}). With this framework, they were able to categorize the United States into different regions of soil-moisture and atmospheric feedback areas using radiosonde data from 89 stations. Different climate

zones that have either positive or negative feedback loops as well as transition zones, and zones that are not controlled by soil-moisture conditions (Figure 2.3). Ferguson & Wood (2011) has expanded this framework with new datasets and tried to expand the classification of land beyond the United States to the whole globe (see Appendix B Figure B 2.1).

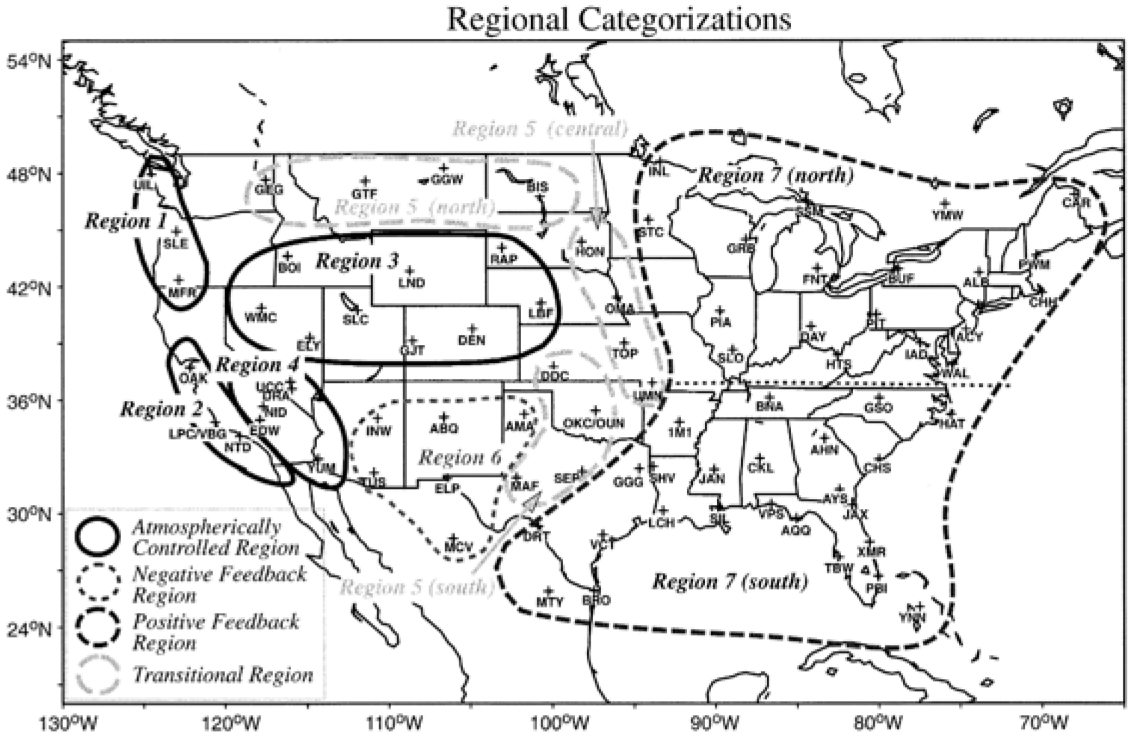

Figure 2.3: Representative regions within the continental United States, based on the CTP-HI_{low} framework. Here region soil-moisture dependent climate regimes are identified for the US. Extracted from Findell & Eltahir (2003b).

More recent studies have benefitted from even better observational and simulation datasets, such as the Global Land Atmosphere Coupling Experiment (GLACE) that have led to discussions on large-scale Soil-Moisture Precipitation (SM-P) feedbacks fand land-atmosphere coupling hotspots (Koster et al., 2004; Santanello et al., 2018). Irrigation and desertification can change the soil moisture and subsequently regional climate due to

land-atmosphere interactions. The effects of soil moisture on the atmosphere can generally be categorized into two different categories of effects: first order and second order effects. The first order effects are local, such as changing of the surface water and energy balances (Adegoke et al., 2003; Alter et al., 2015; Douglas et al., 2009; Im & Eltahir, 2014; Kang & Eltahir, 2019; Qian et al., 2013). Second order effects include land-atmosphere interactions that affect large-scale circulation, sometimes also in remote locations. For example, climate change can warm the land and ocean unevenly, causing anomalous large-scale circulation and remote effects such as rainfall in remote areas (Alter et al., 2015; Entekhabi et al., 1996; Im, Marcella, et al., 2014a; Qian et al., 2020; Tuel & Eltahir, 2020), as well as rainfall downstream of an irrigated area (Im & Eltahir, 2014; Klein & Taylor, 2020; Lu et al., 2017). First-order effects combined with second-order effects can affect rainfall in a region, but also depend on intermediate steps that create an environment that is suitable for rainfall. In the tropics, rainfall is mostly caused by convection and the rising of air parcels due to anomalous heating at the surface due to an ample amount of sunlight. One of the key drivers of rainfall around the tropics is therefore the height of the Lifting Condensation Level (LCL) with regards to the PBL. Generally, irrigation lowers both the PBL and LCL (Alter et al., 2017; Im, Marcella, et al., 2014a; Qian et al., 2013, 2020).

Thermodynamically, irrigation causes an increase in both the Convective Available Potential Energy (CAPE), which increases the likelihood of convective precipitation (Crook, 1996; Pielke Sr., 2001; Z. Yang et al., 2017), and Convective Inhibition (CIN), suppressing initiation of convection (Boucher et al., 2004; Crook, 1996; Sacks et al., 2009). Together, both compete against each other and contribute energy in opposite directions. In the afternoons, however, it is often the case that CIN decreases and the LCL rises, which increases late-afternoon convective initiations (Qian et al., 2020). The potential impacts of land-atmosphere interactions with respect to soil moisture can have significant effects on precipitation either locally or remotely and this in turn can have important consequences for agricultural activities and the livelihoods of people (Im & Eltahir, 2014; Kang & Eltahir, 2019).

2.1 Different Dominating Feedback Mechanisms

Even though we know much about the effects of land-use change on climate on local and larger spatial scales as well as thermodynamic aspects, different studies still show different results. There are generally 2 different views on how soil moisture affects precipitation. One being a positive feedback mechanism, in which soil-moisture increases the amount of subsequent rainfall. This can either be explained through water recycling or through energy considerations such as using MSE (Eltahir, 1998; Eltahir & Bras, 1993; te Wierik et al., 2021). However recent studies have also shown that there exists a negative feedback mechanism for SM-P (Klein & Taylor, 2020; L. Yang, 2018). These studies reason their results through the energy perspective, whereby more sensible heating from the higher surface temperatures can cause the PBL to rise higher and thus cause more precipitation. Some other studies find that both negative and positive feedback exist. In the following, we will look at differences in how studies see the viability of different SM-P mechanisms and, specifically, on the positive and negative feedback loops of soil-moisture and, in extension, land-use changes on local and remote precipitation patterns.

2.2 Positive Feedback

This section looks at studies that have demonstrated positive SM-P feedback.

Kang & Eltahir (2019) detailed the combined relationship of irrigation induced surface cooling, lowering of the PBL and increases of precipitation and specific humidity. The increase in precipitation is due to the interaction with the large-scale circulation above the North China Plain (NCP) as a strong anti-cyclonic circulation interacts with the background regional wind pattern associated with the evolving monsoon circulation along the Taihang mountains. The increases in precipitation and decreases in temperature can be seen in the Figure 2.2.1 (Kang & Eltahir, 2019). We see cooling in the blue areas (Figure 2.2.1(A)) and increases in rainfall in many of the similar areas in the North China Plain (Figure 2.2.1(B)), despite shifted slightly to the south-west. In northern Chongqing, we see both decreases in temperature combined with increases in precipitation, signaling positive SM-P feedback locally.

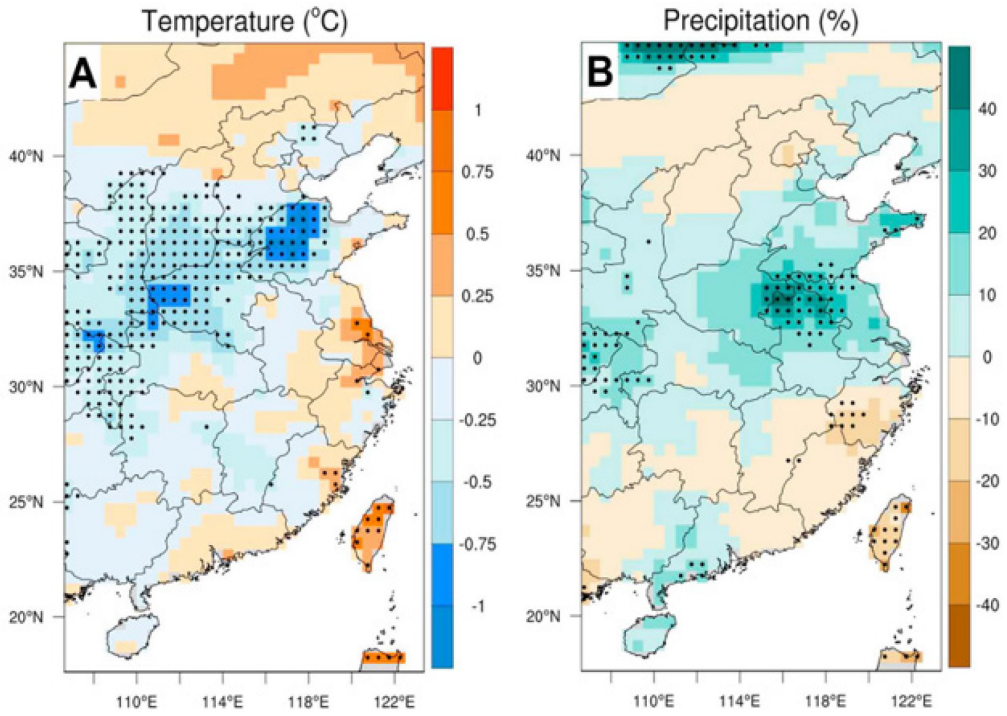

Figure 2.2.1: Figure extracted from Kang & Eltahir (2019). It shows observed spatial changes for surface temperature (A) and precipitation (B) when comparing the difference between before irrigated (1910-1949) and after-irrigated (1970-2009) time periods for the months of May-June-July. The black dots indicate differences that are statistically significant at the 5% Kolmogorov-Smirno test (N=40, p<=0.05).

Using the Granger causality framework, Tuttle & Salvucci (2016) isolates the casual relationship between soil moisture state and the probability of precipitation. They did so by removing the confounding effects of precipitation autocorrelation, low-frequency variability, and atmospheric persistence. Precipitation autocorrelation is removed through a General Linear Model (GLM), which includes both the lagged precipitation and lagged soil moisture. The model also includes a binary indicator variable that determines if there were precipitation days during the previous days. Atmospheric persistence is removed by including lagged pressure data much in the same way. Low-frequency variations, such as seasonal variations in soil-moisture are removed through the inclusion of sinusoids to explain these variables. The results of this purely statistical study based on only

observational data show that there is positive feedback of SM-P on the next-day probability in the western United States (see Figure 2.2.2 below, from Tuttle & Salvucci (2016)). Their results look at two different soil moisture scenarios of dry soils and wet soils based on observations. Wet soils and dry soils are categorized based on being above or below seasonally detrended median soil moisture anomaly. Figure 2.2.2 shows the relative probability of precipitation predicted with a full regression model (including soil moisture) divided by precipitation probabilities predicted without soil moisture. The positive impacts (i.e. impact higher than 1 in wet conditions and lower than 1 in dry conditions) in the west indicate that soil moisture increases the probability of subsequent rainfall. Negative feedback (i.e. impact higher than 1 in dry soil moisture conditions and lower than 1 in wet conditions) dominates the eastern portion of the study area. We have both positive and negative SM-P feedback here.

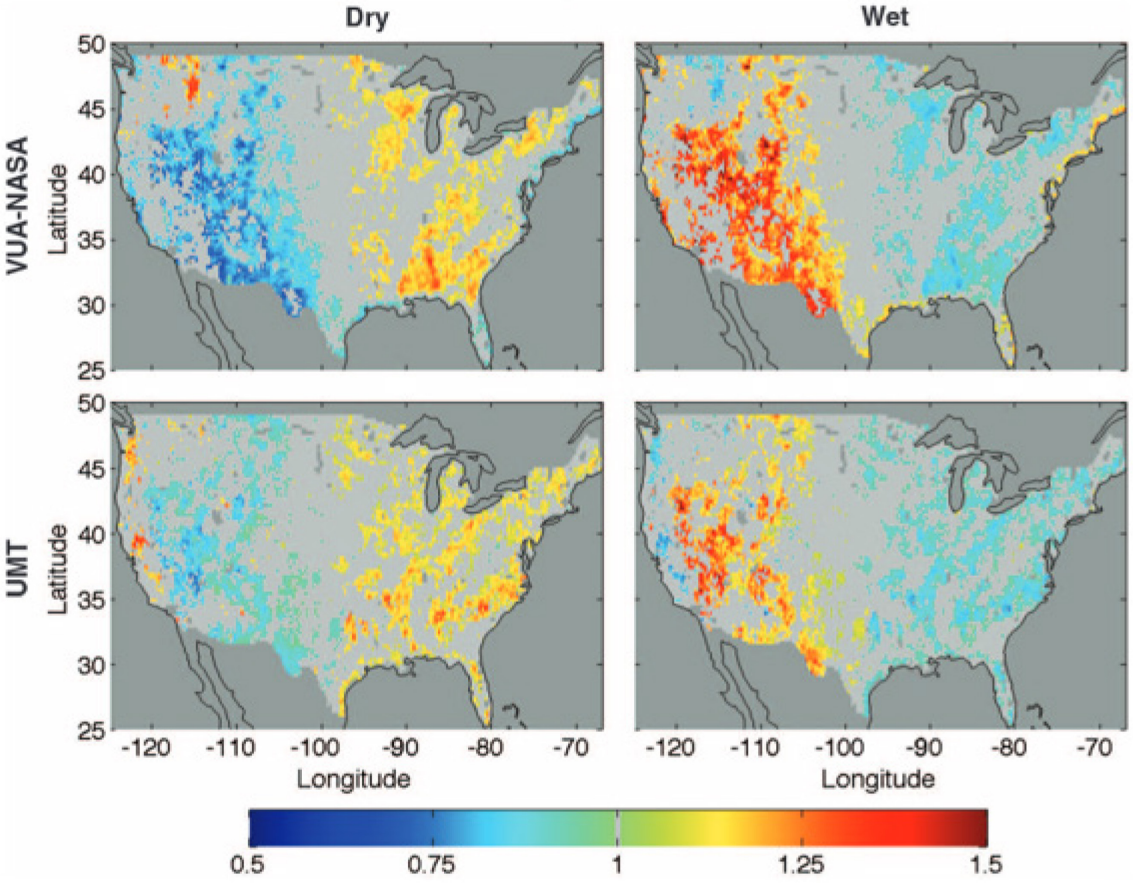

Figure 2.2.2: extracted from Tuttle & Salvucci (2016). This study looks specifically at the impact of soil moisture on next-day precipitation. Here the authors calculate the mean impact of soil moisture on precipitation, calculated as the predicted precipitation probability when soil moisture was included in the regression model divided by the predicted precipitation probability when soil moisture was removed. Blue colors indicate that the inclusion of soil moisture in the model reduced the predicted precipitation probability, while red colors indicate that the probability increased. Light gray areas denote the absence of a statistically significant relationship (alpha = 0.05), and dark gray areas were not tested. Figures on the left show the relative impact below median soil moisture anomaly (dry conditions) and mean relative impact of above median soil moisture anomaly is presented in the right column (wet conditions).

Alter et al. (2015) show through both model simulations and multiple observational validations that rainfall increases remotely (to the east) with irrigation for both July and August as seen in Figure 2.2.3 below. With irrigation, there is also a response in the large-scale circulation (clockwise) and an increase in the amount of water in the nearby Atbara river basin. The mechanism described by Alter et al. (2015) links increase in soil-moisture with the decrease of surface temperature due to evaporative cooling, the development of a clockwise circulation anomaly as well as a high-pressure anomaly over the irrigated area and the interaction with the background winds which causes a convective anomaly thereby resulting in increased precipitation to the east of the irrigated area for both July and August. Increases in specific humidity also results in an environment better suited for rainfall enhancement.

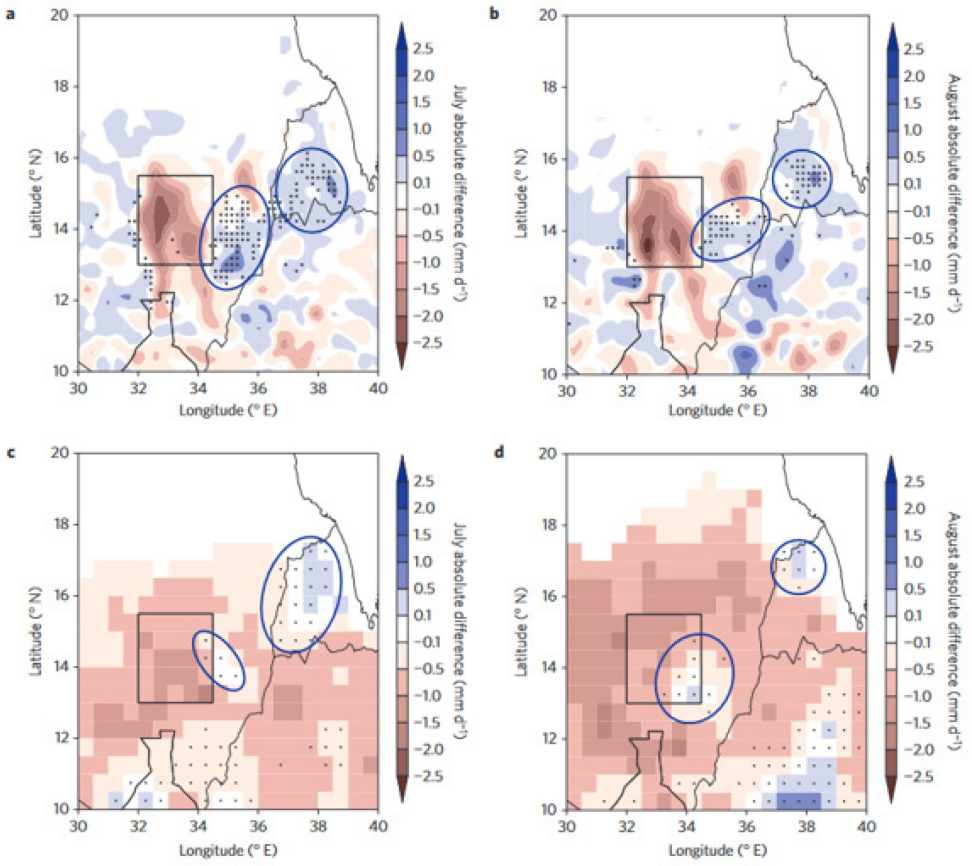

Figure 2.2.3: extracted from Alter et al. (2015). This figure compares the simulated and observed changes in rainfall. a) and b) show absolute differences in ensemble mean

rainfall between irrigation and control simulations for July (a) and August (b). Superimposed dots indicate irrigation-induced rainfall enhancement during at least 70%of the ensemble years. C) and d) show absolute differences in observed rainfall for July (c) and August (d). Superimposed dots indicate grid cells where the value of a rainfall change consistency index >= 80^{th} percentile. Areas with <= 1mm/d in rainfall for the control are masked out to avoid potential inflation due to small amounts.

Yang (2018) shows that there is positive feedback in transitional zones when looking at the soil moisture impact on next-month precipitation (see Figure 2.2.4). Yang (2018) suggests that for negative SM-P feedback to occur, a negative soil moisture - evapotranspiration (SM-E) correlation would be required. In transitional climate zones, i.e. not too wet or dry, SM-E is linear and positive, but this changes when we go to an arid zone, where soil suction is high (water-limited), therefore not necessarily causing a positive correlation between SM-E. For wet soils, E is limited by the potential evapotranspiration (energy-limited).

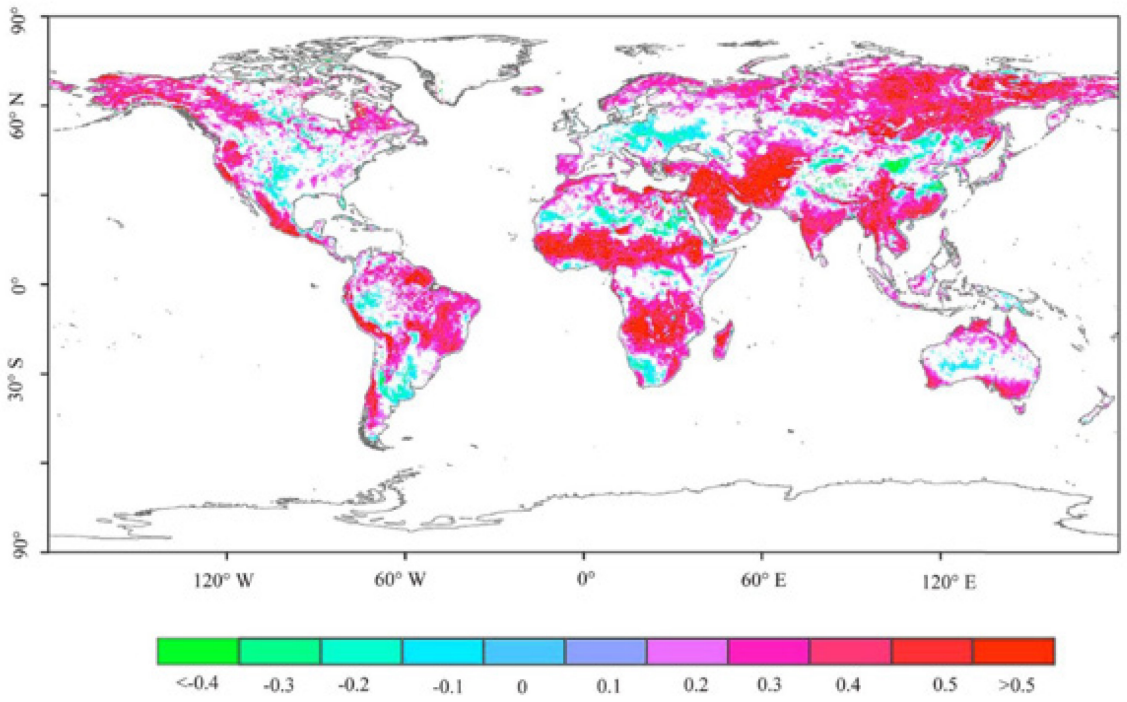

Figure 2.2.4: The correlation between monthly soil moisture and next-month precipitation. We see that most areas on the globe show a positive correlation with regards to SM-P on next-month rainfall and that some mostly transition zones (between wet and dry areas) show negative SM-P feedback. Extracted from Yang (2018).

2.3 Negative Feedback

Here a summary of the results with negative feedback is given. What we learn from the above review, is that many of the studies that showed positive feedback also have areas with negative feedback. Alter et al. (2015) shows, through both model simulations and multiple observational validations, that rainfall decreases locally with irrigation. Yang (2018) shows that there is negative feedback in extremely wet and dry locations (Figure 2.2.4). Tuttle & Salvucci (2016), as mentioned above, shows negative SM-P feedback in the eastern parts of the United States (Figure 2.2.3).

Klein & Taylor (2020) shows with a systematic observational study that mature mesoscale convective systems are positively impacted by dry soils to cause convection remotely on the downstream side of dry patches >= 200km across. This study, in addition to confirming some of the mechanisms of how dry soils increase convection, such as through convergence, increased instability and wind shear, also suggests a specific size that is required to have a significant effect on mesoscale circulations. Even if the mechanism suggested forms negative feedback, it is also stated in the thesis that if we look at a larger zonal length scale, dry patches are causing more convection locally, then more dry and warm land further east, i.e. it is creating areas of stronger rainfall as well as areas of weaker rainfall when compared to the climatology, in a way redistributing the available moisture in the air to cause more extreme events such as floods. This checker style redistribution is continued down the path of the African Easterly Jet.

2.4 Both Feedbacks

After analyzing both studies with positive SM-P feedback and studies with negative SM-P feedback, we find that most of the aforementioned papers present both areas with positive and negative SM-P feedback depending on the climate regime in question and how the local effects interact with larger scale climate characteristics.

Tuttle & Salvucci (2016) and Yang (2018), which both look at the small spatial scales when considering SM-P feedback, show that there are different soil regimes, which favor different feedback mechanisms. Generally, it follows that there are water-limited and energy-limited feedback loops.

2.5 Spatial and Temporal Scales of Feedbacks

We have seen in the previous sections that there are different mechanisms at work to cause a positive or negative feedback between soil-moisture and precipitation, which is also dependent on the geographical location, i.e. orographic features and climate regimes. In this section, we will summarize the information of the studies that have been reviewed into nature of feedback mechanisms, spatial resolutions, feedback scales and time scales.

	Positive effect	Negative effect	Mixed effect	Spatial Resolution**	Affect scale (if applicable)	Effect Scale	Time scale (days)
(Eltahir, 1998)	X			FIFE (15km x 15km)			1
(Findell & Eltahir, 1997)	X			Illinois (~50 x 50km)		State of Illinois	21
(Findell & Eltahir, 2003b)			X	~300 x 300km (point observations)		Contiguous United States	0.5
(Wei & Dirmeyer, 2012)	X			~50 x 50km		Global	
(Klein & Taylor, 2020)		X		3x3km	>= 200 x 200km (arid patches)	mesoscale convective systems	0.5
(Zhou et al., 2019)	X*		X*	~50 x 50km		Global	30
(L. Yang, 2018)			X	25 x 25km		25x25km	30
(Ferguson & Wood, 2011, p.)			X	125 x 125 km		Global	
(Eltahir & Bras, 1993)	X					The Amazons	
(Alter et al., 2015)			X	50 x 50km	~300x 300km (irrigation)	~700x700km	Decades (years)

(Tuttle & Salvucci, 2016)			X	25 x 25km		Contiguous United States	1
(Kang & Eltahir, 2019)	X			50 x 50km	~400 x 400km (NCP irrigation)	Northern China (~1000 x 1000km)	Decades (years)

*This thesis has looked at the correlation between SM and atmospheric aridity expressed in vapor pressure deficit, which is not the same as precipitation.

**Some studies used datasets that had resolutions of 0.5x0.5 degrees. Here they were converted into 50x50km assuming 1 degree = 100km to make different spatial scales more comparable.

Table 2.1: This table compares and contrasts the different studies with regards to their SM-P feedback mechanism (being positive, negative or mixed), the spatial resolution at which SM-P feedback is evaluated, the affect scale (which describes the spatial scale of the initial soil condition of which the effect on precipitation is being studied), the effect scale (the spatial area where there are effects of the examined soil moisture conditions), and feedback time scale (for SM-P).

Our study aims to build upon the conclusions of past studies to provide an additional layer of understanding within the mechanistic pathways from soil moisture to rainfall with the analysis of the changes to PBL and LCL as well as wind patterns associated with rainfall together with the effects of irrigation and desertification in West Africa. The remainder of this thesis is organized as follows: we first discuss the methods, then we look at the results and finally we discuss our results and compare them to other studies in order to reach our conclusion.

3. Methods

3.1 Global and Regional Climate Models

Global Climate Models (GCMs) are a good tool in understanding the physical mechanisms and feedback loops between the ocean, land and atmosphere and have been developed extensively in the past (Figure 3.1.1). As such, they often give credible representations of physical changes on larger continental and global scales (Ceppi et al., 2017; Hamed et al., 2022; Sørland et al., 2018) (Figure 3.1.2). However, they often fall short in capturing the physical mechanisms such as precipitation at smaller scales for local decision makers and other stakeholders to use the information in a meaningful way, as they usually run at resolutions of 2 degrees or larger. This is because certain physical mechanisms such as convection happen at far smaller scales, and running a GCM at those smaller scales would exponentially increase the run time and make the simulations more costly.

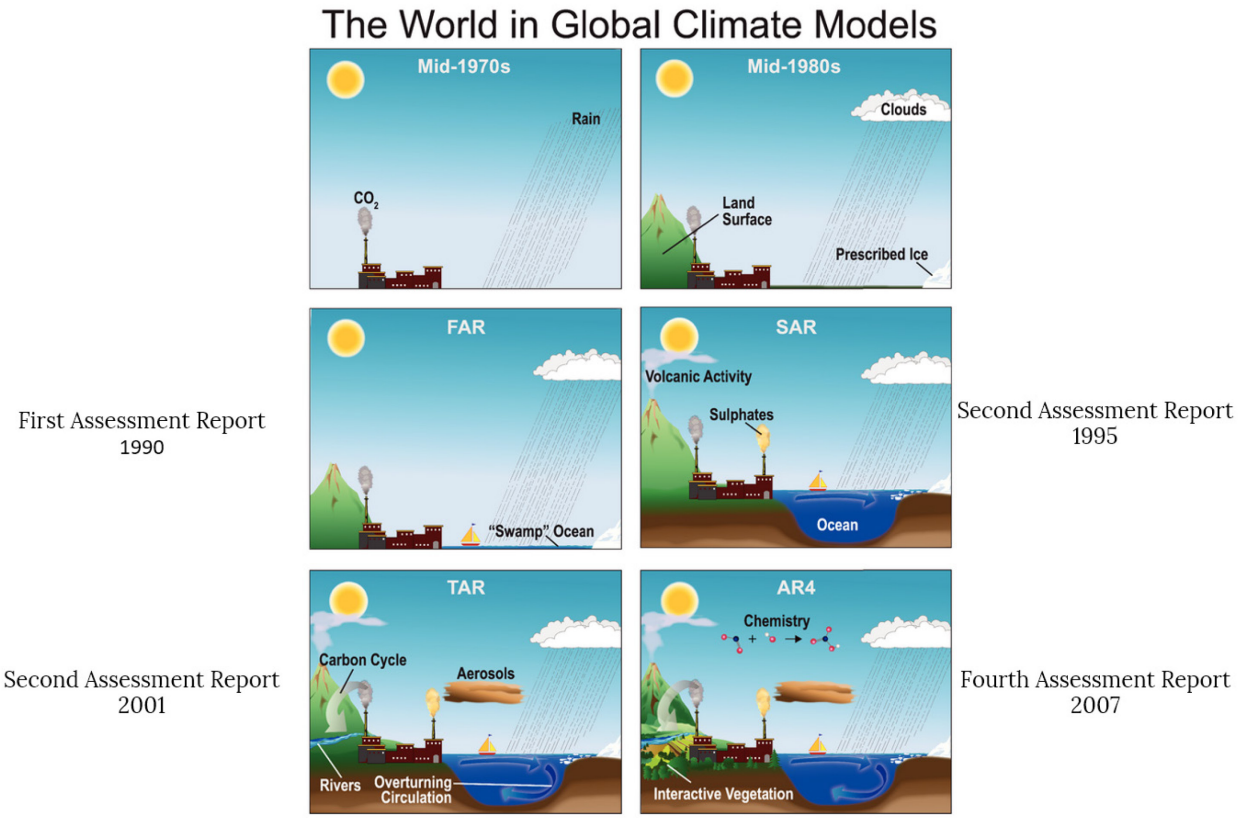

Figure 3.1.1: The continuous development of Global Circulation Models (GCMs) to incorporate more and more climate processes. Graph extracted from IPCC AR4.

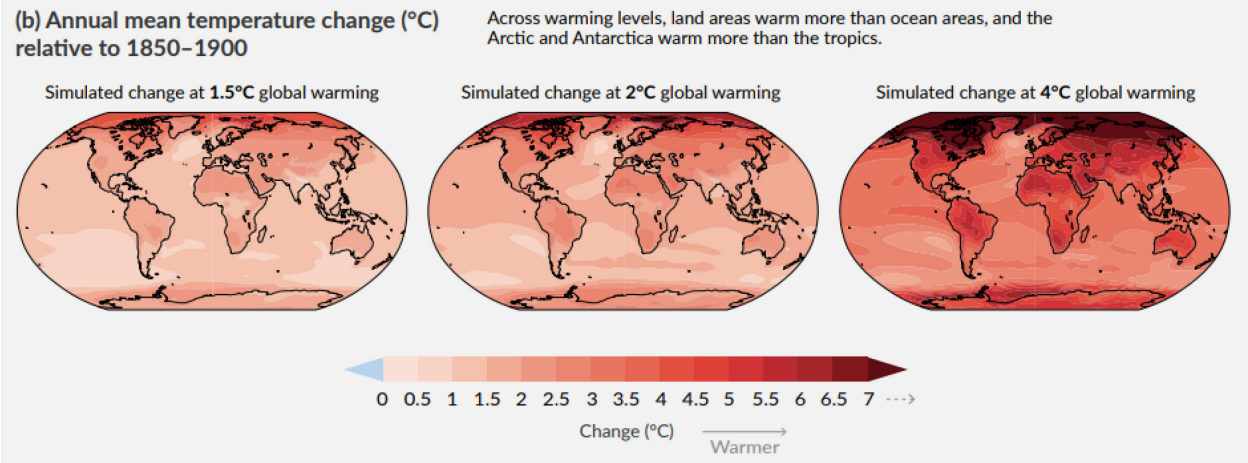

Figure 3.1.2: Changes in global temperature as simulated from GCM ensembles. Graph extracted from IPCC AR6.

For this reason, there is the necessity to downscale GCMs simulations to study local climate feedback loops. One way to study regional climate is to use Regional Climate Models (RCMs). RCMs have the advantage of having finer resolutions, usually in the tens of kilometers, as opposed to hundreds of kilometers for GCMs and are a good tool for representing the smaller scale climate mechanisms without making the running of the models too costly.

3.2 MIT Regional Climate: Model Development

In this study, the MIT Regional Climate Model (MRCM) is used to examine the climatological effects of land-use change within West Africa. MRCM is built upon the Regional Climate Model Version 3 (RegCM3), originally developed by the National Center for Atmospheric Research (NCAR) and maintained by the International Center for Theoretical Physics (ICTP). MRCM retains many of the same structures (Pal et al., 2007), but the Eltahir Research Group has incorporated many modifications over the years to improve the representations of different physical mechanisms. These include an new bare-soil albedo assignment (Marcella, 2012), boundary layer height and boundary layer cloud schemes (Gianotti, 2012), new convective cloud and convective rainfall autoconversion schemes (Gianotti & Eltahir, 2014a, 2014b), and a new irrigation scheme (Marcella & Eltahir, 2014) (Table 3.1). This irrigation scheme has also been implemented over West Africa in the past (Marcella and Eltahir, 2014). Experiments were later performed that validated the accuracy of the model with these updated schemes such as in Im et al., 2014a; Im & Eltahir, 2014b (hereafter referred to as Im14a and Im14b).

Physics	New Features	Key References	
Aerosols & Chemistry	New treatment of lateral boundary for mineral aerosol	Marcella & Eltahir 2010	
	Sub-grid variability of dust emission	Marcella & Eltahir 2011	**Middle East**
Convective Rainfall & Cloud	New convective cloud fraction scheme	Gianotti & Eltahir 2014	
	New convective rainfall autoconversion scheme	Gianotti & Eltahir 2014	**Southeast Asia**
	Modified boundary layer height & boundary layer cloud scheme	Gianotti 2012	
Land Surface	Integrated Biosphere Simulator (IBIS) Land Surface Scheme	Winter et al. 2009	**United States**
	New surface albedo assignment	Marcella & Eltahir 2012	
	New irrigation module	Marcella & Eltahir 2014 Im & Eltahir 2014	**West Africa**

Table 3.1: Table courtesy of Yeonwoo Choi. Table summarizing the improvements of MRCM over the years as well as the study regions they were implemented in on the right-hand side.

Previous work on MRCM simulations has successfully simulated regional climate in West Africa, especially for the monsoon months (Im, Marcella, et al., 2014a; Im & Eltahir, 2014). The version of MRCM used for these simulations has been shown to be highly accurate for simulating monthly rainfall in the Sahel region. It uses the IBIS land-surface scheme combined with the Modified Emmanuel convection scheme (2013, related information accessible on eltahir.mit.edu/conferences). Given these validations, we adopt the same MRCM versions as in Im14a and Im14b to conduct our study on the impact of potential large-scale irrigation and desertification on the WAM and regional rainfall.

In this study, all experiments are run on a 30-year period between 1982 and 2012. The initial and boundary conditions are specified by ERA-Interim, a reanalysis product produced by the European Centre for Medium-Range Weather Forecasts (ECMWF) with a resolution of 1.5 x 1.5 degrees at a 6 hourly interval (Uppala et al., 2008). The sea surface temperatures are given by the National Oceanic and Atmospheric Administration

(NOAA) Optimum Interpolation data (NOAA OI) with a horizontal resolution of 1 x 1 degrees and weekly resolution. [1]

Furthermore, gridded irrigation data from the year 2005 were used in MRCM from the Historical Irrigation Dataset (HID 2005) (S. Siebert et al., 2015) to define the land-use types. Herein, a grid cell is designated as "irrigated cropland" if irrigation covered at least 25% of the total grid cell area. "Irrigated cropland" grid cells are treated/irrigated such that soil moisture in the root zone (top 1 m of the soil) reaches 75% of relative field capacity (field capacity divided by the porosity of a soil layer). At this point, water is added until the root zone reaches soil saturation, which is assumed to be relative field capacity (Marcella & Eltahir, 2014). This irrigation procedure is repeated as necessary for both control (CONT) and sensitivity (EXP) experiments across 30 years from June to August. Compared to irrigation schemes that continuously saturate the root zone, this procedure allows for a more demand-based irrigation system that maintains more realistic levels of soil moisture over irrigated cropland.

3.3 Experimental Design

The model domain and land-use map are shown in Figure 3.4. The whole experimental domain covers West Africa, parts of the Atlantic Ocean and the Mediterranean and is

[1] More detailed model description and general performance of MRCM can be found in previous studies of MRCM simulations over West Africa (Im, et al., 2014; Im, et al., 2014a; Im & Eltahir, 2014; Marcella & Eltahir, 2014).

centered at 3W and 15N with a 50 km horizontal resolution (130 grid points zonally and 114 grid points meridionally). Vertically, the model assumes 18 sigma levels that start at the surface and go up to the 50 hPa level in the atmosphere. The size of the domain was chosen to not have orographic features such as the highlands of Guinea. The assumed boundary conditions affect the model performance on the boundaries of the experiment. Experiments are set up on a 30-year time scale, which should be sufficient in capturing the climatology of a region. This is in contrast with Im14a and Im14b, where the studies span 20 years.

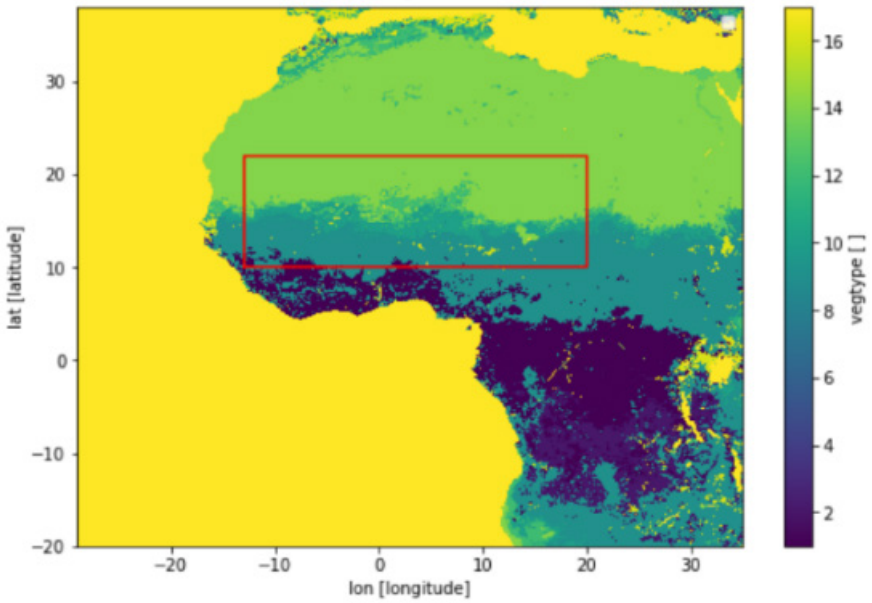

Figure 3.3: Experiment Domain with different land-use types represented by different colors. Land-use types taken from S. Siebert et al. (2015). The red box is the irrigation area between 10-22 N. The graph shows the naturally existing land-use types. The graph in the right with the green color extending to the south is the desert experiment that changes all of the land in northern West Africa into a desert. The different colors represent the different land-use types. The list includes 17 land-use types with 13 being “irrigated cropland” and 14 being “desert”. The complete list from 1-17 is as follows: "tropical evergreen forest","tropical decidduous forest","temperate evergreen broadleaf forest","temperatre evergreen conifer forest","temperate deciduous forest","boreal

evergreen forest","boreal deciduous forest","mixed forest","savanna","grassland","dense shrubland","open shrubland","irrigated crop","desert","polar desert","cropland", and "ocean/water".

3.4 List of Simulations Conducted

As the aim of this study is to understand the effects of land-use change on rainfall patterns in the West Africa, experiments with land-use type changed to irrigated farmland on a large and small scale as well as land-use type changed to desert at different scales were performed. The considerations for these sensitivity experiments are to see if Irrigation on a large scale, as well as on a smaller scale might change the WAM in different ways, to allow rainfall to move further north or increase in magnitude in remote locations. This is because the larger scale irrigation effects are likely not realistic due to the large amount of water required in such scenarios. The smaller scale irrigation is done in 2 ways, first through partial irrigation by the creation of irrigated patches, and secondly by only irrigating a thinner strip of area in the south closer to the tropics. On top of that, we also use scheduling to further minimize water-use of the experiments. This is done by only irrigating in the first week in each month following the irrigation scheme developed previously (Marcella & Eltahir, 2014). The desert experiment is set up to see how rainfall patterns would change in a theoretical desert environment as well as to assess the influence of currently existing vegetation on rainfall and atmospheric characteristics.

There are 2 sets of simulations in this study. One set includes simulations that were conducted with model output at 6-hourly intervals and another that were conducted with output at 3-hourly intervals. Those conducted at 6-hour intervals produced simulation results at 00:00, 06:00, 12:00, 18:00 each day, while the second set of simulations at 3-hour intervals produced results at 00:00, 03:00, 06:00, 09:00, 12:00, 15:00, 18:00, 21:00.

The different 6-hourly simulations were conducted with different irrigation levels, for a total of 10 simulations. These 10 simulations are as follows:

1. no irrigation, control experiment which does not change the land-use type,
2. desertification,
3. 22% desertification of the landscape,
4. 15% of land irrigated,
5. 22% of the land being irrigated,
6. 22% of land being irrigated with larger patch-size,
7. 30% of the land irrigated,
8. 50% of the land irrigated,
9. 100% of the land irrigated,
10. 100% of the land irrigated in a larger area to the coast.

All the above simulations were done with land use specifications as above for the area defined by latitudes between 10 – 22N, 14W – 20E (10W – 20E for the 100% irrigated simulation, and also a simulation that simulates 100% irrigation up until the African coastline in the west) and using the initial and boundary conditions as mentioned in the section 3.2 of this chapter. This latitude zone was chosen based on the results of previous studies that have indicated that this area has a larger effect on increasing rainfall and thus water recycling in the area. There is also one simulation with the latitude of the irrigated zone shifted 5 degrees to the south to 5 – 17N. This simulation was done in order to see if the southward shift of the irrigation zone can have a large effect on climate patterns.

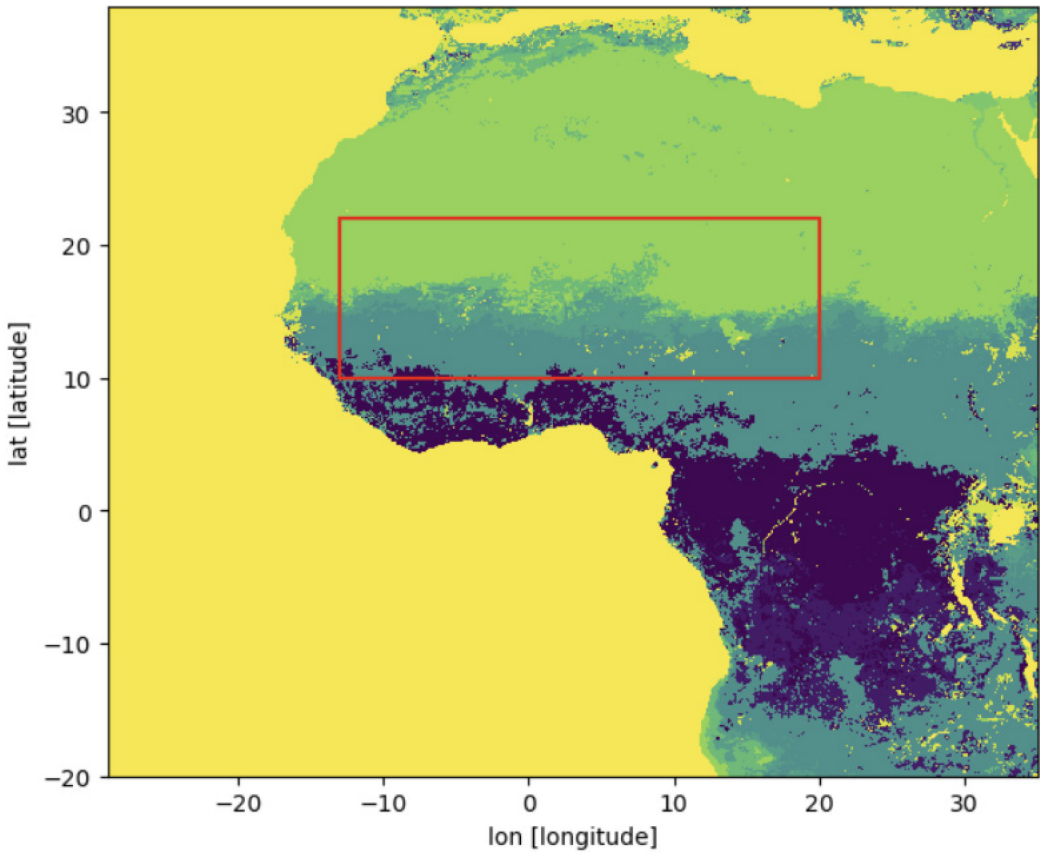

Figure 3.4.1: The entire domain in the graph is the simulation domain. Simulation 1 for 3-hourly and 6-hourly output simulations both use the original land-use types as seen in the above graph. The red box indicates the location of land-use change, where original land-use is changed to be irrigated farmland or desert according to the simulations 2-8, as well as with simulations 1 & 3 for the 3-hourly output simulations.

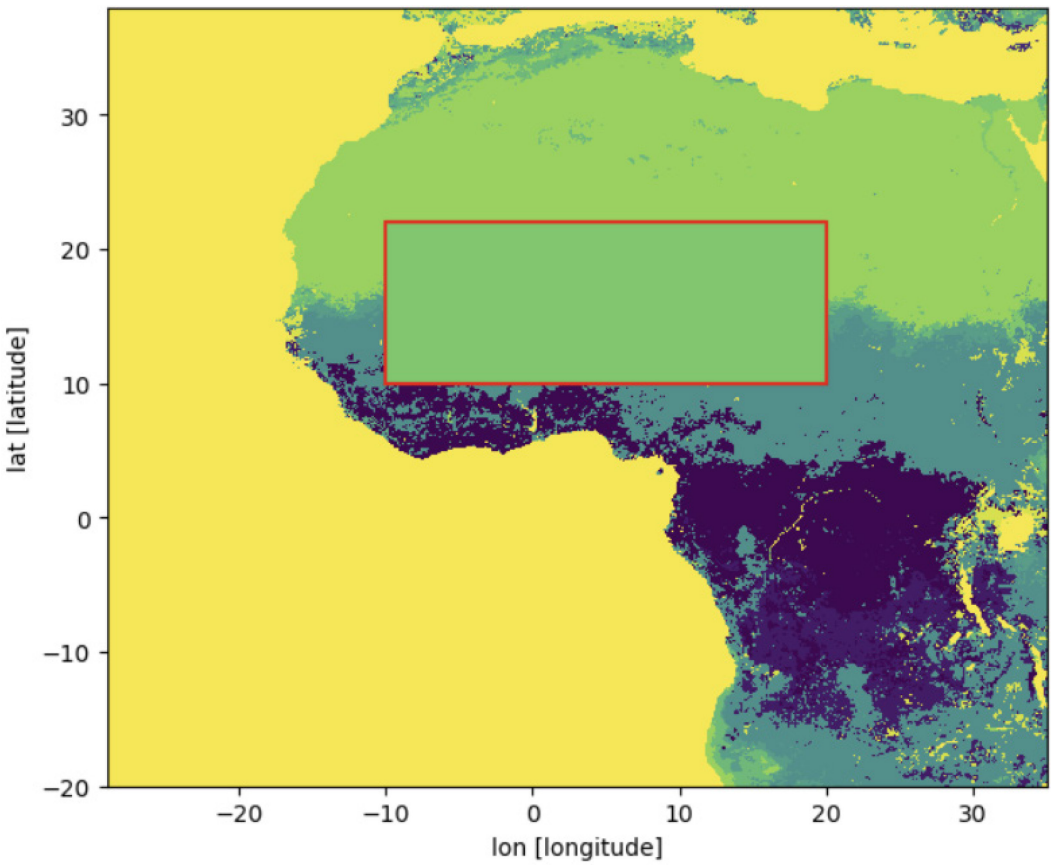

Figure 3.4.2: The entire domain in the graph is the simulation domain. The red box indicates the location of land-use change, where original land-use is changed to be irrigated farmland according to simulation 9.

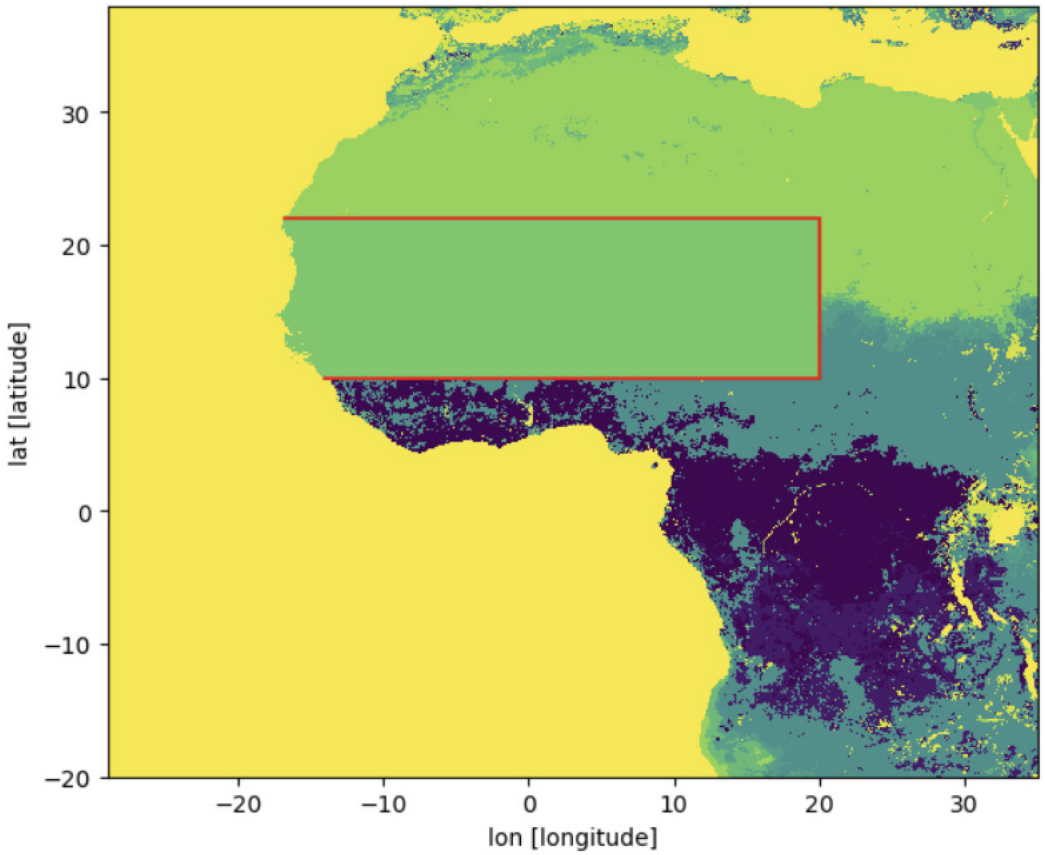

Figure 3.4.3: The entire domain in the graph is the simulation domain. The red box indicates the location of land-use change, where original land-use is changed to be irrigated farmland according to simulation 10.

Apart from 6-hourly output simulations, there were also experiments with 3-hourly output intervals which were conducted to better analyze afternoon 15:00 atmospheric conditions. These simulations include different land-use type setups, for a total of 4 simulations. These 4 simulations are as follows:

1. control experiment,
2. desertification, land-use has changed to be a desert land-use type for an extended area of West Africa,
3. 100% irrigation,
4. 100% irrigation in a slimmer latitudinal band in the south.

The domains are the same as the simulations for 6-hourly output experiments. In addition, there were also experiments conducted in a different geographical location (10 – 14N), which is a slimmer band in the south which would be more realistic in terms of the water distribution infrastructure and availability in West Africa. Here the same simulations of control, desertification and 100% irrigation are conducted.

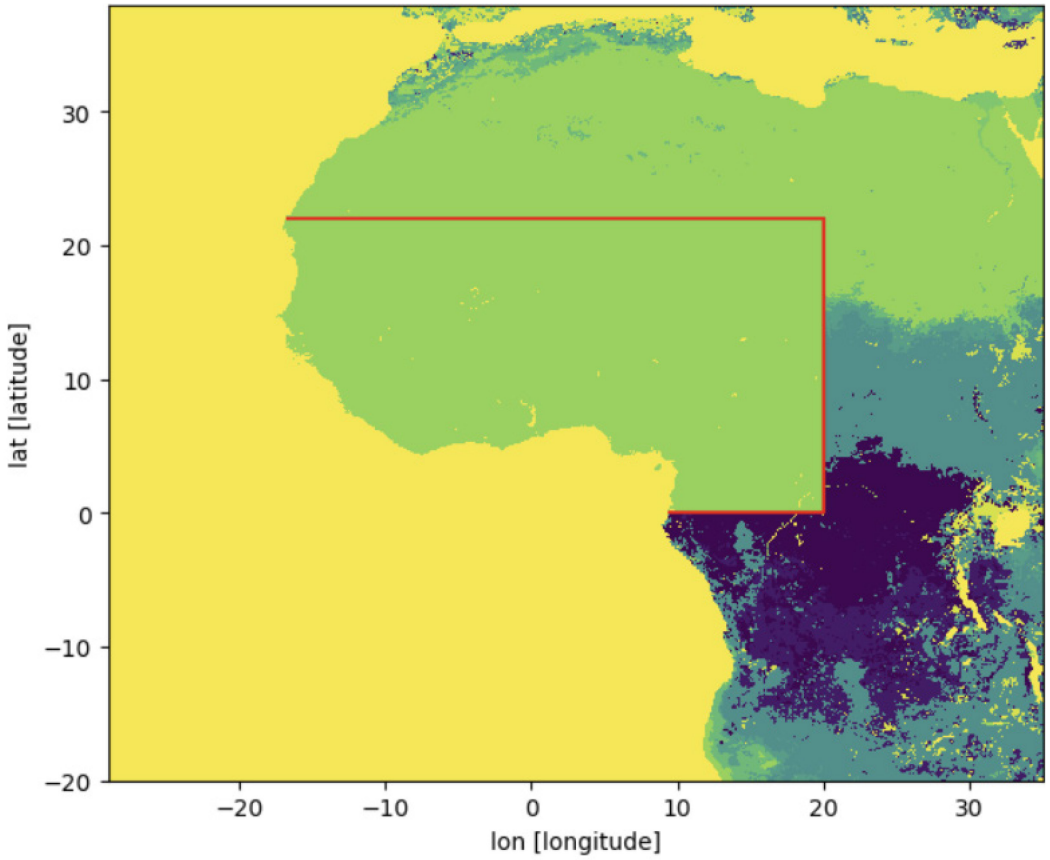

Figure 3.4.4: The entire domain in the graph is the simulation domain. The red box indicates the location of land-use change, where original land-use is changed to be desert according to simulation 2 of the 3-hourly simulation.

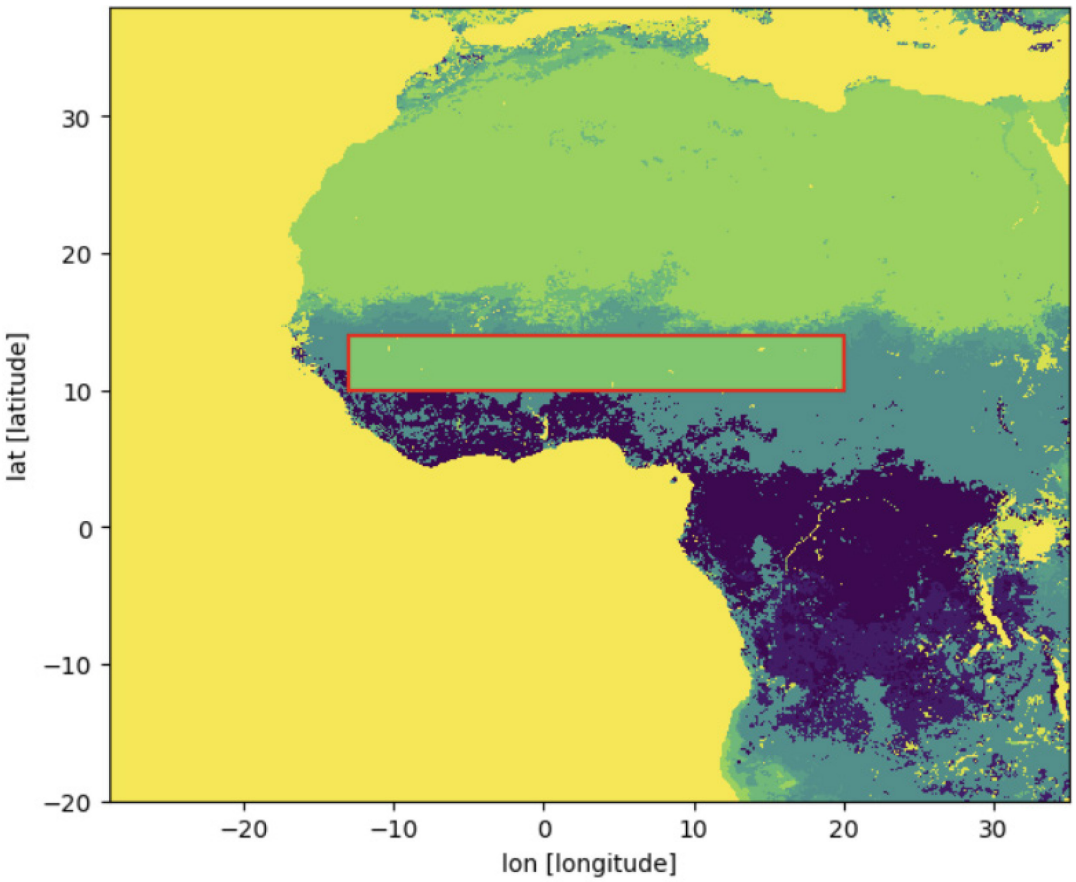

Figure 3.4.5: The entire domain in the graph is the simulation domain. The red box indicates the location of land-use change, where original land-use is changed to be irrigated farmland according to simulation 4 of the 3-hourly simulation.

4. Results

We examine May-September monthly averages of precipitation, evapotranspiration, wind, surface temperature and atmospheric characteristics including Planetary Boundary Layer (PBL) height and Lifting Condensation Level (LCL) height from 31-year (1982-2012) sensitivity experiments listed in section 3.4 (in total of 14 simulations). The region of interest is West Africa (see Figure 3.4.1), and we ultimately want to better understand the effects of land-use change on precipitation as well as other atmospheric variables which are important in controlling intermediate processes that lead to the specific precipitation changes.

4.1 Change in Precipitation (for Experiments with Model Output at 6-hourly Intervals)

For Precipitation change, we look at simulation results showing the difference between the land-use change induced precipitation and the control simulations where we do not

change land-use types. We see a relative increase in precipitation south and south-west of the irrigated area as well as a decrease in precipitation to the north and north-east of this area with increased precipitation. These changes in precipitation can be attributed to a local land-atmosphere coupling effect which reduces land-surface temperatures, reduces the convective available potential energy (CAPE) and ultimately leads to less precipitation as well as the change in wind patterns that alter the large-scale transport of moisture further north. The local land-atmosphere coupling mechanism in reducing local rainfall has been observed in many previous papers (Alter et al., 2015; Im, Marcella, et al., 2014b).

The specific results of seasonal rainfall (May-September) under the different experimental setups (from desertification to irrigation) are now presented below in a series of figures (4.1.1 – 4.1.8) together with their land-use type changes. All of the simulations have the same color scale for the change in rainfall amounts when we subtract the control simulation rainfall amounts from those of the perturbed land-use simulation. The changes in precipitation vary between a decrease of 2 mm/day to an increase of 2.5 mm/day. The results presented here also average the rainfall changes between the months of May through September. The white areas inside the graphs are areas where rainfall changes are beyond or below the previously mentioned [-2.5, 2] mm/day range.

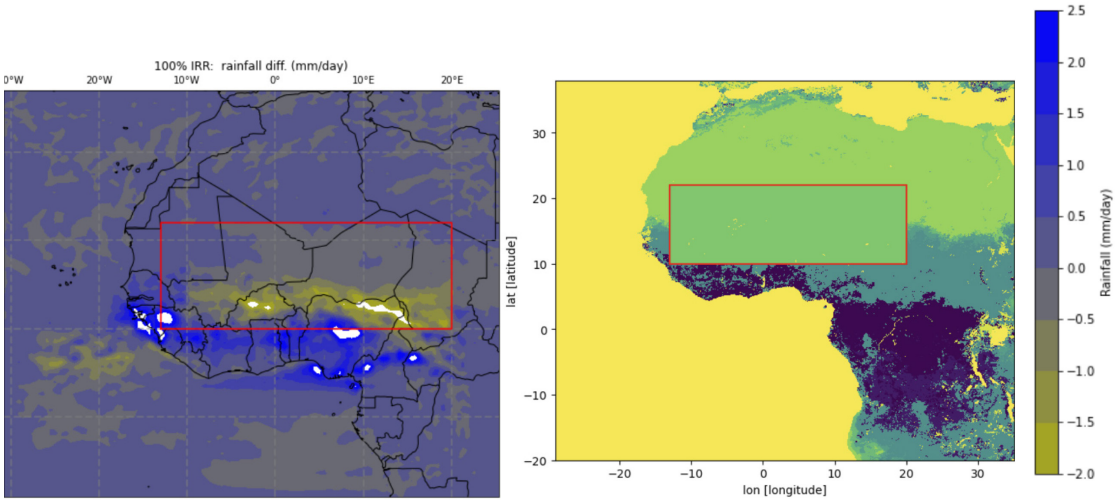

Figure 4.1.1: (Left) Seasonal (May-September) precipitation anomalies (simulation with a change of the land-use type minus the control simulation) with 100% of the lands in the red box indicates the area in which the land-use type has changed, from the original land-use type entirely into the irrigated cropland land-use type. (Right) Land-use type distribution showing the altered land-use type distribution from the original land-use types shown in Figure 3.3.

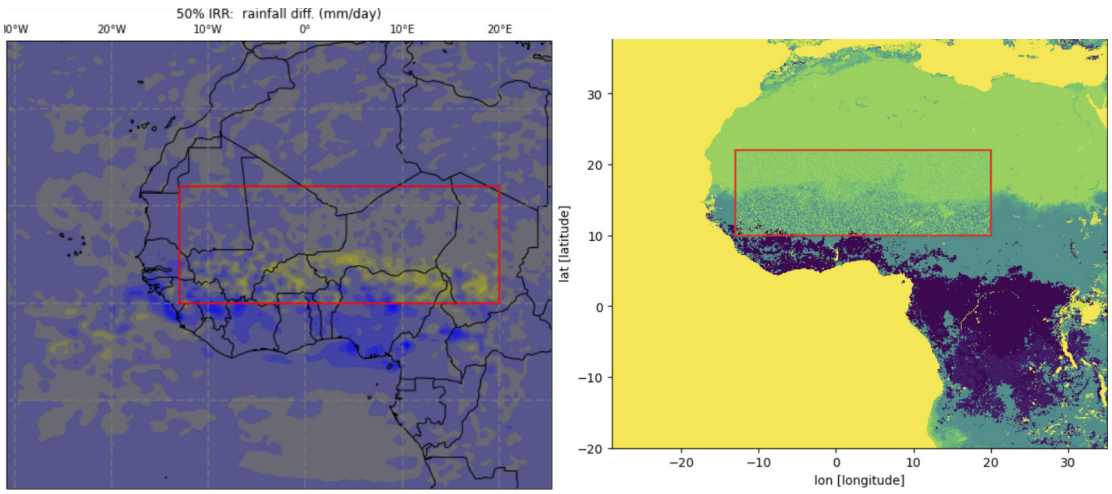

Figure 4.1.2: (Left) Seasonal (May-September) precipitation anomalies (simulation with a change of the land-use type minus the control simulation) with 50% of the lands in the red box indicates the area in which the land-use type has changed (randomly), from the original land-use type into the irrigated cropland land-use type. (Right) Land-use type

distribution showing the altered land-use type distribution from the original land-use types shown in Figure 3.3.

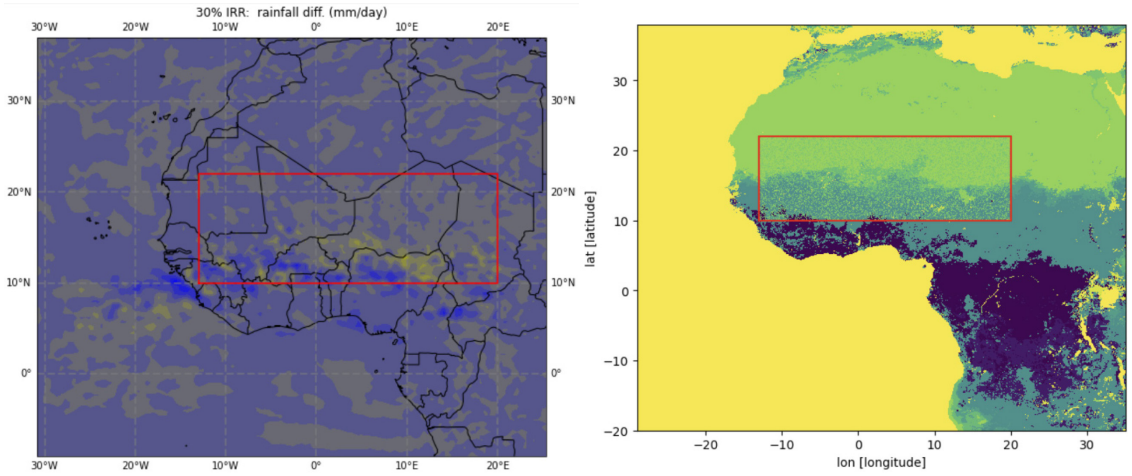

Figure 4.1.3: (Left) Seasonal (May-September) precipitation anomalies (simulation with a change of the land-use type minus the control simulation) with 30% of the lands in the red box indicates the area in which the land-use type has changed (randomly), from the original land-use type into the irrigated cropland land-use type. (Right) Land-use type distribution showing the altered land-use type distribution from the original land-use types shown in Figure 3.3.

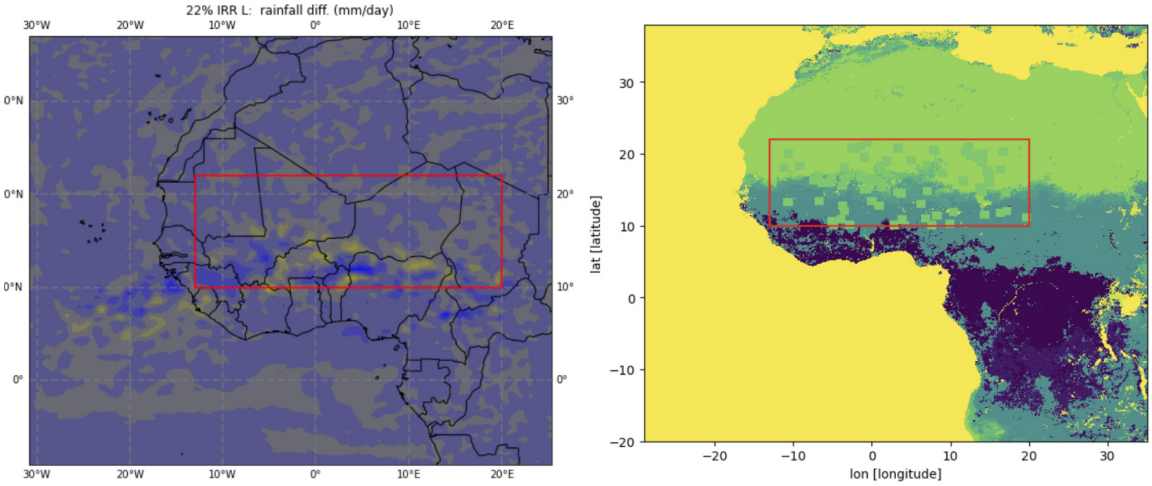

Figure 4.1.4: (Left) Seasonal (May-September) precipitation anomalies (simulation with a change of the land-use type minus the control simulation) with 22% of the lands in the red box indicates the area in which the land-use type has changed (randomly as large

patches; roughly 200km^2 each), from the original land-use type into the irrigated cropland land-use type. (Right) Land-use type distribution showing the altered land-use type distribution from the original land-use types shown in Figure 3.3.

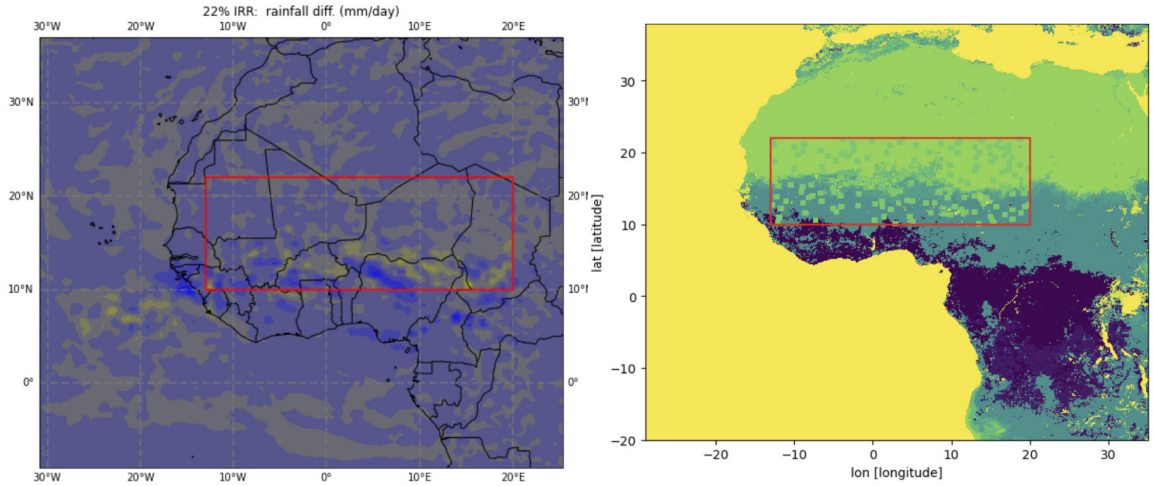

Figure 4.1.5: (Left) Seasonal (May-September) precipitation anomalies (simulation with a change of the land-use type minus the control simulation) with 22% of the lands in the red box indicates the area in which the land-use type has changed (randomly, this time smaller patches roughly 100km^2 each in size), from the original land-use type into the irrigated cropland land-use type. (Right) Land-use type distribution showing the altered land-use type distribution from the original land-use types shown in Figure 3.3.

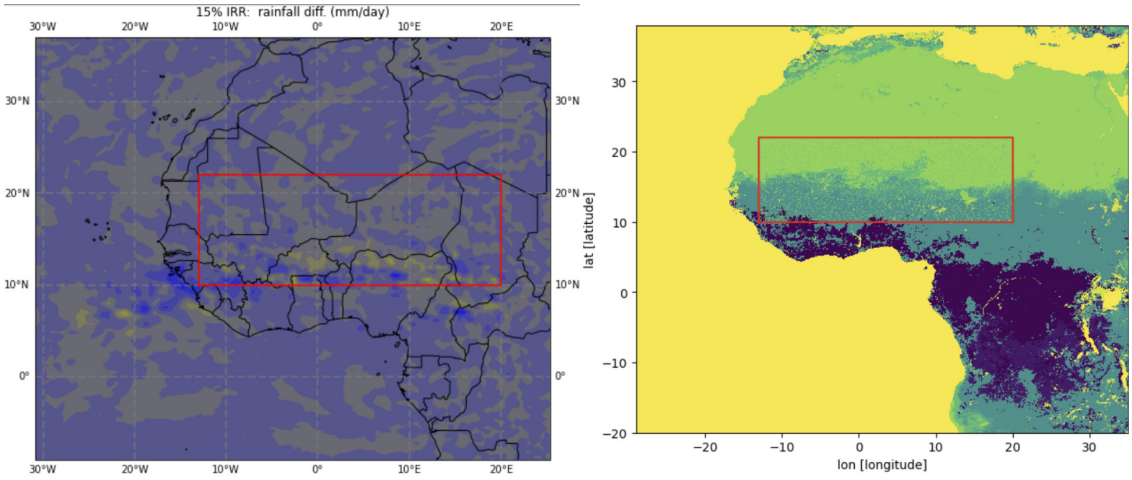

Figure 4.1.6: (Left) Seasonal (May-September) precipitation anomalies (simulation with a change of the land-use type minus the control simulation) with 15% of the lands in the red box indicates the area in which the land-use type has changed (randomly), from the original land-use type into the irrigated cropland land-use type. (Right) Land-use type distribution showing the altered land-use type distribution from the original land-use types shown in Figure 3.3.

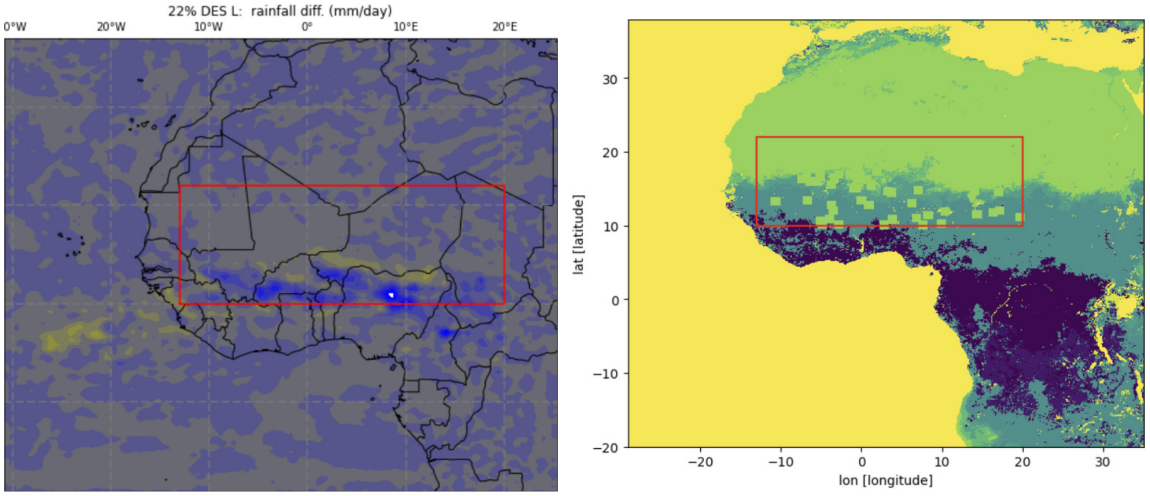

Figure 4.1.7: (Left) Seasonal (May-September) precipitation anomalies (simulation with a change of the land-use type minus the control simulation) with 22% of the lands in the red box indicates the area in which the land-use type has changed (randomly), from the original land-use type into the desert land-use type. (Right) Land-use type distribution showing the altered land-use type distribution from the original land-use types shown in Figure 3.3.

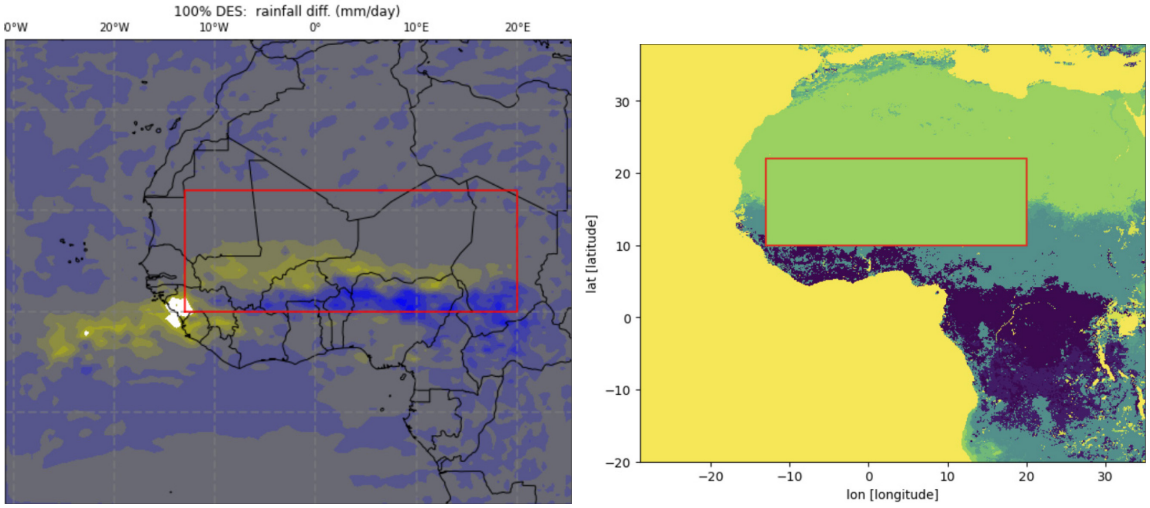

Figure 4.1.8: (Left) Seasonal (May-September) precipitation anomalies (simulation with a change of the land-use type minus the control simulation) with 100% of the lands in the red box indicates the area in which the land-use type has changed (randomly), from the original land-use type into the desert land-use type. (Right) Land-use type distribution showing the altered land-use type distribution from the original land-use types shown in Figure 3.3.

What we see here (Figures 4.1.1 - 4.1.8) is a change in rainfall patterns with land-use change. Specifically, we see an increase in precipitation to the south and south-east of the desertification area, while at the same time we see a decrease in precipitation to the north and north-west (Figure 4.1.8). For the case with just a slight desertification (Figure 4.1.7), we see that there is mostly an increase in precipitation in the southern areas of the land-use change box, which is also the area where most of the land-use type is changed from its original type to the desert land-use type. For irrigated conditions, the general trend is that we see an increase in precipitation at the southern and south-eastern edge and see a decrease to the north-east of the area with increased precipitation (Figure 4.1.1 & Figure 4.1.2). For experiments, where we only irrigate a part of the designated red box (Figure 4.1.3, Figure 4.1.4, Figure 4.1.5, Figure 4.1.6), we consistently see the increase in precipitation along the coast of Guinea as well as along the southern edge of the red box.

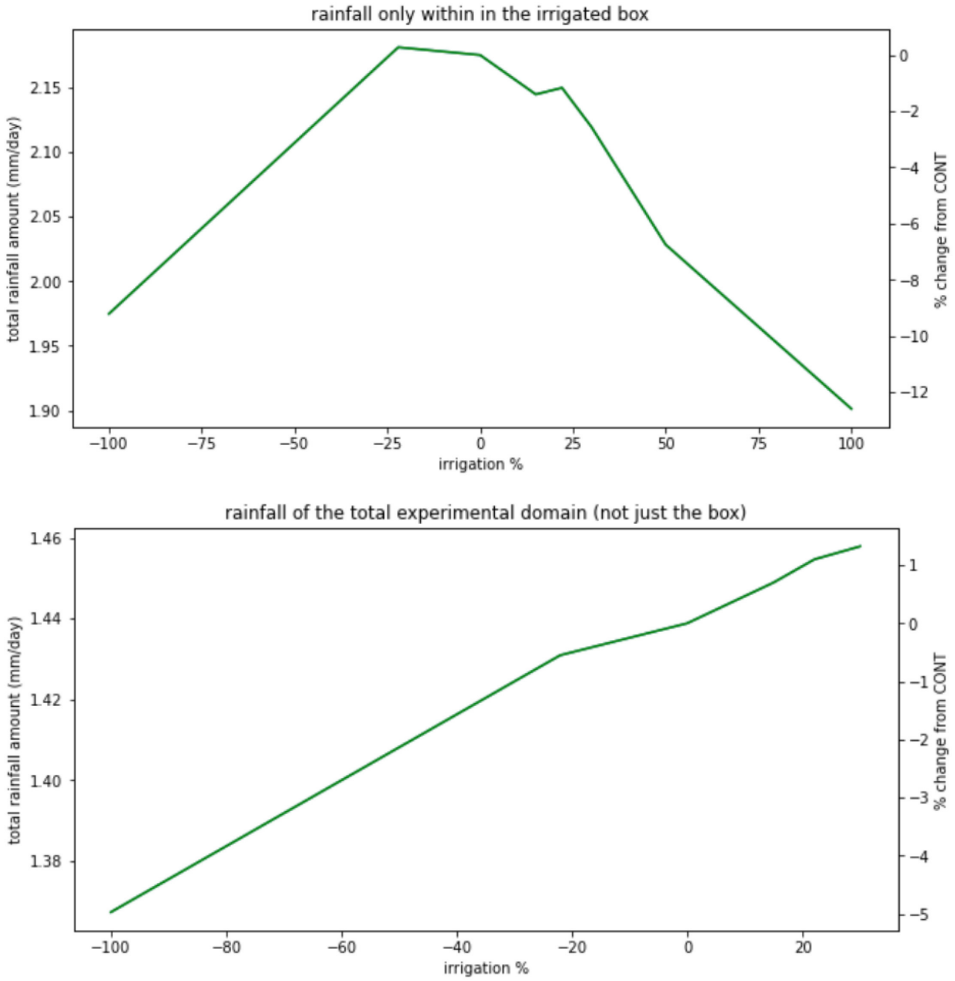

Figure 4.1.9: The overall percentage change in seasonal (May-September) rainfall only within the red box (above figure) where we altered the land-use types and within the entire experimental domain (below figure). Percentages on the x-axis signify the amount of land within the red box that is either altered to be desert (negative percentages) or irrigated cropland (positive percentages) with 0% being the control simulation.

In Figure 4.1.9 (top), we see that the precipitation amount within the red box peaks with experiments where we have a small amount of desertification of roughly 22% being randomly selected to be the desert land-use type inside the red box (Figure 4.1.7) while the smaller perturbations generally produce the most amount of rainfall within the red box. Figure 4.1.9 (bottom) shows the overall change in precipitation within the entire domain increases the more irrigation we add to the experiments. This should be taken with caution, as while we irrigate the lands, much of the extra rainfall falls into the

Atlantic Ocean, and vice versa for the experiments involving changing the land-use types to deserts.

4.2 Change in Evapotranspiration (for Experiments with Model Output at 6-hourly Intervals)

For evapotranspiration change, we look at results showing the difference between the land-use change induced evapotranspiration and the control simulation, where we do not change land-use types. As land-use type is changed from the original land-use type to irrigated farmland (desert) in certain areas, the evapotranspiration increases (decreases) in those areas. Changes are most significant for areas with low rainfall and evapotranspiration originally, depicted by the bright red color, which signifies ~3mm/day increase in evapotranspiration for north/north-eastern areas of the irrigated area (see Figure 4.2.1). Changes in the south are far more gradual, due to the existing wetter soil conditions and the lesser marginal increase in evapotranspiration with irrigation. For desertification, as seen in the first graph, we have a slight decrease in evapotranspiration mostly in the south.

These changes are consistent with other variables. For relative humidity, it increases (decreases) with increasing (decreasing) amounts of irrigated agricultural land in West Africa which are not presented here (see Appendix B Figure B 4.1 – 4.3). For anemom temperature, it decreases (increases) with increasing (decreasing) the irrigated farmland land-use type.

a,b)

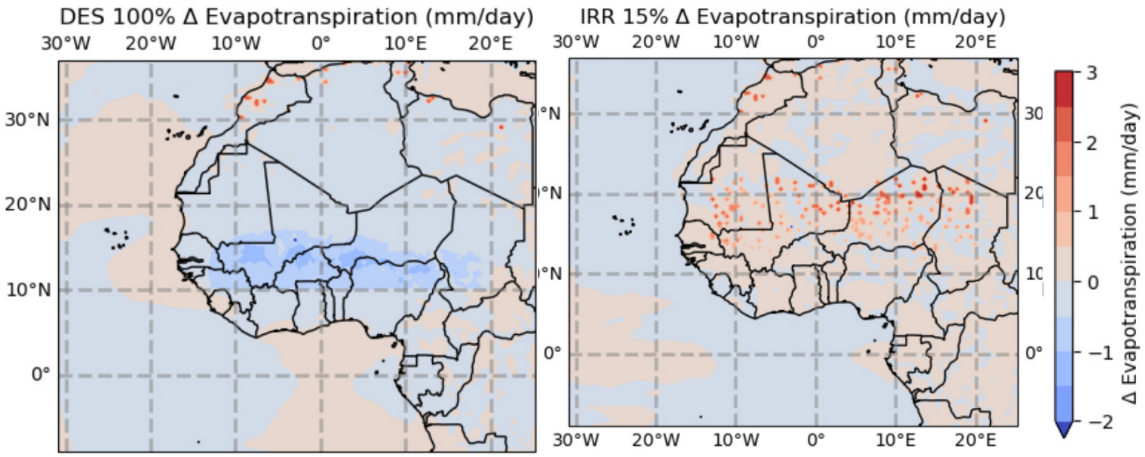
DES 100% Δ Evapotranspiration (mm/day)
IRR 15% Δ Evapotranspiration (mm/day)
30°W
20°W
10°W
0°
10°E
20°E
30°N
20°N
10°N
0°
3
2
1
0
−1
−2
Δ Evapotranspiration (mm/day)

c,d)

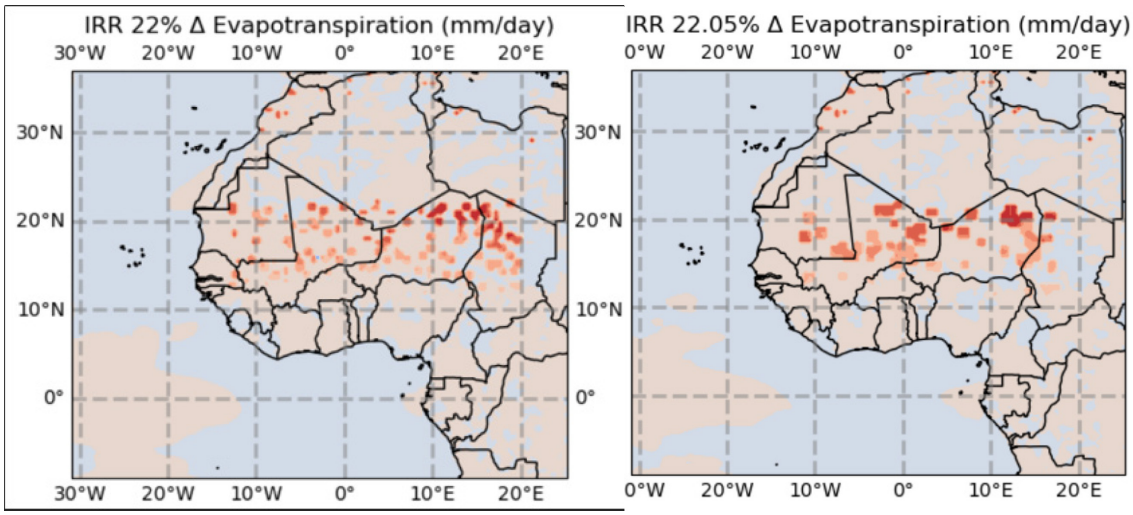
IRR 22% Δ Evapotranspiration (mm/day)
IRR 22.05% Δ Evapotranspiration (mm/day)
30°W
20°W
10°W
0°
10°E
20°E
0°W
30°N
20°N
10°N
0°

e,f)

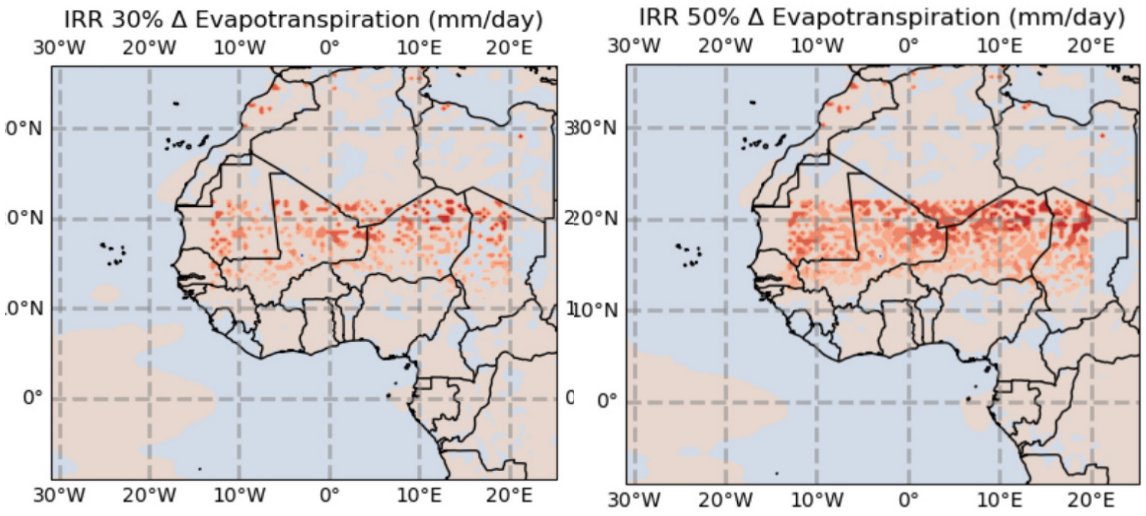

g,h)

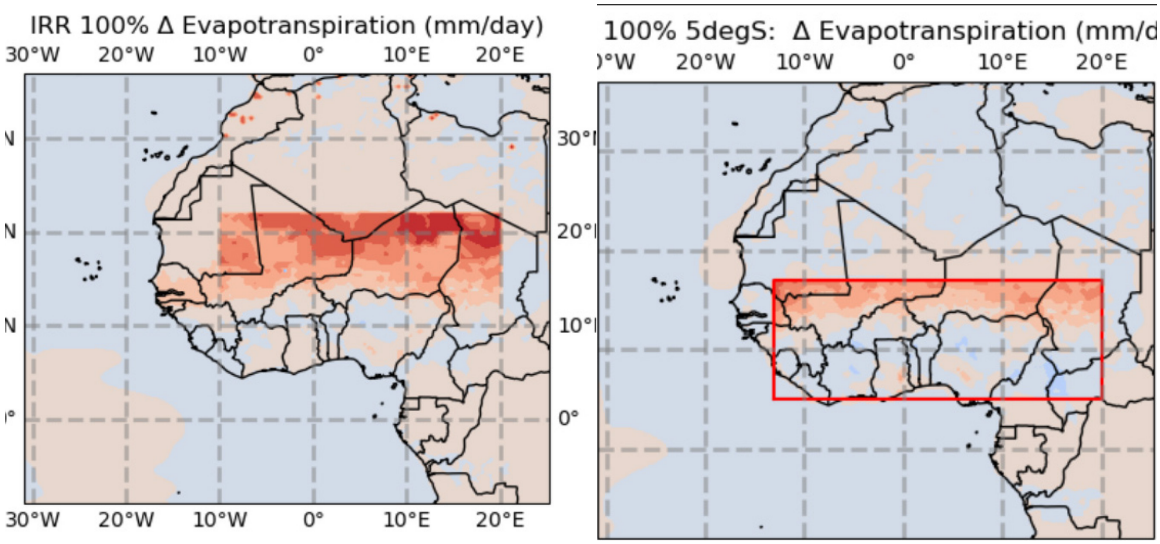

Figure 4.2.1: Changes in June July August (JJA) average evapotranspiration for different sensitivity experiments: 100% of the boxed region being a desert, 15% of the area being irrigated in patches, 22% being irrigated in patches, 22% being irrigated in large patches, 30% being irrigated in patches, 50% being irrigated in patches, 100% being irrigated and 100% being irrigated with the irrigation area shifted 5 degrees to the south (from top to bottom and left to right respectively). Red areas indicate increased evapotranspiration and blue areas indicate decreased evapotranspiration.

4.3 Model Output at 3-hourly Intervals

Even though we have gained a lot of insights from the model output at 6-hourly intervals, it does not tell us about how the atmosphere is behaving under these different land-use type changing scenarios. Specifically, we cannot infer the full set of background mechanisms of why precipitation is increasing or decreasing under different land-use types. To better understand the intermediate mechanisms at work which cause precipitation to increase or decrease, one key piece of information to understand is knowing what is happening in the atmosphere at specific times, such as in the late afternoon around 3PM as PBL reaches its peak height in the late afternoon. This condition allows moisture to be transported to this height through convection, which can then contribute to more condensation and subsequent rainfall, especially when the LCL drops below the PBL. Another perspective on explaining the change in precipitation is through changes in the large-scale atmospheric conditions. One way to do so is to examine the changes in low level wind patterns as they are responsible for transporting moist air and carrying moisture from the tropics to the subtropics during the West African Monsoon (WAM). Both these perspectives will be explored in the results below.

To simplify, we will denote the experimental output at 3-hourly intervals of the control simulation as CONT, the 100% irrigated experiment as IRR and the experiment turning existing land-use types in the West African area into the desert land-use type as specified in Figure 3.4.5 as desA.

4.4 Changes in Wind Pattern

One of the main results from the section looking at changes in precipitation due to land-use change was the increase in precipitation in the south and south-westerly direction of the irrigated area. Even though this coincides with the results from many previous studies that have shown that precipitation increases remotely outside of the irrigated areas (Alter et al., 2015; Seneviratne et al., 2010), it does not explain why precipitation mainly increases towards the south and south-west while decreasing inside the irrigated area. To understand this, we look at how surface winds change with land-use change.

Surface winds in West Africa naturally enter the West African continent from the western Atlantic coastline as well as from the southern coastlines facing the tropical oceans and tropical forested areas. This results in moist oceanic air as well as moist tropical air masses from both the Atlantic Ocean as well as the tropical forests of the tropics carrying moist air northward and eastward into the Sahel region which we understand as the WAM in the months around May to September, which we can also model in the CONT experiment (see Figure 4.4.1). This brings large amounts of moisture feeding precipitation, sometimes more than 16 mm/day to this area which is invaluable for vegetation in the region.

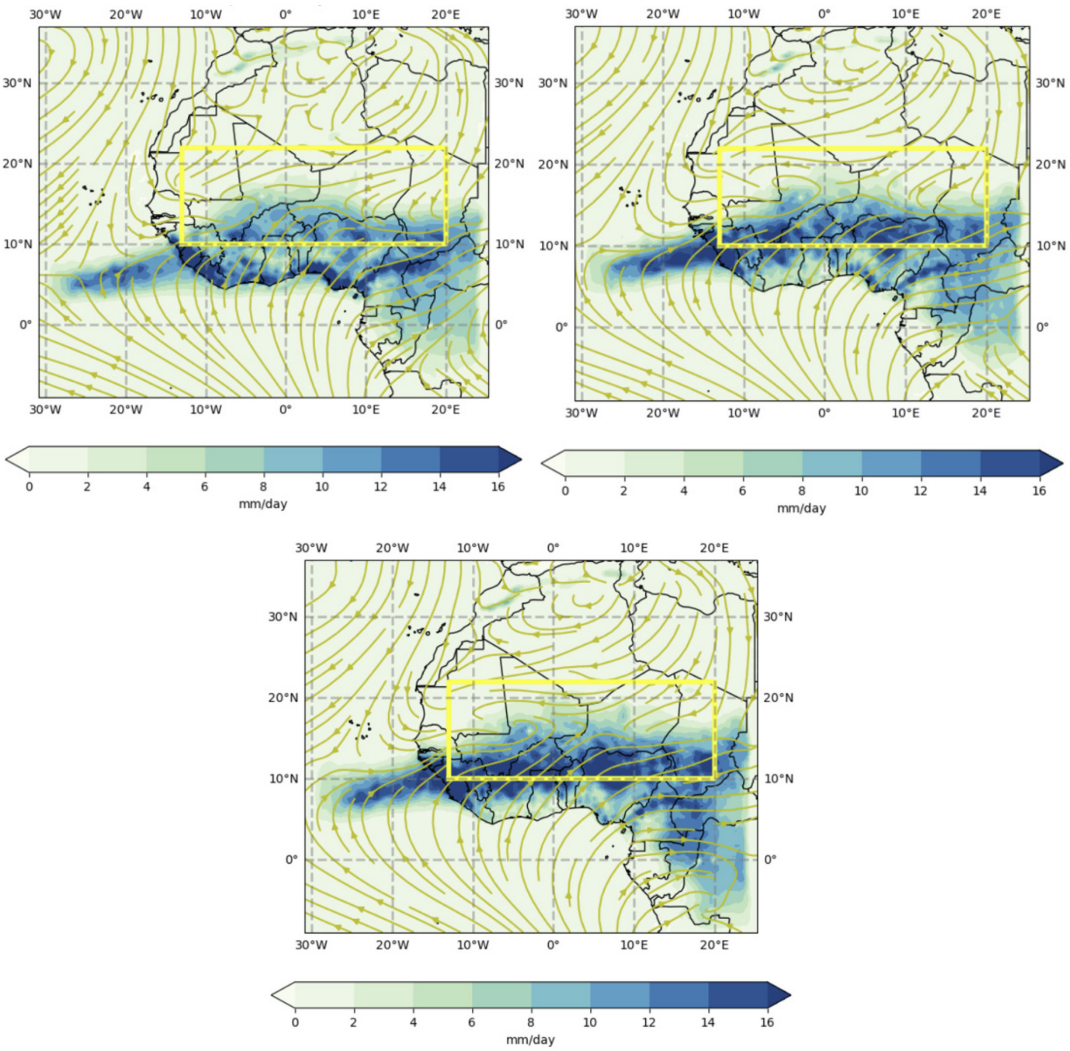

Figure 4.4.1: Wind and precipitation are shown under the control experiment conditions for the months of June, July and August (top-left, top-right and bottom). Precipitation levels are represented by colors from light yellow to dark blue, which range from 0 to >16mm/day respectively. Wind directions are represented by arrows on streamlines in light orange.

If we look at our results from the irrigation IRR experiments, we see that in each of the months of June, July and August, IRR creates anomalous average anemom wind conditions compared to the control simulation (Figure 4.4.3 & Figure 4.4.2), which create diverging centers in the north-western parts of the irrigated area, which decrease convection and cause a decrease in precipitation in the area. At the same time, anomalous southward wind flows prevent moist tropical air from moving northwards, thus thwarting

the WAM in its natural northward movement and pushing more moist air to the south. This causes large amounts of positive anomalous precipitation south of the irrigation area. A similar phenomenon can be seen towards the west, where anomalous wind patterns flowing westwards out of the irrigated area is pushing moist air masses from the Atlantic Ocean back and causing more precipitation along the western edge of the irrigated area.

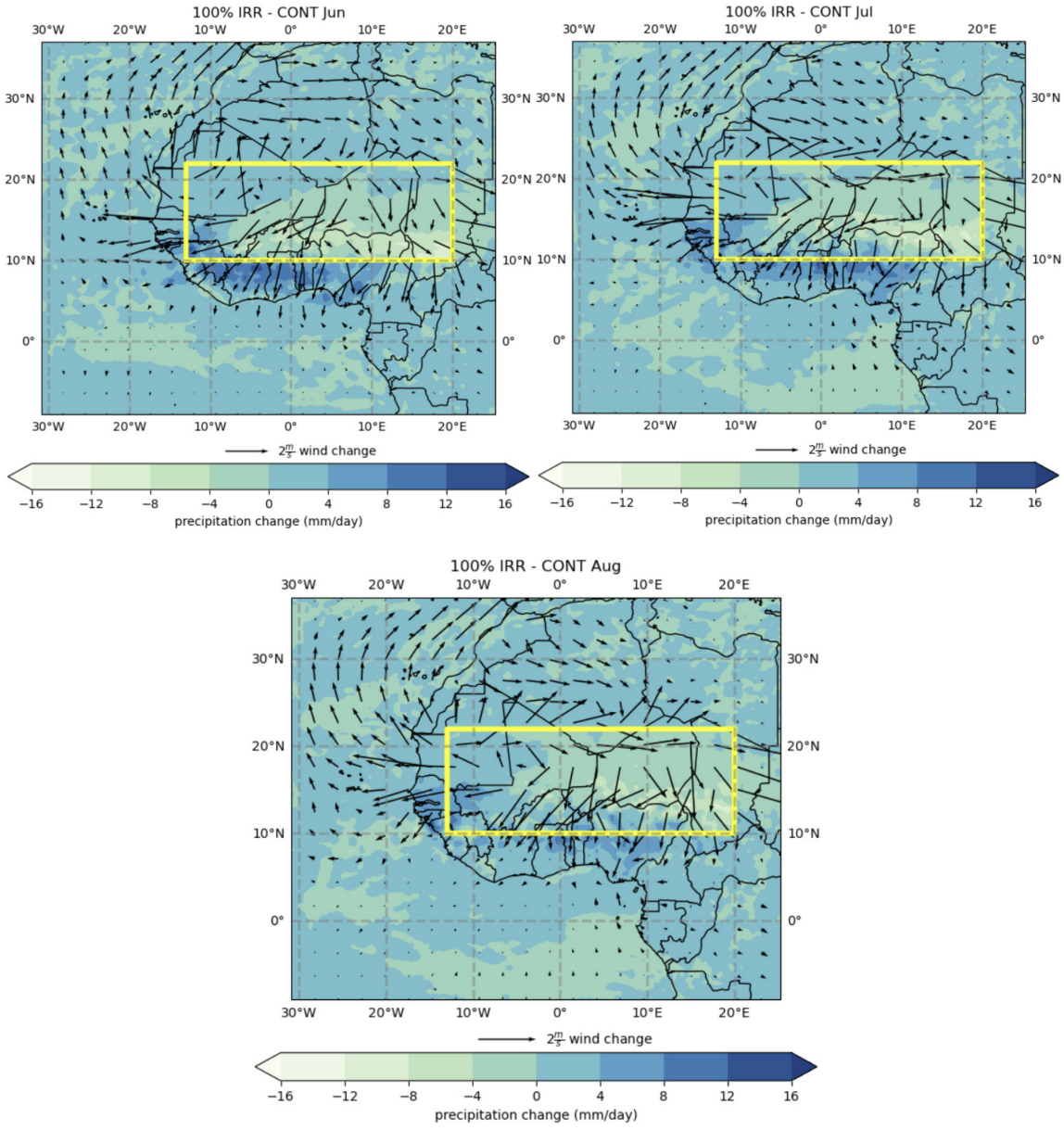

Figure 4.4.2: Wind and precipitation changes when comparing the difference between IRR and CONT are shown for the months of June, July and August (top-left, top-right

and bottom). Precipitation levels are represented by colors from light yellow to dark blue, which ranges from -16mm/day < to > 16mm/day respectively. Wind changes between IRR and CONT are represented by the lengths of the arrows.

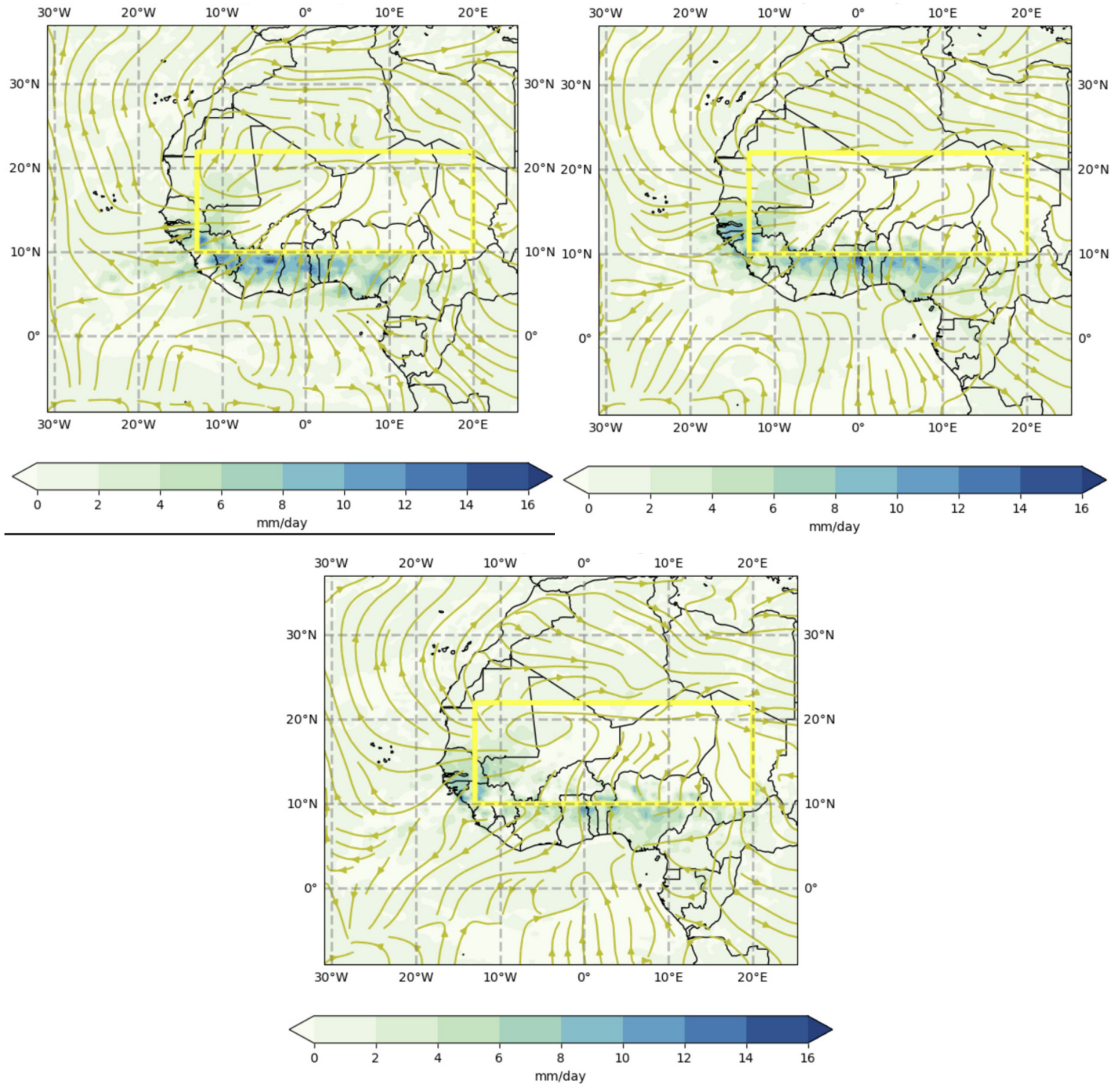

Figure 4.4.3: Wind directional changes when comparing the difference between IRR and CONT are shown for the months of June, July and August (top-left, top-right and bottom). Precipitation levels are represented by colors from light yellow to dark blue, which ranges from 0mm/day < to > 16mm/day respectively.

4.5 Changes in the PBL and LCL and Precipitation

The results of the sensitivity experiments' effects on the PBL and LCL as well as precipitation are compared between the different experimental setups. First the effects of irrigation and desertification on the PBL are examined. For the irrigation experiments, the PBL drops due to the increase of evaporative cooling and subsequent lowering of the PBL due to the decrease in sensible heat flux upwards. Figure 4.5.1a shows the PBL height in the control simulation. We see a clear seasonal northward shift of the maximum height, which is between 3200 and 3600 meters, following the shift of the monsoon rains. This is verified by model output from both surface humidity and rainfall for these months, which is not shown here to keep this thesis concise (see in Appendix Figures B 4.1-4.3). Figure 4.5.1b shows that under IRR, the PBL drops in the north more in July and August and less so in June, while at the same time dropping more in June in the south. Figure 4.5.1c shows the suppression effects of existing vegetation as it shows a lifting of the PBL when there is a desert. The interesting thing is that the pattern presented reflects the soil moisture availability distribution in the different months. Another observation is the dropping of the PBL further north of the Bani river, especially during June and July. This could be due to a blocking mechanism of vegetation that prevents the southwesterly winds from moving northeast.

a)

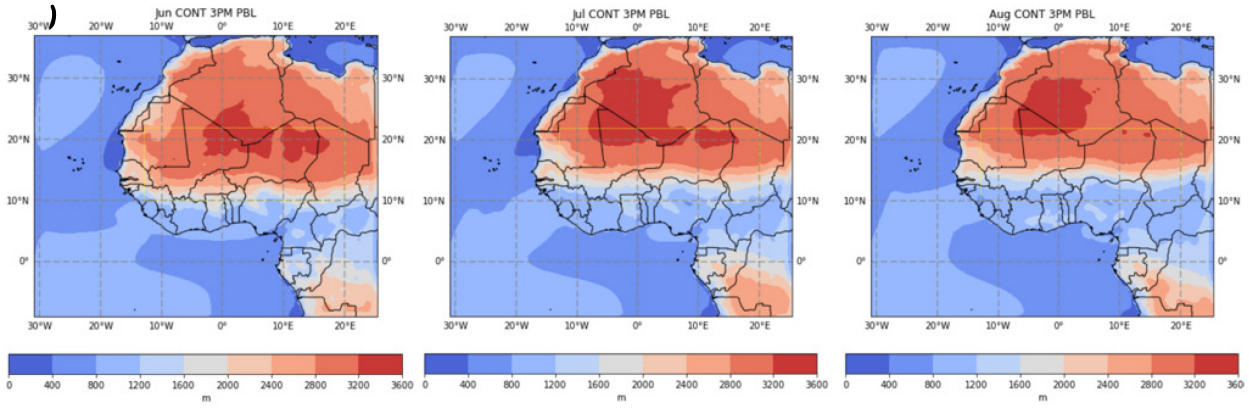

b)

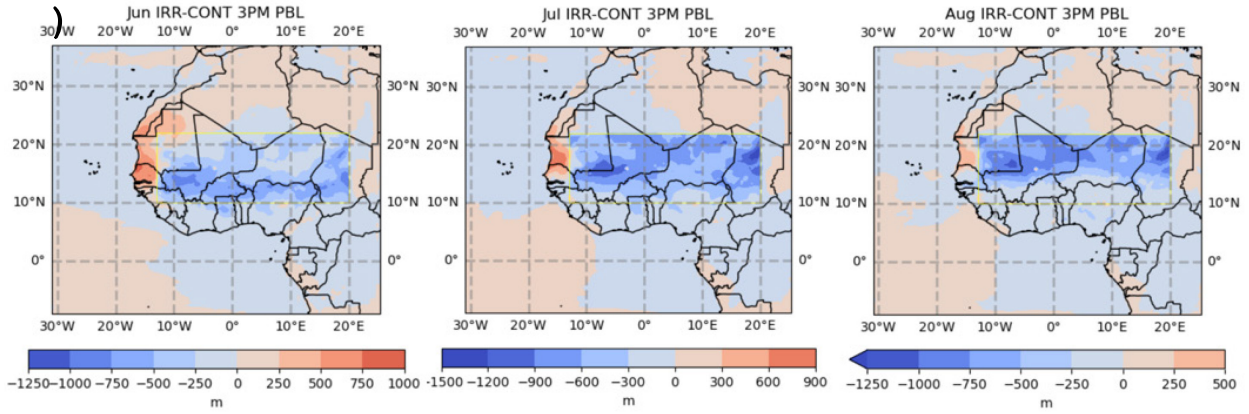

c)

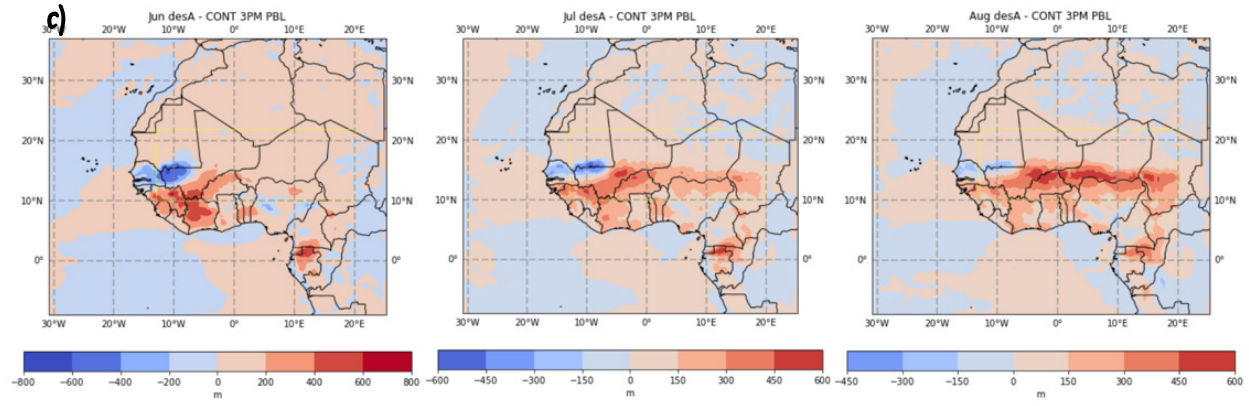

Figure 4.5.1: This figure shows the monthly (June, July, August from left to right) PBL height of the control simulation (a), the irrigated (10 – 22 N) simulation – the control simulation PBL height (b), and the full West Africa desert simulation – the control simulation (c).

a)

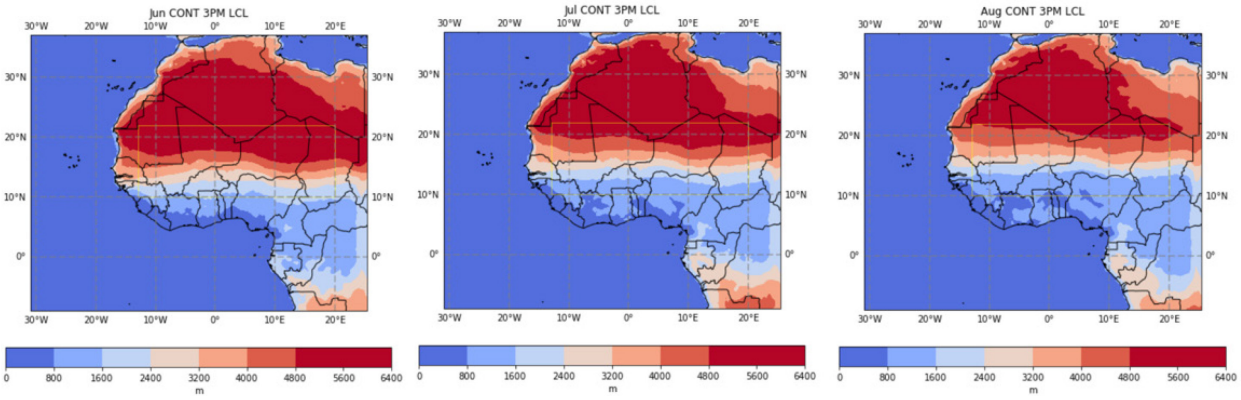

b)

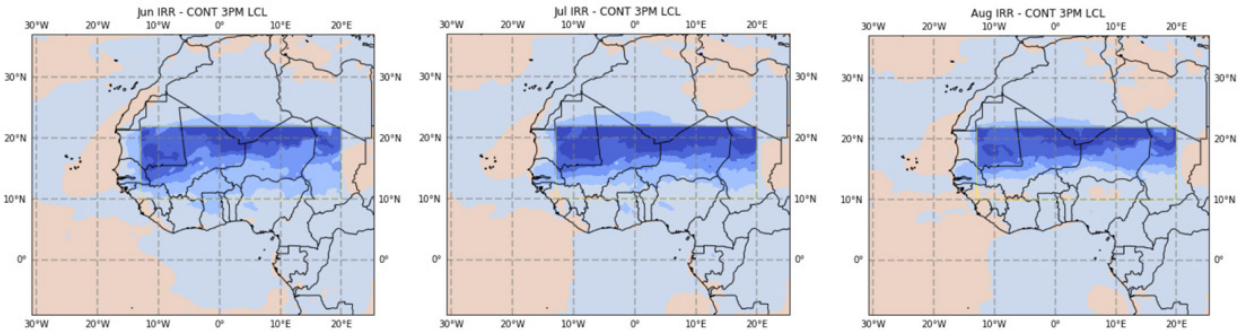

c)

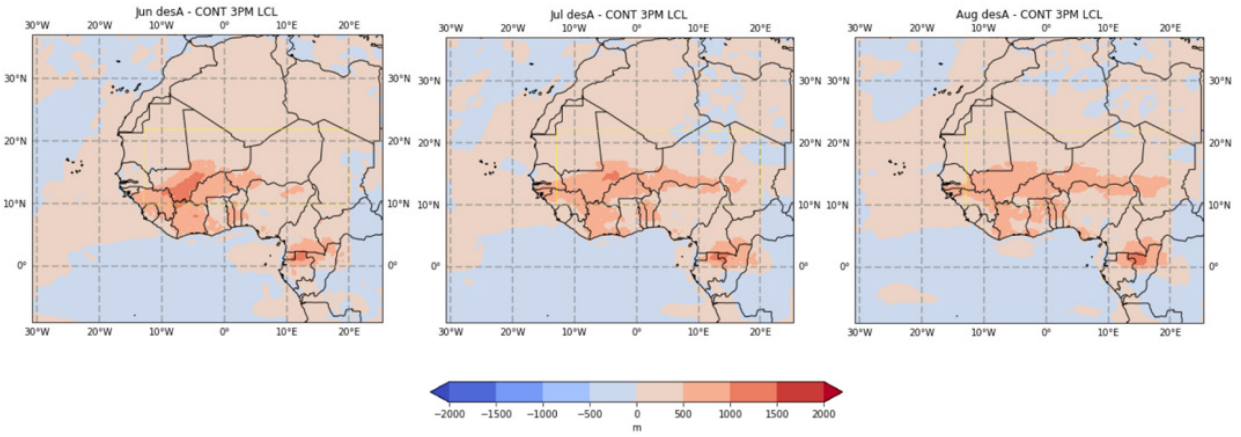

Figure 4.5.2: This figure shows the monthly (June, July, August from left to right) LCL height for the control simulation (a) and the changes caused by the changing of land-use types in the sensitivity experiments for the IRR (b), and desA (c).

Next, the LCL heights are analyzed for both the control simulation and changes that happen in sensitivity experiments. Figure 4.5.2a shows the LCL height in West Africa under the CONT simulation. The maximum height is over 5000 m in the desert while the minimum under 1000 m is along the coast in the south. With irrigation, the LCL drops significantly as Figure 4.5.2b shows, up to 2000 m between 15 – 20 N, while the LCL drops 500 – 1000 m in the southern part of the irrigated area (10 – 15 N). The southern drop is more limited for July and even less so in August. This is due to the changing of the monsoon rainfall location northward as we move forward in time from June to August, as well as the subsequent availability of surface moisture, which is not significantly enhanced with extra irrigation in the southern parts. The relative change in surface moisture is however greatly affected in the northern parts (15 – 20 N) regardless of which month we are in. With desertification, surface moisture is removed, causing the LCL to rise (Fig. 4.5.2d).

We now further analyze the PBL – LCL. The theory is that PBL – LCL gives us an idea if the atmospheric conditions are favorable for rainfall or not. If PBL – LCL is a positive number, it means that the PBL is above the LCL, which means that convection can lead to saturation in the atmosphere and then lead to cloud formation and rainfall. In other words, positive value of PBL – LCL, which means that the PBL is higher up than the LCL, can signify a condition where rainfall is more likely, as turbulent transport inside the PBL can bring a parcel of moist air up to the LCL and cause saturation which then allows clouds to form and rainfall to occur.

$$PBL - LCL > 0 : atmospherically\ suitable\ for\ rainfall$$

For areas around the tropics, such as West Africa, monsoonal rainfall is the dominant mechanism for rainfall. Here, convection of moist air parcels coming from the ocean on the land surface due to surface heating by the sun is the underlying mechanism (*Encyclopedia of Atmospheric Sciences*, 2003). When analyzing PBL – LCL, as well as LCL and PBL separately, the average values of simulation data at 3PM is taken as that is the time where the PBL is assumed to be the highest (while diurnal LCL changes are much smaller), and when rainfall is most likely to happen.

We will compare not only the PBL – LCL, but also how changes of PBL – LCL with the sensitivity experiments compare with the seasonal rainfall amounts. Figure 4.5.3 shows PBL – LCL first (left most figures) for the sensitivity experiment for Jun, July and August, compared then to PBL – LCL of CONT (second figure from the left, hereafter L2), then the figure on the right of that is the difference between sensitivity experiment and control (third from the left, hereafter L3) and finally the figure on the far right (hereafter L4) shows the rainfall difference between the sensitivity experiments and CONT. The key observation to see from these figures is how the PBL – LCL changes between CONT and sensitivity experiments (L3) relates to rainfall changes (L4). The first row of figures shows that convective conditions are very good for IRR (L1), much better than CONT (see all the positive red in L3), however rainfall only increases to the south of the irrigated area (L4). There is a similar pattern for the other months. For the 4th row, where we show the effects of desertification, we see that PBL-LCL drops in L3, and from L1 we see that the conditions for convection are not very good, except for far in the south along the coast. That is also where we see the largest increase in rainfall, together with decreases in rainfall in all other areas L4. The monsoon pushes the band of increased rainfall northward. We see that both irrigation and desertification block the northward movement of the monsoonal rainfall. The possible background mechanisms will be discussed further in section 5.

a)

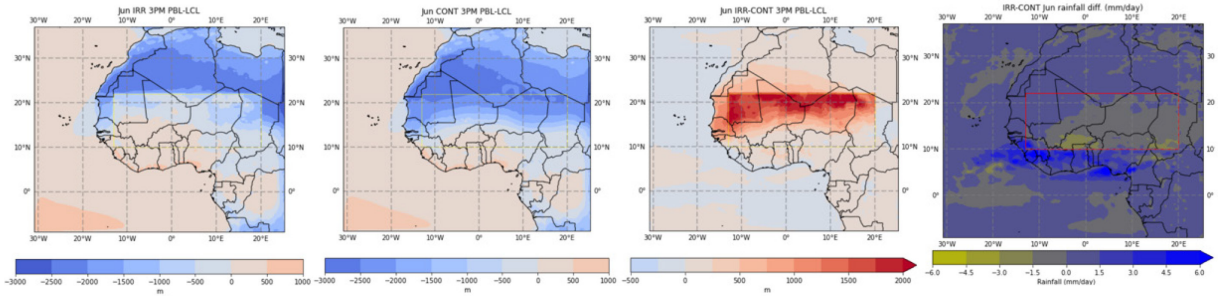
Jun IRR 3PM PBL-LCL
Jun CONT 3PM PBL-LCL
Jun IRR-CONT 3PM PBL-LCL
IRR-CONT Jun rainfall diff. (mm/day)
m
Rainfall (mm/day)

b)

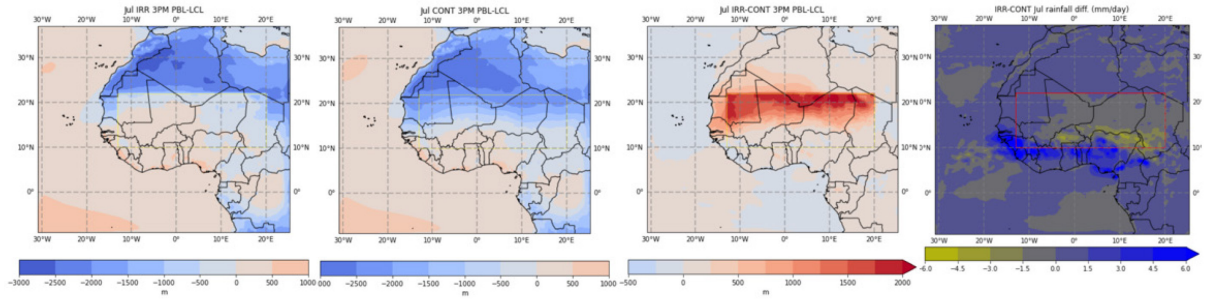
Jul IRR 3PM PBL-LCL
Jul CONT 3PM PBL-LCL
Jul IRR-CONT 3PM PBL-LCL
IRR-CONT Jul rainfall diff. (mm/day)
m
Rainfall (mm/day)

c)

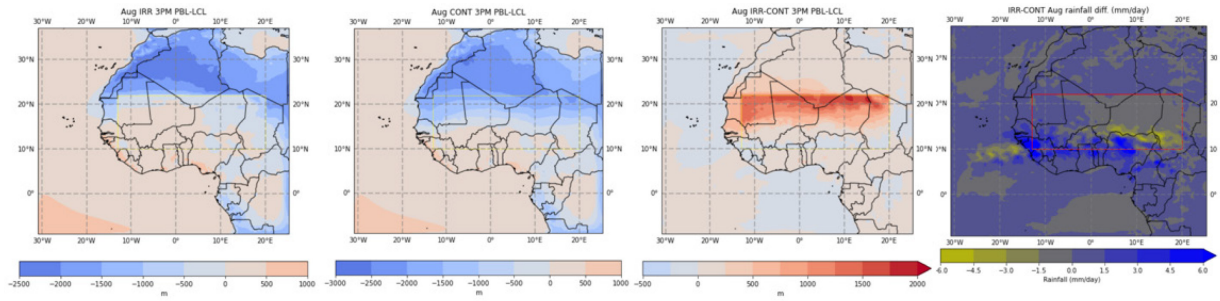
Aug IRR 3PM PBL-LCL
Aug CONT 3PM PBL-LCL
Aug IRR-CONT 3PM PBL-LCL
IRR-CONT Aug rainfall diff. (mm/day)
m
Rainfall (mm/day)

d)

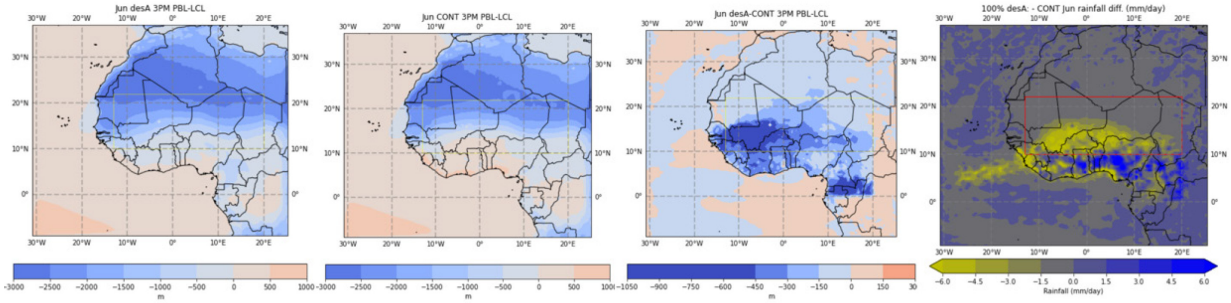
Jun desA 3PM PBL-LCL
Jun CONT 3PM PBL-LCL
Jun desA-CONT 3PM PBL-LCL
100% desA: - CONT Jun rainfall diff. (mm/day)
m
Rainfall (mm/day)

e)

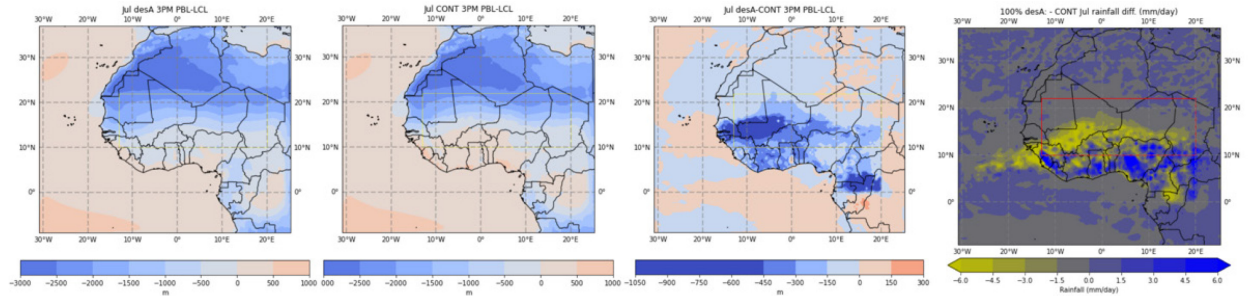

f)

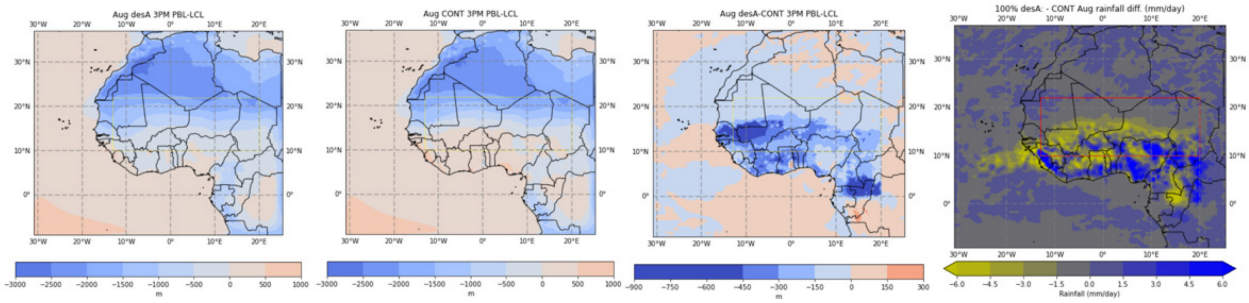

Figure 4.5.3: These figures shows the difference between PBL and LCL (from left to right) for different LULCC setups (L1), the control simulation (L2), the change between the LULCC scenario and the CONT (L3) and the associated rainfall distribution (L4): a) – c): Jun-Aug IRR, d) – e): Jun-Aug desA.

5. Discussion and Conclusions

If we compare our analysis with the other studies that studied land-atmosphere coupling starting from soil-moisture conditions to precipitation, our study specifically looks at the monthly and seasonal rainfall changes during the monsoon season resulting from the changing of land-cover types from simulation experiments conducted in the West African Sahel region. We then try to understand the intermediate mechanisms behind our results after having analyzed different processes in the atmosphere and surface from the simulation output. Variables that we look at to understand the background mechanisms include the Planetary Boundary Layer (PBL), Lifting Condensation Level (LCL), surface temperature, evapotranspiration, surface pressure and surface winds. By comparison, other studies that try to understand the specific coupling mechanisms, may not be looking at specific step-by-step atmospheric processes, or may be looking at other variables different than the ones we listed. Furthermore, there are studies that analyze the positive and negative feedback loops, as well as the spatial distribution of coupling strengths within this process (Green et al., 2017; Jr et al., 2019; Seneviratne et al., 2010).

5.1 Summary of Results and Discussion

The main results of this study are the analysis of large scale effects of irrigation, comparable in size to experiments and analysis done on the North China Plain (Kang & Eltahir, 2018), the US (Alter et al., 2017; Findell & Eltahir, 2003b; Qian et al., 2020; Tuttle & Salvucci, 2016), and in West Africa (Im, Marcella, et al., 2014a; Im & Eltahir, 2014). There are many results from these studies that are similar to our results (see subsequent points (1), (2), (3) and (4)) and also some differences (see (5) and (6)).

(1) Local evaporative cooling effect from irrigation causes surface temperatures to drop in comparison to the control simulation, which assumes no land-use change;

(2) We see that the remote increases in rainfall, outside of the irrigated area, generally holds true, although increasingly less so at larger spatial scales of the irrigation experiment, and this is consistent with many other studies (Alter et al., 2015; Seneviratne et al., 2010);

(3) The desertification experiment highlights what effects the currently existing vegetation in West Africa is having on rainfall and the atmospheric conditions. This way of analyzing the effects of evapotranspiration of vegetation is somewhat unique and far fewer studies have studied land-atmosphere interactions from this perspective. One study looked at deforestation in the Amazon (Eltahir & Bras, 1993) and predicted decreases in precipitation, which is similar to what we found for the months of June and July, where we see an overall decrease in the entire domain. It is also interesting to see that rainfall is not increasing in the north-eastern parts, similar to the irrigation experiments (see Figure 4.5.3 in the above section). This result is interesting, as desertification and irrigation are 2 opposite land-use changes, however the local impact on rainfall shows some similarities;

(4) From the monthly rainfall changes (Figure 4.5.3), we see interesting evidence that might point toward a confirmation of the theory of how dry patches affect

mesoscale convective systems in our simulations. This is because once we switch our land-use type to be a desert, it is similar to having a very large patch of dry land, which, in following the theory by Klein & Taylor (2020) would mean that we should see that mesoscale convective systems, which move in a westerly direction following the African Easterly Jet strengthen, which then would cause more extreme rainfall events downstream and then periods of days without rainfall. Our experimental results show evidence of this by the interchanging of areas which receive more rainfall and then less rainfall under the desertification condition. We do not see similar patterns under the irrigation experiments, which generally show more uniform and aggregated areas of increased and decreased rainfall. We believe that the underlying mechanisms here are different;

(5) The change in LCL and PBL also matches with results from other studies even though other studies are within different climate zones (Qian et al., 2020; Z. Yang et al., 2017), whereby we see an effect which is not at first sight obvious, namely that LCL is more sensitive to LULCC and drops (rises) more under irrigation (desertification) conditions than the PBL in West Africa. Interestingly, however, despite the coherent changes in the surface temperature, evaporation and also in the atmospheric structure, the studies for the US and China (Alter et al., 2017; Kang & Eltahir, 2018, 2019; Qian et al., 2020) have shown mostly positive feedback loops, meaning that the atmospheric structures led to increases in convection and overall rainfall. Even though our experiments also show an overall increase in precipitation in the entire domain, locally, our results show both positive and negative feedback for irrigation and desertification on rainfall despite being at the same large spatial scales as these other studies. The positive feedback loop for SM-P interaction follows the framework set up by Eltahir, 1998, which points toward an increase in moist static energy (MSE), and a subsequent increase in rainfall. This is also the next discussion point;

(6) Our experiments show a clear inversion of LULCC effects, i.e., irrigation exhibits a positive feedback loop and causes more rainfall north up to about 12N, and then switches to cause less rainfall at a certain latitude. This could be because the Sahel is in a transitional zone, which is a zone where evaporation switches

depending on the season between water-limited and energy-limited mechanisms. Transitional zones make hydrological response of the landscape to climate forcing via a non-linear process, which means they are particularly vulnerable to climate variability and change (Dong et al., 2023).

There are some differences between the setup of other studies and those of ours, which might explain the different results that we see. Alter et al. (2017) showed that rainfall increased in the central US both with observations and an MRCM simulation using an experiment with intensified agriculture represented by increased photosynthesis, and singled out the agricultural effects by analyzing GCM simulations that did not have land-use change inside the model run. This is different to what we have in our results as we mostly see rainfall increases outside of the irrigated areas, even though we are also observing a very large area. The reasoning given in the study focused on remote rainfall increases downwind due to local patches of farmland and the overall positive MSE in the region. Im & Eltahir (2014) shows the simulation results of MRCM for 4 different regions that are in or slightly north of the Niger River Basin. The results show that irrigation further north, specifically around 18 – 20 N can increase the rainfall within the basin. This is similar to our experiment with irrigation between 10 – 22 N. However, the spatial scale of the study is much smaller than that of ours.

5.2 Development of a Theory for the Driving Mechanism of Rainfall Changes through PBL, LCL, Surface Winds and Surface Pressure

Some of the key observations from analyzing PBL and LCL for different locations of irrigation and desertification as well its natural state using MRCM simulations are:

(a) The PBL is affected by the availability of soil moisture either through irrigation or the natural monsoonal precipitation, which causes evaporative cooling. This effect is however stronger for intermediately humid areas, which are not too dry nor too wet (i.e. in the Sahel region in general, but this medium humidity region shifts northwards and then back down again with the changes that happen during the monsoon) as seen through the irrigation effects in the drier desert areas, as well as the more humid southern areas of the irrigation zone. Alternatively, this can also be interpreted as areas with intermediate PBL heights. PBL heights at about 2400 m have the largest sensitivity to LULCC.

(b) The LCL behaves similarly to the PBL, however it is more sensitive, meaning the magnitude of the change in meters is larger. Specifically, LCL exhibits a larger change in drier areas which is different to the effects of the PBL, which mostly changes in areas with intermediate heights (transitional zones).

(c) There is an exception to the general understanding of thermodynamics of convective rainfall in the IRR experiment, where despite LCL dropping a lot and almost leveling off with PBL in the north of the irrigated area (thereby creating more optimal thermodynamic conditions for rainfall), there is little rainfall in the area. This points to another mechanism that is preventing rainfall from moving northward during the monsoon season.

We hypothesize that there is a blocking mechanism in place preventing the monsoon to bring moist tropical and oceanic air northward and more inland. An analysis of surface

pressure shows that surface pressure increases significantly in the IRR experiment, causing the northern part of the irrigated area to turn into a high-pressure region, while the changes in surface pressure in desertification experiment (desA) are much smaller (Figure 5.2.1), which does not drive any anomalous circulations. This suggests that large surface pressure anomalies are a possible driving cause behind the lack of convection in IRR in the north and being the cause of a blocking mechanism under which the monsoon rainfall cannot advance northward. When aggregating the results, these observations point toward the theory that both the PBL and LCL heights as well as the large-scale circulation anomalies (caused by LULCC) contribute to convection or the lack thereof.

In fact, after analyzing the surface wind patterns, we see that moist surface air flow is being diverted to the south and south-west in IRR from the irrigated zones which prevents moisture from being carried to the north and north-eastern areas (Figure 4.4.2), thus blocking the monsoon's natural pathway.

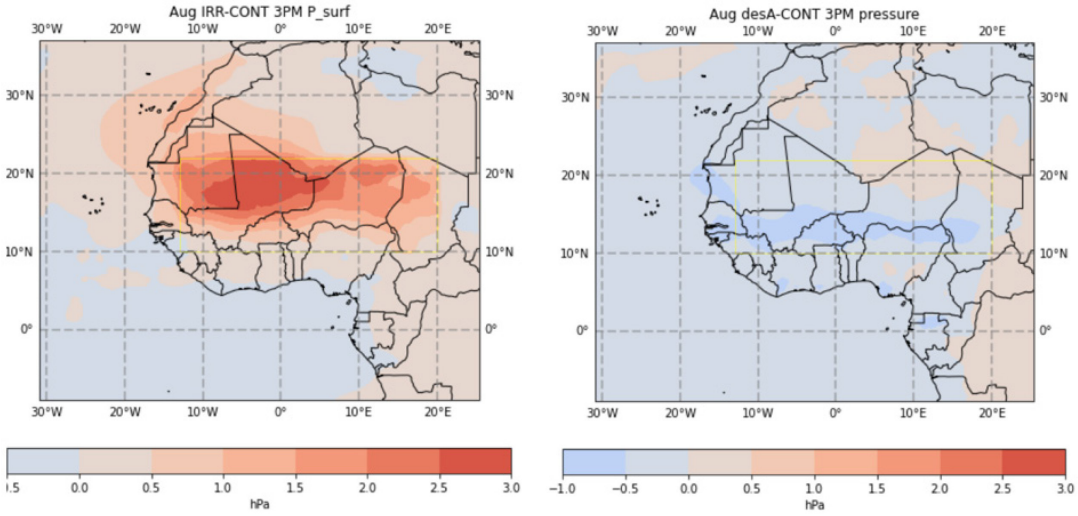

Figure 5.2.1: Changes in surface pressure to CONT between the desertification and irrigation (10 – 22 N) experiments.

5.3 Future Research Directions

Given the many recent papers that have pointed towards the importance of aerosols on climate and precipitation, and how the dominant effects from aerosols on West African rainfall have shifted from North American / European emissions to local West African emissions, another research direction may involve analyzing the aerosol changes under different sensitivity experiments with different land-use changes, and trying to understand if there are any aerosol changes and if those aerosol changes may also have a significant contribution to the precipitation changes in West Africa.

Irrigated agriculture, which has been explored thoroughly in this thesis, is a form of climate change adaptation, as farmers can use it to adapt to climate variability in water scarce areas. Another angle for future research could be to understand the changes in carbon storage associated with different LULCC projects. While extra water resources through extra rainfall can be beneficial to agriculture which is often water-limited, it also increases natural vegetation growth and both agriculture and natural vegetation growth can have a potential positive impact on soil organic carbon storage. This is done as plants fix carbon from the air through photosynthesis, and as parts of the plants, such as the roots stay in the soil which can eventually form soil organic carbon, which is stable and can be stored under the earth for extended periods of time. This means that LULCC projects that change precipitation patterns also have the potential for carbon storage, a nature-based solution to combatting climate change.

Sustainable intensification (SI) is a term that has been coined in recent years as a way to increase food production, while simultaneously reducing environmental impacts and not converting any more land for agricultural purposes in the process (CGIAR, 2015). This concept of SI is controversial, as intensive agriculture is typically associated with a myriad of different environmental impacts, such as decreases in the efficiency of

fertilizer-use and eutrophication. However, correct implementation of SI, with different efficiency improvements, substitutions, and system redesigns in agricultural practices can both increase yields and also has the potential to benefit the environment (Harvey et al., 2014; Haughey et al., 2023).

The current soil organic carbon (SOC) stored in croplands in the top 0.3 m is about 140 Pg (Zomer et al., 2017), which is 10 ~ 16 % of the total SOC in soils around the world in the top 0.3 m of the soil (Sanderman et al., 2017; Scharlemann et al., 2014; Zomer et al., 2017). Additionally, sequestration of SOC on a yearly basis has an estimated potential of 0.9 – 1.85 Pg/year for at least 20 years (Zomer et al., 2017). This estimate does not include the added SOC storing potential of grasslands and through restoration of natural land ecosystems, which also has a large potential, given the degradation of natural land ecosystems due to LULCC (Sanderman et al., 2017).

West Africa specifically is an area with many smallholder farms with croplands making up about 24.7% of the agricultural land, while the rest (75.3%) is comprised of grasslands. Farmland in Africa is far less productive than farms in other parts of the world due to their relative lack of technological means to improve yields (Haughey et al., 2023). This opportunity for growth offers the chance to scale SI practices to increase both food production whilst also increasing SOC to mitigate climate change. The topic of potential changes in soil carbon sequestration under LULCC as well as precipitation changes under LULCC could be explored together to see if synergies exist between increasing agricultural productivity and increasing water availability as a means of climate change adaptation and increasing SOC during this LULCC as a means of climate change mitigation could be done in concert for future agricultural projects.

Bibliography

Adegoke, J. O., Pielke, R. A., Eastman, J., Mahmood, R., & Hubbard, K. G. (2003). Impact of Irrigation on Midsummer Surface Fluxes and Temperature under Dry Synoptic Conditions: A Regional Atmospheric Model Study of the U.S. High Plains. *Monthly Weather Review*, *131*(3), 556–564. https://doi.org/10.1175/1520-0493(2003)131<0556:IOIOMS>2.0.CO;2

Alter, R. E., Douglas, H. C., Winter, J. M., & Eltahir, E. A. B. (2017). Twentieth Century Regional Climate Change During the Summer in the Central United States Attributed to Agricultural Intensification. *Geophysical Research Letters*, 9.

Alter, R. E., Im, E.-S., & Eltahir, E. A. B. (2015). Rainfall consistently enhanced around the Gezira Scheme in East Africa due to irrigation. *Nature Geoscience*, *8*(10), 763–767. https://doi.org/10.1038/ngeo2514

Atiah, W. A., Mengistu Tsidu, G., Amekudzi, L. K., & Yorke, C. (2020). Trends and interannual variability of extreme rainfall indices over Ghana, West Africa. *Theoretical and Applied Climatology*, *140*(3), 1393–1407. https://doi.org/10.1007/s00704-020-03114-6

Berg, A., Lintner, B. R., Findell, K. L., Malyshev, S., Loikith, P. C., & Gentine, P. (2014). Impact of Soil Moisture–Atmosphere Interactions on Surface Temperature Distribution. *Journal of Climate*, *27*(21), 7976–7993. https://doi.org/10.1175/JCLI-D-13-00591.1

Betts, A. K., Ball, J. H., Beljaars, A. C. M., Miller, M. J., & Viterbo, P. A. (1996). The land surface-atmosphere interaction: A review based on observational and global modeling perspectives. *Journal of Geophysical Research: Atmospheres*, *101*(D3), 7209–7225. https://doi.org/10.1029/95JD02135

Biasutti, M. (2019). Rainfall trends in the African Sahel: Characteristics, processes, and causes. *WIREs Climate Change*, *10*(4), e591. https://doi.org/10.1002/wcc.591

Boucher, O., Myhre, G., & Myhre, A. (2004). Direct human influence of irrigation on atmospheric water vapour and climate. *Climate Dynamics*, *22*(6), 597–603. https://doi.org/10.1007/s00382-004-0402-4

Brubaker, K. L., Entekhabi, D., & Eagleson, P. S. (1993). Estimation of continental precipitation recycling. *Journal of Climate; (United States)*, *6:6*. https://doi.org/10.1175/1520-0442(1993)006<1077:EOCPR>2.0.CO;2

Camberlin, P., Janicot, S., & Poccard, I. (2001). Seasonality and atmospheric dynamics of the teleconnection between African rainfall and tropical sea-surface temperature: Atlantic vs. ENSO. *International Journal of Climatology*, *21*(8), 973–1005. https://doi.org/10.1002/joc.673

Ceppi, P., Brient, F., Zelinka, M. D., & Hartmann, D. L. (2017). Cloud feedback mechanisms and their representation in global climate models. *WIREs Climate Change*, *8*(4), e465. https://doi.org/10.1002/wcc.465

CGIAR. (2015, August 20). *Sustainable intensification of agriculture: Oxymoron or real deal?* Water, Land and Ecosystems. https://wle.cgiar.org/thrive/big-questions/sustainable-intensification-agriculture-oxymoron-or-real-deal

Charney, J., Stone, P. H., & Quirk, W. J. (1975). Drought in the Sahara: A Biogeophysical Feedback Mechanism. *Science*, *187*(4175), 434–435. https://doi.org/10.1126/science.187.4175.434

Collins, W. J., Lamarque, J.-F., Schulz, M., Boucher, O., Eyring, V., Hegglin, M. I., Maycock, A., Myhre, G., Prather, M., Shindell, D., & Smith, S. J. (2017). AerChemMIP: Quantifying the effects of chemistry and aerosols in CMIP6. *Geoscientific Model Development*, *10*(2), 585–607. https://doi.org/10.5194/gmd-10-585-2017

Crook, N. A. (1996). Sensitivity of Moist Convection Forced by Boundary Layer Processes to Low-Level Thermodynamic Fields. *Monthly Weather Review*, *124*(8), 1767–1785. https://doi.org/10.1175/1520-0493(1996)124<1767:SOMCFB>2.0.CO;2

Dai, A., & Wigley, T. M. L. (2000). Global patterns of ENSO-induced precipitation. *Geophysical Research Letters*, *27*(9), 1283–1286. https://doi.org/10.1029/1999GL011140

Deser, C., Phillips, A. S., Simpson, I. R., Rosenbloom, N., Coleman, D., Lehner, F., Pendergrass, A. G., DiNezio, P., & Stevenson, S. (2020). Isolating the Evolving

Contributions of Anthropogenic Aerosols and Greenhouse Gases: A New CESM1 Large Ensemble Community Resource. *Journal of Climate*, *33*(18), 7835–7858. https://doi.org/10.1175/JCLI-D-20-0123.1

Dong, J., Akbar, R., Feldman, A. F., Gianotti, D. S., & Entekhabi, D. (2023). Land Surfaces at the Tipping-Point for Water and Energy Balance Coupling. *Water Resources Research*, *59*(2), e2022WR032472. https://doi.org/10.1029/2022WR032472

Douglas, E. M., Beltrán-Przekurat, A., Niyogi, D., Pielke, R. A., & Vörösmarty, C. J. (2009). The impact of agricultural intensification and irrigation on land–atmosphere interactions and Indian monsoon precipitation—A mesoscale modeling perspective. *Global and Planetary Change*, *67*(1), 117–128. https://doi.org/10.1016/j.gloplacha.2008.12.007

Eltahir, E. A. B. (1998). A Soil Moisture-Rainfall Feedback Mechanism: 1. Theory and observations. *Water Resources Research*, *34*(4), 765–776. https://doi.org/10.1029/97WR03499

Eltahir, E. A. B., & Bras, R. L. (1993). On the response of the tropical atmosphere tio large-scale deforestation. *Quarterly Journal of the Royal Meteorological Society*, *119*(512), 779–793. https://doi.org/10.1002/qj.49711951209

Encyclopedia of Atmospheric Sciences. (2003). Acamedic.

Entekhabi, D., Rodriguez-Iturbe, I., & Castelli, F. (1996). Mutual interaction of soil moisture state and atmospheric processes. *Journal of Hydrology*, *184*(1), 3–17. https://doi.org/10.1016/0022-1694(95)02965-6

Ferguson, C. R., & Wood, E. F. (2011). Observed Land–Atmosphere Coupling from Satellite Remote Sensing and Reanalysis. *Journal of Hydrometeorology*, *12*(6), 1221–1254. https://doi.org/10.1175/2011JHM1380.1

Findell, K. L., & Eltahir, E. A. B. (1997). An analysis of the soil moisture-rainfall feedback, based on direct observations from Illinois. *Water Resources Research*, *33*(4), 725–735. https://doi.org/10.1029/96WR03756

Findell, K. L., & Eltahir, E. A. B. (2003a). Atmospheric Controls on Soil Moisture–Boundary Layer Interactions. Part I: Framework Development. *Journal of*

Hydrometeorology, *4*(3), 552–569. https://doi.org/10.1175/1525-7541(2003)004<0552:ACOSML>2.0.CO;2

Findell, K. L., & Eltahir, E. A. B. (2003b). Atmospheric Controls on Soil Moisture–Boundary Layer Interactions. Part II: Feedbacks within the Continental United States. *Journal of Hydrometeorology*, *4*(3), 570–583. https://doi.org/10.1175/1525-7541(2003)004<0570:ACOSML>2.0.CO;2

Gianotti, R. L., & Eltahir, E. A. B. (2014a). Regional Climate Modeling over the Maritime Continent. Part I: New Parameterization for Convective Cloud Fraction. *Journal of Climate*, *27*(4), 1488–1503. https://doi.org/10.1175/JCLI-D-13-00127.1

Gianotti, R. L., & Eltahir, E. A. B. (2014b). Regional Climate Modeling over the Maritime Continent. Part II: New Parameterization for Autoconversion of Convective Rainfall. *Journal of Climate*, *27*(4), 1504–1523. https://doi.org/10.1175/JCLI-D-13-00171.1

Gianotti, R. L. (Rebecca L. (2012). *Convective cloud and rainfall processes over the Maritime Continent: Simulation and analysis of the diurnal cycle* [Thesis, Massachusetts Institute of Technology]. https://dspace.mit.edu/handle/1721.1/79488

Gong, C., & Eltahir, E. (1996). Sources of moisture for rainfall in West Africa. *Water Resources Research*, *32*(10), 3115–3121. https://doi.org/10.1029/96WR01940

Green, J. K., Konings, A. G., Alemohammad, S. H., Berry, J., Entekhabi, D., Kolassa, J., Lee, J.-E., & Gentine, P. (2017). Regionally strong feedbacks between the atmosphere and terrestrial biosphere. *Nature Geoscience*, *10*(6), Article 6. https://doi.org/10.1038/ngeo2957

Gu, G., & Adler, R. F. (2004). Seasonal Evolution and Variability Associated with the West African Monsoon System. *Journal of Climate*, *17*(17), 3364–3377. https://doi.org/10.1175/1520-0442(2004)017<3364:SEAVAW>2.0.CO;2

Hamed, M. M., Nashwan, M. S., & Shahid, S. (2022). A novel selection method of CMIP6 GCMs for robust climate projection. *International Journal of Climatology*, *42*(8), 4258–4272. https://doi.org/10.1002/joc.7461

Harvey, C. A., Chacón, M., Donatti, C. I., Garen, E., Hannah, L., Andrade, A., Bede, L., Brown, D., Calle, A., Chará, J., Clement, C., Gray, E., Hoang, M. H., Minang, P.,

Rodríguez, A. M., Seeberg-Elverfeldt, C., Semroc, B., Shames, S., Smukler, S., … Wollenberg, E. (2014). Climate-Smart Landscapes: Opportunities and Challenges for Integrating Adaptation and Mitigation in Tropical Agriculture. *Conservation Letters*, *7*(2), 77–90. https://doi.org/10.1111/conl.12066

Haughey, E., Neogi, S., Portugal-Pereira, J., van Diemen, R., & Slade, R. B. (2023). Sustainable intensification and carbon sequestration research in agricultural systems: A systematic review. *Environmental Science & Policy*, *143*, 14–23. https://doi.org/10.1016/j.envsci.2023.02.018

Hirasawa, H., Kushner, P. J., Sigmond, M., Fyfe, J., & Deser, C. (2022). Evolving Sahel Rainfall Response to Anthropogenic Aerosols Driven by Shifting Regional Oceanic and Emission Influences. *Journal of Climate*, *35*(11), 3181–3193. https://doi.org/10.1175/JCLI-D-21-0795.1

Hollinger, F., & Staatz, J. M. (2015). *Agricultural growth in West Africa: Market and policy drivers*. African Development Bank and the Food and Agriculture Organization of the United Nations ; African Development Bank.

Huang, J., Adams, A., Wang, C., & Zhang, C. (2009). Black Carbon and West African Monsoon precipitation: Observations and simulations. *Annales Geophysicae*, *27*(11), 4171–4181. https://doi.org/10.5194/angeo-27-4171-2009

Im, E.-S., & Eltahir, E. A. B. (2014). Enhancement of rainfall and runoff upstream from irrigation location in a climate model of West Africa. *Water Resources Research*, *50*(11), 8651–8674. https://doi.org/10.1002/2014WR015592

Im, E.-S., Gianotti, R. L., & Eltahir, E. A. B. (2014). Improving the Simulation of the West African Monsoon Using the MIT Regional Climate Model. *Journal of Climate*, *27*(6), 2209–2229. https://doi.org/10.1175/JCLI-D-13-00188.1

Im, E.-S., Marcella, M. P., & Eltahir, E. A. B. (2014a). Impact of Potential Large-Scale Irrigation on the West African Monsoon and Its Dependence on Location of Irrigated Area. *Journal of Climate*, *27*(3), 994–1009. https://doi.org/10.1175/JCLI-D-13-00290.1

Im, E.-S., Marcella, M. P., & Eltahir, E. A. B. (2014b). Impact of Potential Large-Scale Irrigation on the West African Monsoon and Its Dependence on Location of Irrigated Area. *Journal of Climate*, *27*(3), 994–1009. https://doi.org/10.1175/JCLI-D-13-00290.1

Jr, J. A. S., Lawston, P., Kumar, S., & Dennis, E. (2019). Understanding the Impacts of Soil Moisture Initial Conditions on NWP in the Context of Land–Atmosphere Coupling. *Journal of Hydrometeorology*, *20*(5), 793–819. https://doi.org/10.1175/JHM-D-18-0186.1

Kang, S., & Eltahir, E. A. B. (2018). North China Plain threatened by deadly heatwaves due to climate change and irrigation. *Nature Communications*, *9*(1), 2894. https://doi.org/10.1038/s41467-018-05252-y

Kang, S., & Eltahir, E. A. B. (2019). Impact of Irrigation on Regional Climate Over Eastern China. *Geophysical Research Letters*, *46*(10), 5499–5505. https://doi.org/10.1029/2019GL082396

Klein, C., & Taylor, C. M. (2020). Dry soils can intensify mesoscale convective systems. *Proceedings of the National Academy of Sciences*, *117*(35), 21132–21137. https://doi.org/10.1073/pnas.2007998117

Koster, R. D., Dirmeyer, P. A., Guo, Z., Bonan, G., Chan, E., Cox, P., Gordon, C. T., Kanae, S., Kowalczyk, E., Lawrence, D., Liu, P., Lu, C.-H., Malyshev, S., McAvaney, B., Mitchell, K., Mocko, D., Oki, T., Oleson, K., Pitman, A., … Yamada, T. (2004). Regions of Strong Coupling Between Soil Moisture and Precipitation. *Science*, *305*(5687), 1138–1140. https://doi.org/10.1126/science.1100217

Lavaysse, C., Flamant, C., Janicot, S., Parker, D., Lafore, J.-P., Sultan, B., & Pelon, J. (2009). Seasonal evolution of the West African Heat Low: A climatological perspective. *Climate Dynamics*, *33*, 313–330. https://doi.org/10.1007/s00382-009-0553-4

Liu, W., Zhang, Q., Li, C., Xu, L., & Xiao, W. (2022). The influence of soil moisture on convective activity: A review. *Theoretical and Applied Climatology*, *149*(1), 221–232. https://doi.org/10.1007/s00704-022-04046-z

Lobell, D., Bala, G., Mirin, A., Phillips, T., Maxwell, R., & Rotman, D. (2009). Regional Differences in the Influence of Irrigation on Climate. *Journal of Climate*, *22*(8), 2248–2255. https://doi.org/10.1175/2008JCLI2703.1

Lu, Y., Harding, K., & Kueppers, L. (2017). Irrigation Effects on Land–Atmosphere Coupling Strength in the United States. *Journal of Climate*, *30*(10), 3671–3685. https://doi.org/10.1175/JCLI-D-15-0706.1

Marcella, M. P. (2012). *Biosphere-atmosphere interactions over semi-arid regions: Modeling the role of mineral aerosols and irrigation in the regional climate system* [Thesis, Massachusetts Institute of Technology]. https://dspace.mit.edu/handle/1721.1/79490

Marcella, M. P., & Eltahir, E. A. B. (2014). Introducing an Irrigation Scheme to a Regional Climate Model: A Case Study over West Africa. *Journal of Climate*, *27*(15), 5708–5723. https://doi.org/10.1175/JCLI-D-13-00116.1

McArthur, J. W., & Sachs, J. D. (2019). Agriculture, Aid, and Economic Growth in Africa. *The World Bank Economic Review*, *33*(1), 1–20. https://doi.org/10.1093/wber/lhx029

Monerie, P.-A., Dittus, A. J., Wilcox, L. J., & Turner, A. G. (2023). Uncertainty in Simulating Twentieth Century West African Precipitation Trends: The Role of Anthropogenic Aerosol Emissions. *Earth's Future*, *11*(2), e2022EF002995. https://doi.org/10.1029/2022EF002995

Nnamchi, H. C., & Li, J. (2011). Influence of the South Atlantic Ocean Dipole on West African Summer Precipitation. *Journal of Climate*, *24*(4), 1184–1197.

Pal, J. S., & Eltahir, E. A. B. (2001). Pathways Relating Soil Moisture Conditions to Future Summer Rainfall within a Model of the Land–Atmosphere System. *Journal of Climate*, *14*(6), 1227–1242. https://doi.org/10.1175/1520-0442(2001)014<1227:PRSMCT>2.0.CO;2

Pal, J. S., Giorgi, F., Bi, X., Elguindi, N., Solmon, F., Gao, X., Rauscher, S. A., Francisco, R., Zakey, A., Winter, J., Ashfaq, M., Syed, F. S., Bell, J. L., Diffenbaugh, N. S., Karmacharya, J., Konaré, A., Martinez, D., Rocha, R. P. da, Sloan, L. C., & Steiner, A. L. (2007). Regional Climate Modeling for the Developing World: The ICTP RegCM3 and RegCNET. *Bulletin of the American Meteorological Society*, *88*(9), 1395–1410. https://doi.org/10.1175/BAMS-88-9-1395

Pielke Sr., R. A. (2001). Influence of the spatial distribution of vegetation and soils on the prediction of cumulus Convective rainfall. *Reviews of Geophysics*, *39*(2), 151–177. https://doi.org/10.1029/1999RG000072

Potapov, P., Turubanova, S., Hansen, M. C., Tyukavina, A., Zalles, V., Khan, A., Song, X.-P., Pickens, A., Shen, Q., & Cortez, J. (2022). Global maps of cropland extent and change show accelerated cropland expansion in the twenty-first century. *Nature Food*, *3*(1), Article 1. https://doi.org/10.1038/s43016-021-00429-z

Qian, Y., Huang, M., Yang, B., & Berg, L. K. (2013). A Modeling Study of Irrigation Effects on Surface Fluxes and Land–Air–Cloud Interactions in the Southern Great Plains. *Journal of Hydrometeorology*, *14*(3), 700–721. https://doi.org/10.1175/JHM-D-12-0134.1

Qian, Y., Yang, Z., Feng, Z., Liu, Y., Gustafson, W. I., Berg, L. K., Huang, M., Yang, B., & Ma, H.-Y. (2020). Neglecting irrigation contributes to the simulated summertime warm-and-dry bias in the central United States. *Npj Climate and Atmospheric Science*, *3*(1), Article 1. https://doi.org/10.1038/s41612-020-00135-w

Rodríguez-Fonseca, B., Janicot, S., Mohino, E., Losada, T., Bader, J., Caminade, C., Chauvin, F., Fontaine, B., García-Serrano, J., Gervois, S., Joly, M., Polo, I., Ruti, P., Roucou, P., & Voldoire, A. (2011). Interannual and decadal SST-forced responses of the West African monsoon. *Atmospheric Science Letters*, *12*(1), 67–74. https://doi.org/10.1002/asl.308

Sacks, W. J., Cook, B. I., Buenning, N., Levis, S., & Helkowski, J. H. (2009). Effects of global irrigation on the near-surface climate. *Climate Dynamics*, *33*(2), 159–175. https://doi.org/10.1007/s00382-008-0445-z

Sanderman, J., Hengl, T., & Fiske, G. J. (2017). Soil carbon debt of 12,000 years of human land use. *Proceedings of the National Academy of Sciences*, *114*(36), 9575–9580. https://doi.org/10.1073/pnas.1706103114

Santanello, J. A., Dirmeyer, P. A., Ferguson, C. R., Findell, K. L., Tawfik, A. B., Berg, A., Ek, M., Gentine, P., Guillod, B. P., van Heerwaarden, C., Roundy, J., & Wulfmeyer, V. (2018). Land–Atmosphere Interactions: The LoCo Perspective. *Bulletin of the American Meteorological Society*, *99*(6), 1253–1272. https://doi.org/10.1175/BAMS-D-17-0001.1

Savenije, H. H. G. (1995). Does moisture feedback affect rainfall significantly? *Physics and Chemistry of the Earth*, *20*(5), 507–513. https://doi.org/10.1016/S0079-1946(96)00014-6

Scharlemann, J. P., Tanner, E. V., Hiederer, R., & Kapos, V. (2014). Global soil carbon: Understanding and managing the largest terrestrial carbon pool. *Carbon Management*, *5*(1), 81–91. https://doi.org/10.4155/cmt.13.77

Sellers, P., Hall, F., Margolis, H., Kelly, B., Baldocchi, D., Hartog, G. den, Cihlar, J., Ryan, M. G., Goodison, B., Crill, P., Ranson, K. J., Lettenmaier, D., & Wickland, D. E. (1995). The Boreal Ecosystem–Atmosphere Study (BOREAS): An Overview and Early Results from the 1994 Field Year. *Bulletin of the American Meteorological Society*, *76*(9), 1549–1577. https://doi.org/10.1175/1520-0477(1995)076<1549:TBESAO>2.0.CO;2

Sellers, P. J., Hall, F. G., Asrar, G., Strebel, D. E., & Murphy, R. E. (1992). An overview of the First International Satellite Land Surface Climatology Project (ISLSCP) Field Experiment (FIFE). *Journal of Geophysical Research: Atmospheres*, *97*(D17), 18345–18371. https://doi.org/10.1029/92JD02111

Seneviratne, S. I., Corti, T., Davin, E. L., Hirschi, M., Jaeger, E. B., Lehner, I., Orlowsky, B., & Teuling, A. J. (2010). Investigating soil moisture–climate interactions in a changing climate: A review. *Earth-Science Reviews*, *99*(3–4), 125–161. https://doi.org/10.1016/j.earscirev.2010.02.004

Shindell, D., Parsons, L., Faluvegi, G., Hicks, K., Kuylenstierna, J., & Heaps, C. (2023). The important role of African emissions reductions in projected local rainfall changes. *Npj Climate and Atmospheric Science*, *6*(1), Article 1. https://doi.org/10.1038/s41612-023-00382-7

Siebert, A. (2014). Hydroclimate Extremes in Africa: Variability, Observations and Modeled Projections. *Geography Compass*, *8*(6), 351–367. https://doi.org/10.1111/gec3.12136

Siebert, A., Ryser, P., Ndiaye, D., Diop, L., Mbengue, A., Sal, A., Konte, O., Ndiaye, O., Trzaska, S., Robertson, A., Hansen, J., Singh, B., Cousin, R., & Faniriantsoa, R. (2021).

A Multi-Model Approach to Forecasting Seasonal Rainfall Characteristics in Senegal. *2021*, H55G-0813.

Siebert, S., Kummu, M., Porkka, M., Döll, P., Ramankutty, N., & Scanlon, B. R. (2015). A global data set of the extent of irrigated land from 1900 to 2005. *Hydrology and Earth System Sciences*, *19*(3), 1521–1545. https://doi.org/10.5194/hess-19-1521-2015

Sørland, S. L., Schär, C., Lüthi, D., & Kjellström, E. (2018). Bias patterns and climate change signals in GCM-RCM model chains. *Environmental Research Letters*, *13*(7), 074017. https://doi.org/10.1088/1748-9326/aacc77

Taylor, C. M., de Jeu, R. A. M., Guichard, F., Harris, P. P., & Dorigo, W. A. (2012). Afternoon rain more likely over drier soils. *Nature*, *489*(7416), 423–426. https://doi.org/10.1038/nature11377

te Wierik, S. A., Cammeraat, E. L. H., Gupta, J., & Artzy-Randrup, Y. A. (2021). Reviewing the Impact of Land Use and Land-Use Change on Moisture Recycling and Precipitation Patterns. *Water Resources Research*, *57*(7). https://doi.org/10.1029/2020WR029234

Teye, J. K., & Nikoi, E. G. A. (2022). Climate-Induced Migration in West Africa. In J. K. Teye (Ed.), *Migration in West Africa: IMISCOE Regional Reader* (pp. 79–105). Springer International Publishing. https://doi.org/10.1007/978-3-030-97322-3_5

Thorncroft, C. D., Nguyen, H., Zhang, C., & Peyrillé, P. (2011). Annual cycle of the West African monsoon: Regional circulations and associated water vapour transport. *Quarterly Journal of the Royal Meteorological Society*, *137*(654), 129–147. https://doi.org/10.1002/qj.728

Tripathi, H. G., Woollen, E. S., Carvalho, M., Parr, C. L., & Ryan, C. M. (2021). Agricultural expansion in African savannas: Effects on diversity and composition of trees and mammals. *Biodiversity and Conservation*, *30*(11), 3279–3297. https://doi.org/10.1007/s10531-021-02249-w

Tuel, A., & Eltahir, E. a. B. (2020). Why Is the Mediterranean a Climate Change Hot Spot? *Journal of Climate*, *33*(14), 5829–5843. https://doi.org/10.1175/JCLI-D-19-0910.1

Turner, B. L., Lambin, E. F., & Reenberg, A. (2007). The emergence of land change science for global environmental change and sustainability. *Proceedings of the National Academy of Sciences*, *104*(52), 20666–20671. https://doi.org/10.1073/pnas.0704119104

Tuttle, S., & Salvucci, G. (2016). Empirical evidence of contrasting soil moisture–precipitation feedbacks across the United States. *Science*, *352*(6287), 825–828. https://doi.org/10.1126/science.aaa7185

Uppala, S., Dee, D., Kobayashi, S., Berrisford, P., & Simmons, A. (2008). *Towards a climate data assimilation system: Status update of ERA-Interim*. https://doi.org/10.21957/BYINOX4WOT

Wang, G., & Eltahir, E. A. B. (2007). Biosphere-atmosphere interactions over West Africa. II: Multiple climate equilibria. *Quarterly Journal of the Royal Meteorological Society*, *126*(565), 1261–1280. https://doi.org/10.1002/qj.49712656504

Wei, J., & Dirmeyer, P. A. (2012). Dissecting soil moisture-precipitation coupling: SOIL MOISTURE-PRECIPITATION COUOPLING. *Geophysical Research Letters*, *39*(19), n/a-n/a. https://doi.org/10.1029/2012GL053038

Worou, K., Goosse, H., Fichefet, T., & Kucharski, F. (2021). *Weakened impact of the Atlantic Niño on the future equatorial Atlantic and Guinean Coast rainfall* [Preprint]. Dynamics of the Earth system: models. https://doi.org/10.5194/esd-2021-46

Yang, L. (2018). Negative soil moisture-precipitation feedback in dry and wet regions. *SCIEntIfIC REPOrTS*, 9.

Yang, Z., Dominguez, F., Zeng, X., Hu, H., Gupta, H., & Yang, B. (2017). Impact of Irrigation over the California Central Valley on Regional Climate. *Journal of Hydrometeorology*, *18*(5), 1341–1357. https://doi.org/10.1175/JHM-D-16-0158.1

Zheng, X., & Eltahir, E. A. B. (1998). The Role of Vegetation in the Dynamics of West African Monsoons. *JOURNAL OF CLIMATE*, *11*.

Zheng, X., Eltahir, E. A. B., & Emanuel, K. A. (1999). A mechanism relating tropical Atlantic spring sea surface temperature and west African rainfall. *Quarterly Journal of the Royal Meteorological Society*, *125*(556), 1129–1163. https://doi.org/10.1002/qj.1999.49712555604

Zhou, S., Williams, A. P., Berg, A. M., Cook, B. I., Zhang, Y., Hagemann, S., Lorenz, R., Seneviratne, S. I., & Gentine, P. (2019). Land–atmosphere feedbacks exacerbate concurrent soil drought and atmospheric aridity. *Proceedings of the National Academy of Sciences*, *116*(38), 18848–18853. https://doi.org/10.1073/pnas.1904955116

Zhou, S., Williams, A. P., Lintner, B. R., Berg, A. M., Zhang, Y., Keenan, T. F., Cook, B. I., Hagemann, S., Seneviratne, S. I., & Gentine, P. (2021). Soil moisture–atmosphere feedbacks mitigate declining water availability in drylands. *Nature Climate Change*, *11*(1), 38–44. https://doi.org/10.1038/s41558-020-00945-z

Zomer, R. J., Bossio, D. A., Sommer, R., & Verchot, L. V. (2017). Global Sequestration Potential of Increased Organic Carbon in Cropland Soils. *Scientific Reports*, *7*(1), 15554. https://doi.org/10.1038/s41598-017-15794-8

Appendix A Definitions

CTP is defined as the following:

$$\mathrm{CTP} = g \int_{Z_{\mathrm{PSurfStd-300}}}^{Z_{\mathrm{PSurfStd-100}}} \left(\frac{T_{\mathrm{parcel}} - T_{\mathrm{env}}}{T_{\mathrm{env}}} \right) dz$$

CTP is here the integral of the area between the sounding profile, T_{env} and a moist adiabat T_{parcel} raised from ~1km to ~3km.

HI is defined as:

$$\mathrm{HI} = (T_{\mathrm{PSurfStd-50}} - T_{d,\mathrm{PSurfStd-50}}) + (T_{\mathrm{PSurfStd-150}} - T_{d,\mathrm{PSurfStd-150}})$$

HI defines the sum of the dewpoint depressions at 50 and 150 mb above the ground surface.

In the study, thresholds for HI and CTP were defined as between 5 and 15 degrees Celsius in HI and above 0 J/kg for the necessary condition for land-surface controlled convection to happen. All other conditions are implausible in the model either due to an atmosphere that is too stable or a has too little moisture. The cut-off points for this framework is given in the Figure below (from Findell & Eltahir, 2003b).

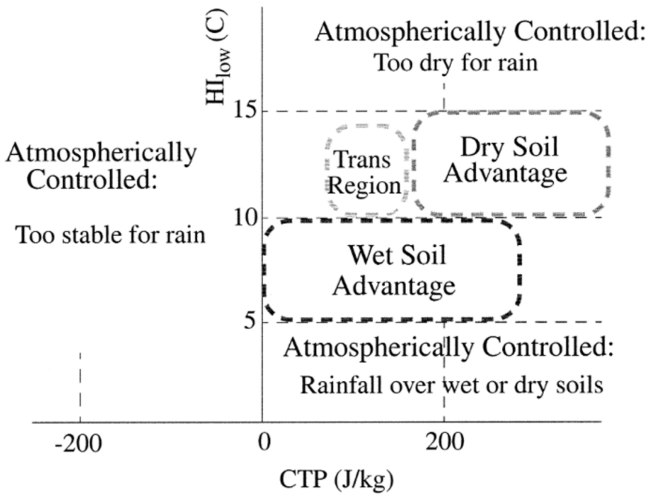
Atmospherically Controlled:
Too dry for rain
HIlow (C)
15
Trans Region
Dry Soil Advantage
Atmospherically Controlled:
Too stable for rain
10
Wet Soil Advantage
5
Atmospherically Controlled:
Rainfall over wet or dry soils
-200
0
200
CTP (J/kg)

Appendix B Figures

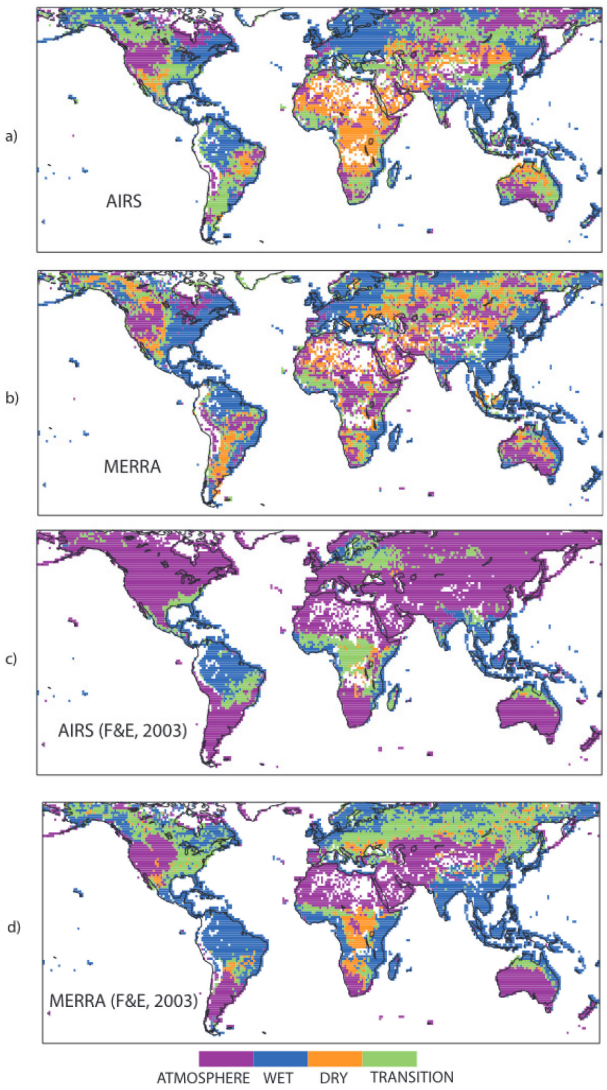

FIG. 8. (a) AIRS- and (b) MERRA-derived global regime classification for 2002–09 convective seasons, following the classification protocol of this study (Fig. 7). (c),(d) As in (a)–(b), but using the unmodified classification scheme of F&E2003. Only AIRS-available days were included. The absence of color (i.e., white) indicates an insufficient number ($n < 40$) of AIRS retrievals. On a global basis, 200 ± 118 days contributed to the classification, with a median of 166.

Figure B 2.1: Extracted from (Ferguson & Wood, 2011). Here different climate regimes are defined similar to (Findell & Eltahir, 2003b).

a,b)

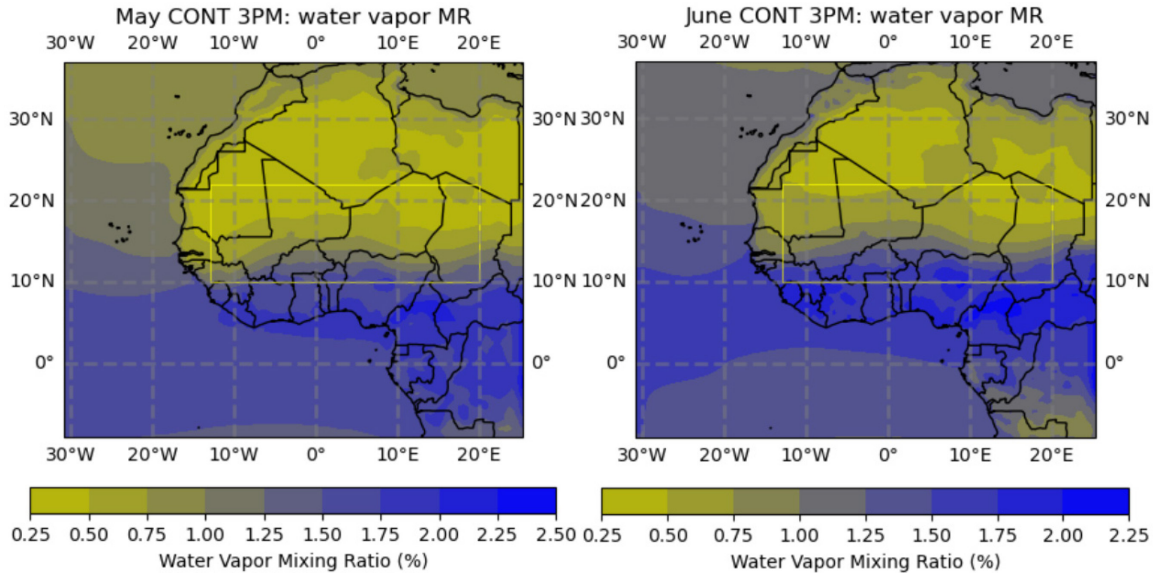
May CONT 3PM: water vapor MR
June CONT 3PM: water vapor MR
30°W 20°W 10°W 0° 10°E 20°E
30°N 20°N 10°N 0°
0.25 0.50 0.75 1.00 1.25 1.50 1.75 2.00 2.25 2.50
0.25 0.50 0.75 1.00 1.25 1.50 1.75 2.00 2.25
Water Vapor Mixing Ratio (%)
Water Vapor Mixing Ratio (%)

c,d)

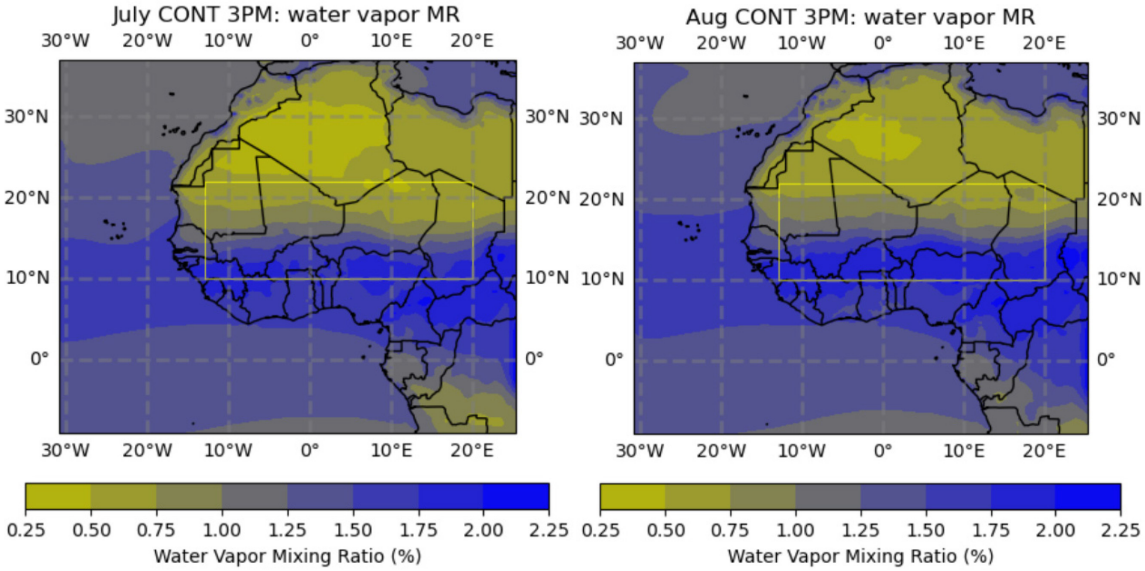
July CONT 3PM: water vapor MR
Aug CONT 3PM: water vapor MR
30°W 20°W 10°W 0° 10°E 20°E
30°N 20°N 10°N 0°
0.25 0.50 0.75 1.00 1.25 1.50 1.75 2.00 2.25
0.25 0.50 0.75 1.00 1.25 1.50 1.75 2.00 2.25
Water Vapor Mixing Ratio (%)
Water Vapor Mixing Ratio (%)

e)

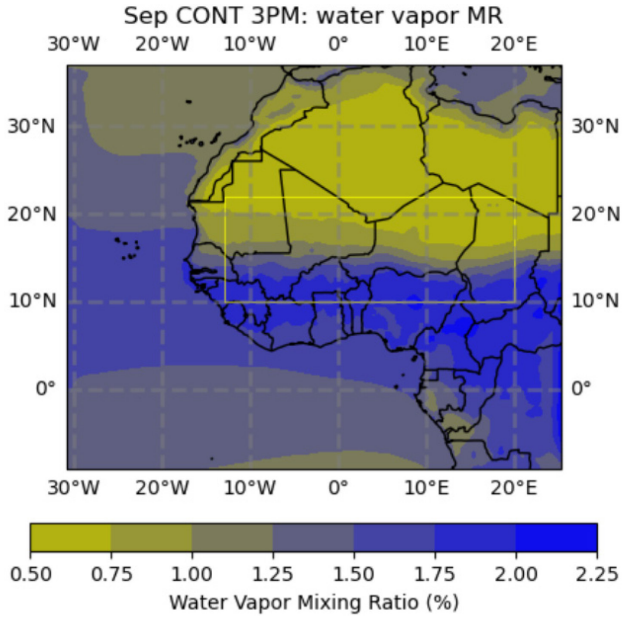

Figure B 4.1: Monthly (May - September) Water Vapor Mixing Ratio (%) at 3PM in the afternoon for the control experiment (CONT) (no change to the land-use types).

a,b)

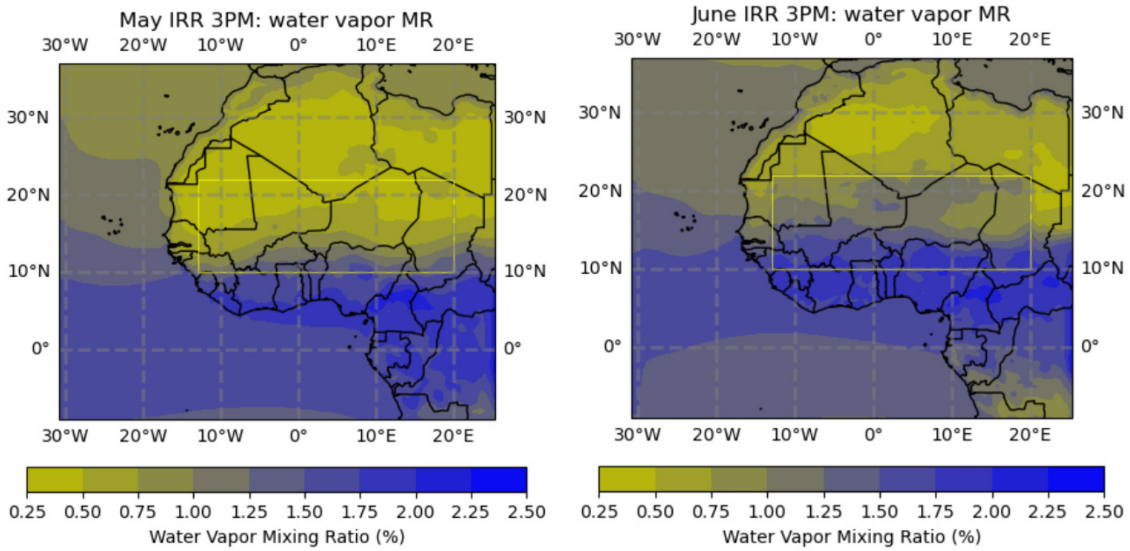

c,d)

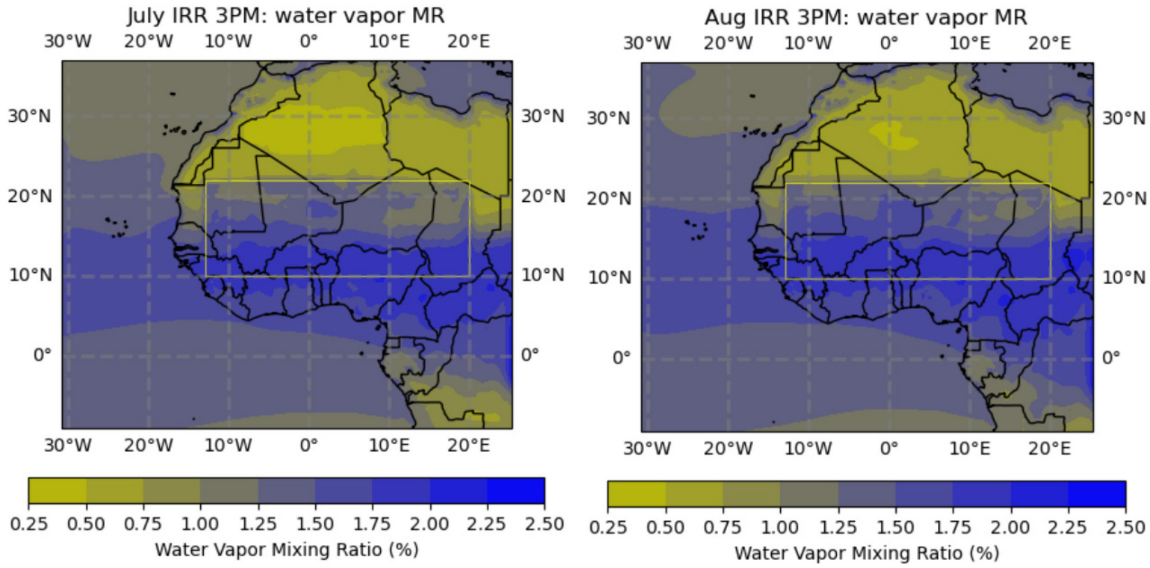

e)

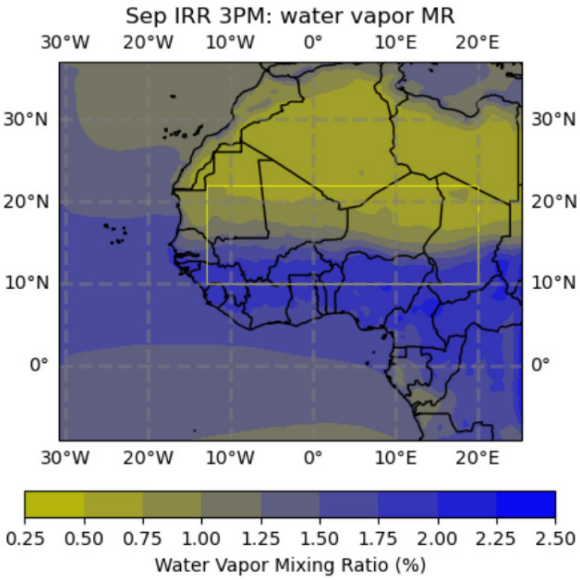

Figure B 4.2: Monthly (May - September) Water Vapor Mixing Ratio (%) at 3PM in the afternoon for irrigated experiments (100% of the box is irrigated under scheduling between June and August).

a,b)

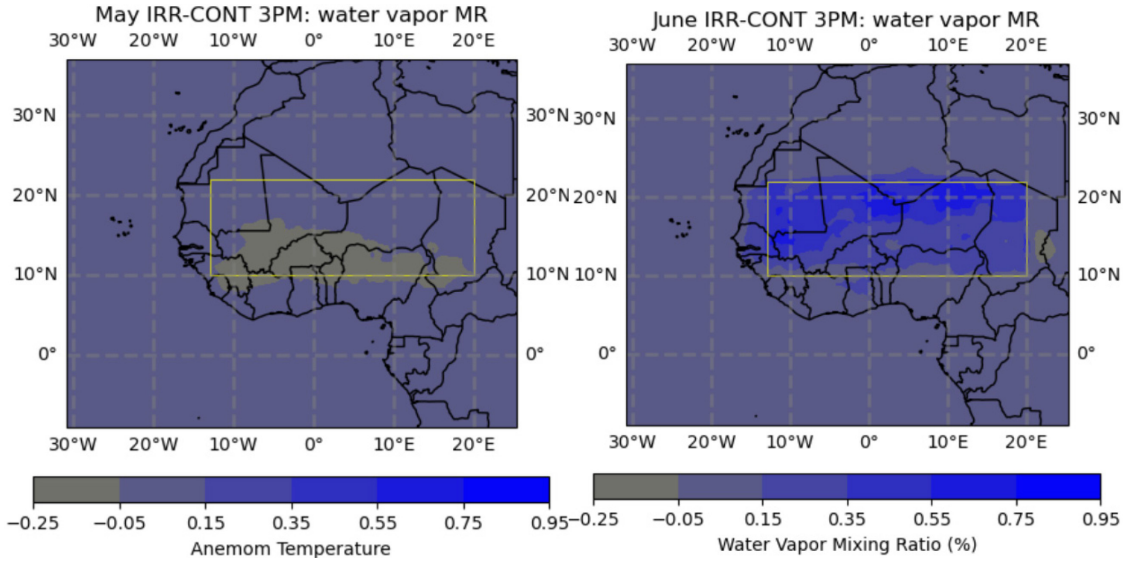
May IRR-CONT 3PM: water vapor MR
June IRR-CONT 3PM: water vapor MR
30°W 20°W 10°W 0° 10°E 20°E
30°N 20°N 10°N 0°
−0.25 −0.05 0.15 0.35 0.55 0.75 0.95
Anemom Temperature
Water Vapor Mixing Ratio (%)

c,d)

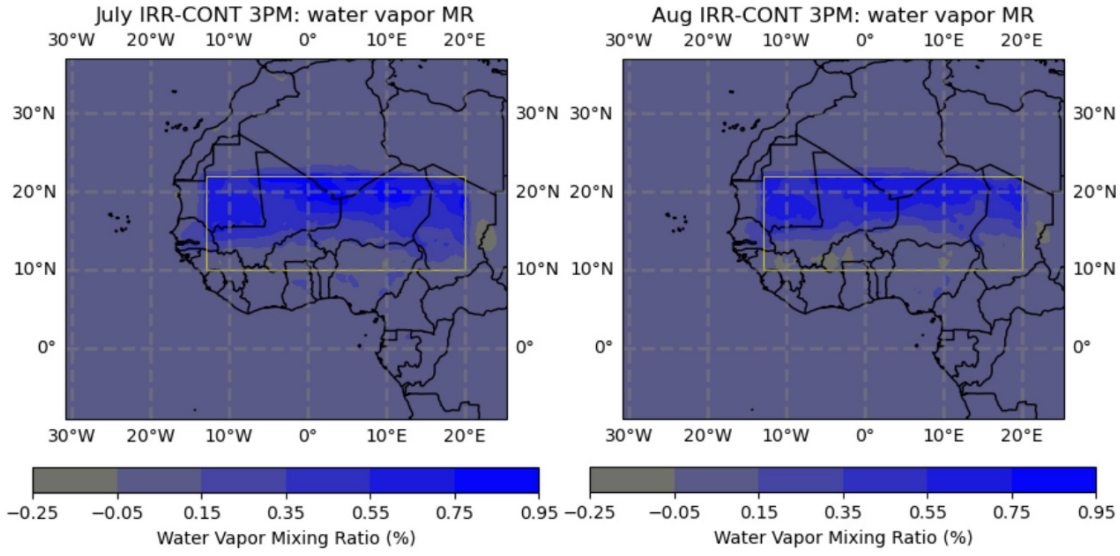
July IRR-CONT 3PM: water vapor MR
Aug IRR-CONT 3PM: water vapor MR
30°W 20°W 10°W 0° 10°E 20°E
30°N 20°N 10°N 0°
−0.25 −0.05 0.15 0.35 0.55 0.75 0.95
Water Vapor Mixing Ratio (%)

e)

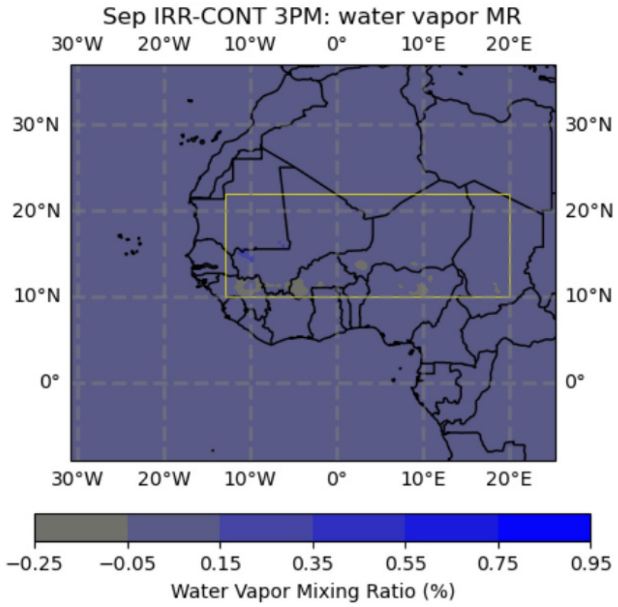

Figure B 4.3: Monthly (May - September) Water Vapor Mixing Ratio (%) at 3PM in the afternoon for the irrigated experiment – control experiment difference (IRR - CONT) (100% of the box is irrigated under scheduling between June and August).

List of Tables

List of Figures

between before irrigated (1910-1949) and after-irrigated (1970-2009) time periods for the months of May-June-July. The black dots indicate differences that are statistically significant at the 5% Kolmogorov-Smirno test (N=40, p<=0.05).

Figure 2.2.2: extracted from Tuttle & Salvucci (2016). This study looks specifically at the impact of soil moisture on next-day precipitation. Here the authors calculate the mean impact of soil moisture on precipitation, calculated as the predicted precipitation probability when soil moisture was included in the regression model divided by the predicted precipitation probability when soil moisture was removed. Blue colors indicate that the inclusion of soil moisture in the model reduced the predicted precipitation probability, while red colors indicate that the probability increased. Light gray areas denote the absence of a statistically significant relationship (alpha = 0.05), and dark gray areas were not tested. Figures on the left show the relative impact below median soil moisture anomaly (dry conditions) and mean relative impact of above median soil moisture anomaly is presented in the right column (wet conditions).

Figure 2.2.3: extracted from Alter et al. (2015). This figure compares the simulated and observed changes in rainfall. a) and b) show absolute differences in ensemble mean rainfall between irrigation and control simulations for July (a) and August (b). Superimposed dots indicate irrigation-induced rainfall enhancement during at least 70%of the ensemble years. C) and d) show absolute differences in observed rainfall for July (c) and August (d). Superimposed dots indicate grid cells where the value of a rainfall change consistency index >= 80^{th} percentile. Areas with <= 1mm/d in rainfall for the control are masked out to avoid potential inflation due to small amounts.

Figure 2.2.4: The correlation between monthly soil moisture and next-month precipitation. We see that most areas on the globe show a positive correlation with regards to SM-P on next-month rainfall and that some mostly transition zones (between wet and dry areas) show negative SM-P feedback. Extracted from Yang (2018).

Figure 3.1.1: The continuous development of Global Circulation Models (GCMs) to incorporate more and more climate processes. Graph extracted from IPCC AR4.

Figure 3.1.2: Changes in global temperature as simulated from GCM ensembles. Graph extracted from IPCC AR6.

Figure 3.3: Experiment Domain with different land-use types represented by different colors. The red box is the irrigation area between 10-22 N. The left graph shows the naturally existing land-use types. The graph in the right with the green color extending to the south is the desert experiment that changes all of the land in northern West Africa into a desert. The different colors represent the different land-use types. The list includes 17 land-use types with 13 being “irrigated cropland” and 14 being “desert”. The complete list from 1-17 is as follows: "tropical evergreen forest","tropical decidduous forest","temperate evergreen broadleaf forest","temperatre evergreen conifer forest","temperate deciduous forest","boreal evergreen forest","boreal deciduous forest","mixed forest","savanna","grassland","dense shrubland","open shrubland","irrigated crop","desert","polar desert","cropland", and "ocean/water".

Figure 3.4.1: The entire domain in the graph is the simulation domain. Simulation 1 for both 3-hourly and 6-hourly output simulations both use the original land-use types as seen in the above graph. Red box indicates the location of land-use change, where original land-use is changed to be irrigated farmland or desert according to the simulations 2-8, as well as with simulations 1 & 3 for the 3-hourly output simulations.

Figure 3.4.2: The entire domain in the graph is the simulation domain. Red box indicates the location of land-use change, where original land-use is changed to be irrigated farmland according to simulation 9.

Figure 3.4.3: The entire domain in the graph is the simulation domain. Red box indicates the location of land-use change, where original land-use is changed to be irrigated farmland according to simulation 10.

Figure 3.4.4: The entire domain in the graph is the simulation domain. Red box indicates the location of land-use change, where original land-use is changed to be desert according to simulation 2 of the 3-hourly simulation.

Figure 3.4.5: The entire domain in the graph is the simulation domain. Red box indicates the location of land-use change, where original land-use is changed to be irrigated farmland according to simulation 4 of the 3-hourly simulation.

Figure 4.1.1: (Left) Seasonal (May-September) precipitation anomalies (simulation with a change of the land-use type minus the control simulation) with 100% of the lands in the red box indicates the area in which the land-use type has changed, from the original land-use type entirely into the irrigated cropland land-use type. (Right) Land-use type distribution showing the altered land-use type distribution from the original land-use types shown in Figure 3.3.

Figure 4.1.2: (Left) Seasonal (May-September) precipitation anomalies (simulation with a change of the land-use type minus the control simulation) with 50% of the lands in the red box indicates the area in which the land-use type has changed (randomly), from the original land-use type into the irrigated cropland land-use type. (Right) Land-use type distribution showing the altered land-use type distribution from the original land-use types shown in Figure 3.3.

Figure 4.1.3: (Left) Seasonal (May-September) precipitation anomalies (simulation with a change of the land-use type minus the control simulation) with 30% of the lands in the red box indicates the area in which the land-use type has changed (randomly), from the original land-use type into the irrigated cropland land-use type. (Right) Land-use type

distribution showing the altered land-use type distribution from the original land-use types shown in Figure 3.3.

Figure 4.1.4: (Left) Seasonal (May-September) precipitation anomalies (simulation with a change of the land-use type minus the control simulation) with 22% of the lands in the red box indicates the area in which the land-use type has changed (randomly as large patches; roughly 200km^2 each), from the original land-use type into the irrigated cropland land-use type. (Right) Land-use type distribution showing the altered land-use type distribution from the original land-use types shown in Figure 3.3.

Figure 4.1.5: (Left) Seasonal (May-September) precipitation anomalies (simulation with a change of the land-use type minus the control simulation) with 22% of the lands in the red box indicates the area in which the land-use type has changed (randomly, this time smaller patches roughly 100km^2 each in size), from the original land-use type into the irrigated cropland land-use type. (Right) Land-use type distribution showing the altered land-use type distribution from the original land-use types shown in Figure 3.3.

Figure 4.1.6: (Left) Seasonal (May-September) precipitation anomalies (simulation with a change of the land-use type minus the control simulation) with 15% of the lands in the red box indicates the area in which the land-use type has changed (randomly), from the original land-use type into the irrigated cropland land-use type. (Right) Land-use type distribution showing the altered land-use type distribution from the original land-use types shown in Figure 3.3.

Figure 4.1.7: (Left) Seasonal (May-September) precipitation anomalies (simulation with a change of the land-use type minus the control simulation) with 22% of the lands in the red box indicates the area in which the land-use type has changed (randomly), from the original land-use type into the desert land-use type. (Right) Land-use type distribution showing the altered land-use type distribution from the original land-use types shown in Figure 3.3.

Figure 4.1.8: (Left) Seasonal (May-September) precipitation anomalies (simulation with a change of the land-use type minus the control simulation) with 100% of the lands in the red box indicates the area in which the land-use type has changed (randomly), from the original land-use type into the desert land-use type. (Right) Land-use type distribution showing the altered land-use type distribution from the original land-use types shown in Figure 3.3.

Figure 4.1.9: The overall percentage change in seasonal (May-September) rainfall only within the red box (above figure) where we altered the land-use types and within the entire experimental domain (below figure). Percentages on the x-axis signify the amount of land within the red box that is either altered to be desert (negative percentages) or irrigated cropland (positive percentages) with 0% being the CONT simulation.

Figure 4.2.1: Changes in JJA average evapotranspiration for different sensitivity experiments: 100% of the boxed region being a desert, 15% of the area being irrigated in patches, 22% being irrigated in patches, 22% being irrigated in large patches, 30% being irrigated in patches, 50% being irrigated in patches, 100% being irrigated and 100% being irrigated with the irrigation area shifted 5 degrees to the south (from top to bottom and left to right respectively). Red areas indicate increased evapotranspiration and blue areas indicate decreased evapotranspiration.

Figure 4.4.1: Wind and precipitation are shown under the control experiment conditions for the months of June, July and August (top-left, top-right and bottom). Precipitation levels are represented by colors from light yellow to dark blue, which range from 0 to >16mm/day respectively. Wind directions are represented by arrows on streamlines in light orange.

Figure 4.4.2: Wind and precipitation changes when comparing the difference between IRR and CONT are shown for the months of June, July and August (top-left, top-right

and bottom). Precipitation levels are represented by colors from light yellow to dark blue, which ranges from -16mm/day < to > 16mm/day respectively. Wind changes between IRR and CONT are represented by the lengths of the arrows.

Figure 4.4.3: Wind directional changes when comparing the difference between IRR and CONT are shown for the months of June, July and August (top-left, top-right and bottom). Precipitation levels are represented by colors from light yellow to dark blue, which ranges from 0mm/day < to > 16mm/day respectively.

Figure 4.5.1: This figure shows the monthly (June, July, August from left to right) PBL height of the control simulation (a), the irrigated (10 – 22 N) simulation – the control simulation PBL height (b), and the full West Africa desert simulation – the control simulation (c).

Figure 4.5.2: This figure shows the monthly (June, July, August from left to right) LCL height for the control simulation (a) and the changes caused by the changing of land-use types in the sensitivity experiments for the IRR (b), and desA (c).

Figure 4.5.3: These figures shows the difference between PBL and LCL (from left to right) for different LULCC setups (L1), the control simulation (L2), the change between the LULCC scenario and the CONT (L3) and the associated rainfall distribution (L4): a) – c): Jun-Aug IRR, d) – e): Jun-Aug desA.

Figure 5.2.1: Changes in surface pressure to CONT between the desertification and irrigation (10 – 22 N) experiments.